



**UNIVERSIDADE FEDERAL
DE SANTA CATARINA**

UNIVERSIDADE FEDERAL DE SANTA CATARINA
CAMPUS BLUMENAU
DEPARTAMENTO DE ENGENHARIAS
CURSO DE ENGENHARIA DE MATERIAIS

EDUARDO SZPOGANICZ

**INFLUENCE OF POLYSILOXANE-BASED CORE-SHELL PARTICLE SIZE AND
CONTENT ON MECHANICAL PERFORMANCE OF EPOXY RESIN**

BLUMENAU

2019

Eduardo Szpoganicz

**INFLUENCE OF POLYSILOXANE-BASED CORE-SHELL PARTICLE SIZE AND
CONTENT ON MECHANICAL PERFORMANCE OF EPOXY RESIN**

Bachelor's Thesis Project on Material Engineering from the Federal University of Santa Catarina – Blumenau Center, as a requirement to obtain a Bachelor's Degree in Materials Engineering.
Advisor: Prof. Dr. Johnny de Nardi Martins

Blumenau

2019

Influence of polysiloxane-based core-shell particle size and content on mechanical performance of epoxy resin/
Eduardo Szpoganicz ; Orientador, Johnny de Nardi Martins,
2019.

Trabalho de Conclusão de curso (graduação) - Universidade
Federal de Santa Catarina, Campus Blumenau, Graduação em
Engenharia de Materiais, Blumenau, 2019.

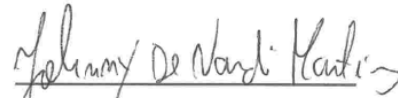
I - Material Science and Engineering, II - epoxy resin, III
- polysiloxane core-shell particles, IV - fracture
toughness of thermoset polymers, V - high-performance
polymers, VI - network density.

Eduardo Szpoganicz

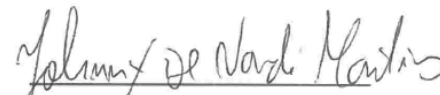
**INFLUENCE OF POLYSILOXANE-BASED CORE-SHELL PARTICLE SIZE AND
CONTENT ON MECHANICAL PERFORMANCE OF EPOXY RESIN**

This Bachelor's Thesis Project was considered appropriate for obtaining the Title of Materials Engineering and approved in its final form by the Course of Materials Engineering.

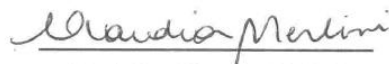
Blumenau, November 20th, 2019


Prof. Dr. Johnny de Nardi Martins
Course Coordinator

Examining Chair:


Prof. Dr. Johnny De Nardi Martins
Advisor

Universidade Federal de Santa Catarina



Prof. Dr. Claudia Merlini

Examining Chair

Universidade Federal de Santa Catarina



Prof. Dr. Wanderson Santana da Silva

Examining Chair

Universidade Federal de Santa Catarina

This work is dedicated to all Professors and Supervisors which I had during my graduation and my curricular internships.

ACKNOWLEDGEMENTS

First of all, I would like to recognize the Federal University of Santa Catarina and all the professors involved in the undergraduate course of Materials Engineering at the Blumenau campus, for providing the best of knowledge in the fundamental topics of science.

To the Polymer Engineering Department – Universität Bayreuth led by Prof. Dr-Ing. Volker Altstädt, which provided me a period of research and the project to perform this Bachelor work. Here, I include the materials and testing devices, which were essential to this project.

To Professor Dr. Johnny de Nardi Martins, who was responsible for my first contact with the Polymer Engineering Department, integrally advisor of this work, and my Professor during my whole graduation. Professor Johnny has always been present in the progress of this work, always collaborating with corrections and adjustments, besides playing an excellent orientation role. Nevertheless, as a friend, always providing me important advises.

To my directly supervisor in Germany, M.Sc. Fabian Hübner, who was always present to clarify information and collaborate with the progress of this work. Also, to his important role as a good friend, granting the best of my performance and motivation at the Polymer Engineering Department.

To my old friend and Bachelor's advisor since my 2th year of graduation, Prof. Dr. Daniel Ponce, who chose me as student for scientific initiation activities since then. Prof. Daniel always sought the best of my performance, has always been present and participated in my understandings. It is with great joy that today I consider great part of my performance models in engineering as a result of my works with Prof. Daniel.

To the students and technicians who somehow contributed to this project. To the PhD students Martin, Simon, Markus, Alper, Merve, Nick and Dominik who guided me and provided me help whenever it was needed. To the Master's students Justus, Marcel, Nico, Fränki, Linda and Phillip, who were always available to help me inside and outside the Department. To the technicians Ute Kuhn and Andreas Mainz, who were helping and providing the necessary assistance to the testing and measurements used in this work.

To my family who never denied any kind of help when necessary. Especially to my mother, whose was protagonist in my whole education and principles since my whole life, providing me the best of motivation and life conduct.

ABSTRACT

Epoxy resins are a class of thermoset polymers that have several uses in both high and low performance industrial application. The high network density in the molecular structure of these resins gives place to an exceptional combination of mechanical, chemical and heat resistance properties. However, the increase in the network density will lead the material to brittleness and poor resistance to crack initiation and propagation, which results in low fracture toughness. The addition of elastomeric particles promotes important toughness mechanism on epoxy resin systems. Eventually, these particles will be related to a decrease tendency in the stiffness, and possibly to the thermal stability. Eventually, these effects will be associated with the particles properties, like structure, size and content.

This bachelor's work is an investigation of the use of the polysiloxane-based core-shell particles (PCS) in epoxy resin, analyzing the increase in fracture toughness and the transversal effects in others properties, like loss of stiffness and thermomechanical stability. The investigation seeks for a relation between these behaviors with the particles parameters, being them particle size (microsized and nanosized particles) and the particle content (no particle, 1, 3 and 5 wt. %). In addition, this relation is given by two different epoxy resin systems (low and high network density systems). The mechanical properties investigated were the fracture toughness through the critical stress intensity factor (K_{IC}) testing, and the stiffness by the tensile testing. The glass transition temperature (T_g) and the network density were measured by dynamic mechanical analysis (DMA). In parallel, the fracture surfaces was analyzed by scanning electron microscopy (SEM), and the particles size and size distribution were evaluated.

For the low network density system, the influence of particle size was not very significant. Both particles size have shown to improve very expressively the fracture toughness, reaching 2.79 MPa m^{1/2} K_{IC} values. The stiffness and thermomechanical stability did not present expressive modifications. For the high network density system, the fracture toughness was less, but also relatively expressively improved, reaching until 0.81 MPa m^{1/2} K_{IC} . The nanosized particles have shown present better performance. For this last case, the microsized particles had a significant effect on the network density structure, but didn't influence expressively the T_g .

Keywords: Epoxy resin, polysiloxane-based core-shell particles, epoxy resin toughening, thermal performance of resins, network density.

RESUMO

As resinas epóxi são uma classe de polímeros termorrígidos que têm várias utilizações em aplicações industriais de alto e baixo desempenho. A alta densidade de ligações cruzadas na rede molecular dessas resinas atribui uma combinação excepcional de propriedades mecânicas, químicas e de resistência ao calor. Porém, o aumento na densidade da rede levará o material à fragilidade e baixa resistência à iniciação e propagação de trincas, resultando em baixa tenacidade à fratura. A adição de partículas elastoméricas promove importantes mecanismos de tenacidade em sistemas de resina epóxi. Eventualmente, esses efeitos serão associados às propriedades das partículas, como estrutura, tamanho e quantidade.

Este trabalho é uma investigação do uso de partículas PCS em resina epóxi, analisando o aumento da tenacidade à fratura e os efeitos transversais em outras propriedades, como perda de rigidez e estabilidade termomecânica. A investigação buscou uma relação entre esses comportamentos com os parâmetros das partículas, sendo estes, tamanho de partícula (partículas micrométricas e nanométricas) e a quantidade em massa (sem partículas, 1, 3 e 5 wt. %). Além disso, essa relação foi dada por dois sistemas diferentes de resina epóxi. As propriedades mecânicas investigadas são: A tenacidade à fratura através do ensaio K_{IC} , e a resistência mecânica através do ensaio de tração. Por meio da análise mecânica dinâmica (DMA) foram analisados a temperatura de transição vítrea (T_g) e a densidade de ligações cruzadas. Em paralelo, as superfícies da fratura foram analisadas por microscopia eletrônica de varredura (SEM), onde foi avaliado o tamanho e distribuição das partículas.

Para o sistema de baixa densidade de ligações cruzadas, a influência do tamanho das partículas não se apresentou muito significativa, alcançando valores de $2.79 \text{ MPa m}^{1/2} K_{IC}$. Ambos tamanhos de partícula mostraram expressiva melhora na tenacidade à fratura. A rigidez e a estabilidade termomecânica não apresentam modificações significativas. Para o sistema de alta densidade de ligações cruzadas, houve um aumento da tenacidade à fratura menor, mas relativamente expressivo, atingindo valores de até $0.81 \text{ MPa m}^{1/2} K_{IC}$. As partículas nanométricas apresentaram melhor desempenho em propriedades mecânicas para o sistema de alta densidade de ligações cruzadas. Para este caso, as partículas micrométricas tiveram um efeito significativo na densidade ligações cruzadas da rede, mas tiveram pouca influência na T_g .

Palavras-chave: Resina epóxi, partículas de polisiloxano *core-shell*, tenacificação de resina epoxy, desempenho térmico de resinas, densidade de ligações cruzadas.

FIGURES LIST

Figure 1 – Chemical structure of the epoxy group (left), amine-epoxy functional group opening mechanism (right).....	21
Figure 2 – Chemical structure of (a) diglycidyl ether of bisphenol-A, (b) tetraglycidyl methylene dianiline, (c) cycloaliphatic epoxy resin	22
Figure 3 – Epoxy resin physical properties as a function of the temperature.....	23
Figure 4 – Glass transition temperature as a function of crosslink density	24
Figure 5 – Formation of resin-hardener networks through the curing process.....	25
Figure 6 – Straight ramp-up of a common curing cycle of epoxy resin system	26
Figure 7 – Glass transition temperature as a function the cure index	27
Figure 8 – Effect of molecular weight between crosslinks on the physical state of epoxy resin	28
Figure 9 – Modes of loading: Mode I opening mode, mode II in-plane shear, and mode III anti-plane shear	29
Figure 10 – Typical test geometry for characterizing epoxy toughness by compact tension test.....	30
Figure 11 – Schematic representations of unstable crack propagation in a load-displacement relation.....	32
Figure 12 – Schematic representations of stable brittle crack propagation in a load-displacement relation.....	33
Figure 13 – Schematic representations of stable ductile propagation in a load-displacement relation.....	33
Figure 14 – (a) Crack behavior without the presence of particles, (b) Crack pinning mechanism as toughening with the use of particles.....	35
Figure 15 – Possible self-assembly micellar structures for core-shell particles	37
Figure 16 – A schematic representation of the different toughening mechanism involved in the fracture.....	39
Figure 17 – A schematic representation of the bisphenol-A molecular structure.....	41
Figure 18 – Illustrative molecular structure of polyetheramine.....	41
Figure 19 – Illustrative molecular structure of NMA.....	41
Figure 20 – Physical form of the low viscous masterbatch and the illustration of the PCS particles preformed ...	42
Figure 21 – Physical form of the toughener, followed by its copolymer structure, and its final form as self-assembled core-shell nanoparticle after curing	43
Figure 22 – Speedmixer DCA 150.1 FVZ.....	45
Figure 23 – Dimensions and geometry of mold cavity, consequently epoxy resin system dimensions and geometry resulting after curing	46
Figure 24 – (a) Specimen geometry and dimensions associated with ISO 13586 as a function of the size W , (b) schematic illustration of K_{IC} testing on the universal testing machine.....	47
Figure 25 – Dependency of fracture toughness K_C , K_{IC} at room temperature on specimen thickness (a) under quasi-static load for PVC-C with $K_{Ic} = 110 \text{ MPa mm}^{1/2}$ and for PP with $K_{Ic} = 139 \text{ MPa mm}^{1/2}$ (b) at traverse speed $V_T = 8.3 \times 10^{-4} \text{ m s}^{-1}$	48
Figure 26 – Specimen geometry and dimensions following ISO 13586.....	48
Figure 27 – (a) Specimen ready for K_{IC} testing, (b) schematic view of the practical testing.....	49
Figure 28 – Scanning Electron Microscope Zeiss Leo 1530.....	50
Figure 29 – Schematic illustration of cavity formation on the bulk, (a) side view before the crack propagation, (b) side view after the crack propagation, (c) top view from surface fracture.....	50

Figure 30 – Tensile testing specimen machined following DIN EN ISO 527-2 Type B	51
Figure 31 – Universal testing machine Zwick Z1475	52
Figure 32 – (a) Schematic structure of a DMA measurement. (b) general results of storage modulus in function of temperature.....	53
Figure 33 – Gabo Eplexor 500N DMA machine utilized for DMA measuring	53
Figure 34 – Fracture toughness for DGEBA-PEA-Particle systems as a function of particle size and content.....	55
Figure 35 – Fracture toughness for DGEBA-NMA-Particle systems as a function of particle size and content ...	57
Figure 36 – Fracture toughness for resin systems as a function of particle size and content	58
Figure 37 – Fracture surface SEM image for the DGEBA-PEA neat system	59
Figure 38 – Fracture surface SEM image for the DGEBA-PEA modified with 1 wt. % of microsized particle system with different magnifications, left (5.00 k), right (15.00 k)	60
Figure 39 – Fracture surface SEM image for the DGEBA-PEA modified with 1 wt. % of nanosized particle system with different magnifications, left (2.50 k), right (15.00 k)	60
Figure 40 – Fracture surface SEM image for the DGEBA-NMA neat system	61
Figure 41 – Fracture surface SEM image for the DGEBA-NMA modified with 1 wt. % of microsized particle system with different magnifications, left (5.00 k), right (15.00 k)	62
Figure 42 – Fracture surface SEM image for the DGEBA-NMA modified with 1 wt. % of nanosized particle system with different magnifications, left (2.50 k), right (15.00 k).....	62
Figure 43 – Practical measurement of fracture toughness (K_{IC}) from one DGEBA-NMA unmodified specimen, attached with a SEM image from the specimen fracture surface	63
Figure 44 – Practical measurement of fracture toughness (K_{IC}) from one DGEBA-NMA modified with 1 wt. % nanosized PCS specimen, attached with a SEM image from the specimen fracture surface	62
Figure 45 – Particle size and size distribution for DGEBA-PEA-Microsized system	65
Figure 46 – Particle size and size distribution for DGEBA-PEA-Nanosized system	65
Figure 47 – Particle size and size distribution for DGEBA-NMA-Microsized system	66
Figure 48 – Particle size and size distribution for DGEBA-NMA-Nanosized system	67
Figure 49 – Practical tensile curves for DGEBA-PEA neat and modified with 1 wt. % PCS particles, attached with the most important results	68
Figure 50 – Practical tensile curves for DGEBA-NMA neat and modified with 1 wt. % PCS particles, attached with the most important results	69
Figure 51 – T_g evaluated from DMA for DGEBA-PEA-Particle systems as function of particle size and content	71
Figure 52 – T_g evaluated from DMA for DGEBA-NMA-Particle systems as function of particle size and content	71
Figure 53 – $\tan \delta$ curve as a function of temperature for DGEBA-PEA modified with 1 wt. % of particles.....	72
Figure 54 – Network density for DGEBA-PEA-Particle system as a function of the particle size and content	75
Figure 55 – Network density for DGEBA-NMA-Particle system as a function of the particle size and content ..	75
Figure 56 – DMA results as a plot of storage modulus (E'), loss modulus (E'') and $\tan \delta$ (E''/E') for low network system unmodified	84

Figure 57 – DMA results as a plot of storage modulus (E'), loss modulus (E'') and $\tan \delta$ (E''/E') for low network system modified with 1 wt. % of microsized particles	84
Figure 58 – DMA results as a plot of storage modulus (E'), loss modulus (E'') and $\tan \delta$ (E''/E') for low network system modified with 3 wt. % of microsized particles	85
Figure 59 – DMA results as a plot of storage modulus (E'), loss modulus (E'') and $\tan \delta$ (E''/E') for low network system modified with 5 wt. % of microsized particles	85
Figure 60 – DMA results as a plot of storage modulus (E'), loss modulus (E'') and $\tan \delta$ (E''/E') for low network system modified with 1 wt. % of nanosized particles	86
Figure 61 – DMA results as a plot of storage modulus (E'), loss modulus (E'') and $\tan \delta$ (E''/E') for low network system modified with 3 wt. % of nanosized particles	86
Figure 62 – DMA results as a plot of storage modulus (E'), loss modulus (E'') and $\tan \delta$ (E''/E') for low network system modified with 5 wt. % of nanosized particles	87
Figure 63 – DMA results as a plot of storage modulus (E'), loss modulus (E'') and $\tan \delta$ (E''/E') for high network system unmodified	87
Figure 64 – DMA results as a plot of storage modulus (E'), loss modulus (E'') and $\tan \delta$ (E''/E') for high network system modified with 1 wt. % of microsized particles	88
Figure 65 – DMA results as a plot of storage modulus (E'), loss modulus (E'') and $\tan \delta$ (E''/E') for high network system modified with 3 wt. % of microsized particles	88
Figure 66 – DMA results as a plot of storage modulus (E'), loss modulus (E'') and $\tan \delta$ (E''/E') for high network system modified with 5 wt. % of microsized particles	89
Figure 67 – DMA results as a plot of storage modulus (E'), loss modulus (E'') and $\tan \delta$ (E''/E') for high network system modified with 1 wt. % of nanosized particles	89
Figure 68 – DMA results as a plot of storage modulus (E'), loss modulus (E'') and $\tan \delta$ (E''/E') for high network system modified with 3 wt. % of nanosized particles	90
Figure 69 – DMA results as a plot of storage modulus (E'), loss modulus (E'') and $\tan \delta$ (E''/E') for high network system modified with 5 wt. % of nanosized particles	90

TABLES LIST

Table 1 – Description of each material weight for the final material system, following the balance establish from the equations 9, 10, 11 and 12.....	45
Table 2 – Curing cycle settled for DGEBA-D230 (left) and DGEBA-NMA (right) systems.....	46
Table 3 – Fracture toughness general results for all resin-particles systems.....	59
Table 4 – T_g for a high network density system as a function of a microsized particle content.....	73
Table 5 – Glass transition general results for all resin-particles systems.....	73
Table 6 – Network density general results for all resin-particles systems	76

ABBREVIATIONS AND ACRONYMS

PCS	Polysiloxane-Based Core-Shell
wt. %	Weight in Percentage
K_{IC}	Critical Stress Intensity Factor
T_g	Glass Transition Temperature
DMA	Dynamic Mechanical Analysis
SEM	Scanning Electron Microscopy
EEW	Epoxy Equivalent Weight
IPDA	Isophorone Diamine
TETA	Triethylenetetramine
T_{use}	Temperature of Use
C	Cure Index
T_{g0}	Initial Glass Transition Temperature
$T_{g\infty}$	Glass Transition Temperature of the “Fully Cured” Resin
G_C	Strain Energy Release Rate
C	Compliance of the Cracked Specimen
a	Crack Length
P_C	Critical Load for the Onset of Crack Propagation
U	Energy under the Load-Displacement
B	Specimen Thickness
D	Specimen Height
ϕ	Calibration Factor
G_{Ic}	Fracture Energy Associated with Mode I
G_{IIc}	Fracture Energy Associated with Mode II
G_{IIIc}	Fracture Energy Associated with Mode III
K_I	Stress Intensity Factor Mode I
Y	Geometrical Factor

σ	Applied Normal Stress
K_{IC}	Critical Stress Intensity Factor Mode I
σ_c	Critical Applied Normal Stress
DDS	Diaminodiphenylsulfone
CSR	Core-Shell Rubber
G_{ICU}	Fracture Energy of Untoughened Epoxy
Ψ	Toughening Contribution
ΔG_r	Rubber-Bridging Model
ΔG_s	Localized Shear Banding Energy
ΔG_v	Plastic Void Growth Energy
DGEBA	Diglycidylether of Bisphenol-A
PEA	Polyetheramine
NMA	Norbornene Methyl Anhydride
PMMA	Poly(methyl methacrylate)
PCL	Polycaprolactone
AEW	Curing Agent Equivalent Weight
W_e	Epoxy Final Weight
W_{ca}	Curing Agent Final Weight
FW	Total Weight of the System
EW	Epoxy Weight
CAW	Curing Agent Weight
PW	Particle Weight
AW	Weight of Additives
B	Plate Thickness
W	Fracture Toughness Specimen Length
E'	Storage Modulus
E''	Loss Modulus

$\tan \delta$	Storage and Loss Modulus Rate
ν_c	Network Density
E_R	Rubbery Modulus
A	Front Factor
R	Gas Constant
T	Temperature in Kelvin
2D	Two Dimensions
3D	Three Dimensions
E	Young's Modulus
σ_M	Maximum Tensile Stress
ε_B	Elongation at Break
da/dN	Fatigue Crack Growth Rate Measurement

SUMMARY

1. Introduction	17
2. Aims and Motivations	19
3. State of the Art	20
3.1. Epoxy Resins	20
3.2. Curing Agents for Epoxy Resin.....	23
3.3. Network Structure.....	25
3.4. Fracture Mechanics	28
3.4.1. Modes of Crack Propagation	31
3.4.2. Microstructural Effects	34
3.5. Toughness Modifiers	34
3.5.1. Polysiloxane-Based Core-Shell	36
3.5.2. Particle Size Effects	37
3.5.3. Volume Content Effects.....	38
3.5.4. Math Modeling of Toughening	38
4. Materials and Methods	40
4.1. Materials.....	40
4.1.1. Epoxy Resin	40
4.1.2. Curing Agents.....	41
4.1.3. Toughness Modifiers	42
4.2. Methods	43
4.2.1. Material Formulation and Testing	43
4.2.1.1. Fracture Toughness Testing (K_{IC}).....	47
4.2.1.2. Scanning Electron Microscope (SEM)	49
4.2.1.3. Particle Size and Distribution Evaluation	50
4.2.1.4. Tensile Testing	51
4.2.1.5. Dynamic Mechanical Analysis (DMA)	52
4.2.1.6. Network Density Calculation	54

5. Results and Discussion	55
5.1. Mechanical Properties	55
5.1.1. Fracture Toughness	55
5.1.2. Fractography	59
5.1.3. Particle Size and Size Distribution	64
5.1.4. Tensile Properties	67
5.2. Thermomechanical Properties	70
5.2.1. Glass Transition Temperature (T_g)	70
5.2.2. Network Density	74
6. Conclusions	77
7. Suggestions for Future Works	79
References	80
Appendix A	84

1. Introduction

Epoxy polymers are extensively used in industrial applications such as adhesives, coatings and composite materials. This is because epoxies have properties that make them attractive for high-performance applications, including high strength and modulus, creep performance, thermal and chemical resistance. A wide range of commercial epoxy resins and curing agents are currently available, which allows for the optimization for specific applications using an appropriate combination of both (DEKKER, 1988). Especially low viscous epoxy resin as casting systems find many applications in the sector of automotive, aviation and aerospace, since lightweight properties gather more and more importance due to weight savings and system optimizations. Although, have been reported through several works that for high thermomechanical properties performance, the neat epoxy resin presents to be very hard and brittle, which restricts its applications without the presence of modifiers. (LEVITA, 1991; AZIMI, *et al.*, 1996; UTALOFF, *et al.*, 2018).

Early studies have shown that the addition of rubber particles can greatly improve the fracture toughness of epoxy polymers (UTALOFF, *et al.*, 2018; CHONG, 2015). More recently, the emergence of nanoscale modifiers has attracted much attention, whether by preformed particles or phase separating structures. The morphology of these new modifiers has been extensively studied, however, the contributions of such complex microstructures to the mechanical and fracture performance is still not well understood. (CHONG, 2015). The microstructures that these new modifiers provide are complex, and a proper understanding of how these are related to the composite performance will be exploited. There are few literature bringing comparative analyses between particle properties and network density of epoxy systems. (CHONG, 2015)

Extensive research has focused on improving the fracture toughness of epoxies through hard and soft particulate additives, as well as the manipulation of the epoxy chemistry and chain structure (CHONG, 2015). Rubber toughening like polysiloxane-based core-shell (PCS) is a common approach for improving the fracture toughness in epoxy thermosets. Mechanisms of thermoset toughening by particulate fillers include crack bridging, shear band yielding, particle cavitation, void growth and many others. Many of these same mechanisms are available even in nanoscale. Although, it is important to notice that the usage of toughening modifiers usually leads to side effects, like a decrease of the tensile resistance

modulus, and thermomechanical properties like T_g . Therefore, the modification of a resin system should consider not only fracture toughness improvement but balance other properties. (CHEN, *et al.*, 2013)

Furthermore, it is possible to notice that not only the fracture toughness improvement, but the transversal effects of adding particles are correlated to the network density structure of the resin system. As the network density improves, the system gets more closed and compact. This makes the system more sensitive to network disorder, decreasing the toughening effect and improving the undesirable collateral effects. On the other hand, low network density systems have proved to be more suitable for improvement with a low register of network disorder (UTALOFF, *et al.*, 2018).

Eventually, the particles properties will be correlated to the particles–network interaction, which brings two main important facts to be analyzed. The particle size and content clearly, will correspond in how these particles fit in the structure, how they interact with the epoxy system, and also how they promote different mechanical and thermomechanical behavior on the matrix. (CHONG, 2015; CHEN, *et al.*, 2013)

The need for epoxy resin for high-performance application improvement still shows a lot of space to improve, which provide a stable meaning for this work. Nevertheless, the investigation on the particle size and content effects correlated with different networks structures has not been much explored by the literature. Therefore, this bachelor's work aim for finding great balance in the use of PCS particles on fracture toughness without decrease on mechanical and thermomechanical stability, stablishing a scientific overview about the particles size and content with the epoxy network structure and properties.

2. Aims and Motivations

The main goal of this work was to investigate the effects of polysiloxane-based core-shell particles on the mechanical and thermomechanical properties of epoxy resin systems, analyzing the particles size and content parameters, and the resin network density.

For that, it was defined the following specific goals:

- Perform the formulation of high and low network density epoxy resin systems with two different curing agents, with addition of nanosized and microsized PCS particles in different contents;
- Evaluation of fracture toughness improvement;
- Evaluation of particles effect on Elastic modulus;
- Evaluation of particles effect on thermomechanical properties;
- Establish a correlation of the particles parameters with the mechanical and thermomechanical behavior of both epoxy resins systems;
- Evaluation of engineering applications related to the results.

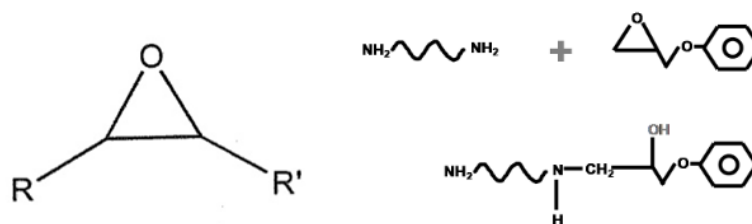
3. State of the Art

3.1. Epoxy Resin

Epoxy resins are classified as thermoset materials and are extensively used in structural and specialty composite applications, due to their unique combination of properties unreachable with other thermoset materials (DEKKER, 1988). Due to their molecular weight, it is found available in a wide variety of physical forms (from high melting solids to low viscosity liquid), and therefore, they are amenable to a wide range of processes, then afterwards to applications. Epoxies offer relatively high strength, low shrinkage, excellent adhesion to various substrates, effective electrical insulation, chemical and solvent resistance, among many others. (DEKKER, 1988) It also counts with several easy ways of curing without the evolution of volatiles or by a broad of others chemical species. Epoxy resins are also chemically compatible with most substrates and tend to wet surfaces easily, marking them favorable suited to composites applications. These resins are of particular interest to structural engineers because they are able to provide an exclusive balance between chemical and mechanical properties combined with extreme processing versatility. In all cases, thermoset resins may be tailored to some degree to satisfy particular requirements, so formulation and processing information are often maintained as trade secrets. (ELLIS, 1993; TOMUTA, 2014).

There are three basic elements of an epoxy resin formulation that must be understood when selecting a thermoset system: The base resin, curing agents, and the additives. When the formulation of epoxy resin for a particular use is made, it is necessary to know what each of these components contributes to the physical performance of the part during and after production. Epoxy resins comprise a group which possesses the same category of reactive functional groups, the epoxy or oxirane-group (ELLIS, 1993). Their chemistry and technology have been reported in many literature reviews, and Figure 1 (left) illustrates the epoxy functional group, while Figure 1 (right) illustrate the epoxy functional group opening mechanism. (DEKKER, 1988) The epoxy group will be defined by its reactivity towards both nucleophilic and electrophilic species and it is thus susceptible to a wide range of curing agents. These curing agents are of two types: they may be either catalysts or hardeners. (DEKKER, 1988)

Figure 1 – Chemical structure of the epoxy group (left), amine-epoxy functional group opening mechanism (right)



Source: Adapted from Dekker, 1988

Catalysts are usually drawn from tertiary amines or Lewis acids, and they function by initiating the ionic polymerization of the epoxy compound to produce polyether structures. The reaction by hardeners will follow both primary and secondary amines, as well as hydrogen-bonding catalysts and promoters, which can be shown to have a considerable effect on the activation barrier of the curing reaction. An epoxy group reacts with one amine-hydrogen (Figure 1, right), resulting in a hydrogen attached directly to a nitrogen atom. Therefore, every time that an epoxy group is opened, one hydroxyl group is generated. Initial chemical reaction builds linear molecular weight, the molecules get longer in a polyaddition reaction, without the formation of sub-products. The process of curing an epoxy resin converts the initially low molecular weight resin into its thermoset form, which is a space network or three-dimensional chemical structure. (DEKKER, 1988; ELLIS, 1993)

Epoxy resins used in commercial composite applications can be divided into two main fields of applications regarding thermomechanical behavior: high-temperature and low-temperature performance, considering the material T_g as reference. The T_g is the temperature below which a polymer exists in the glassy state, and only the vibration motion is present, whereas above this temperature, individual molecular segments are able to move relative to each other in what is termed the rubbery state. (CHONG, 2015) Therefore, the mechanical performance of a material above its T_g is typically several orders of magnitude lower than its value below the T_g , that can be also affected by the presence of absorbed moisture or solvents. (CHONG, 2015) It is also important to mention that the main factor regarding the resin T_g characteristic is the cross-linking density. If the T_g is very high, due to the high amount of crosslinks, the material tends to be very brittle and fragile, with a low resistance to crack propagation. By the other hand, lower T_g resins due to the low density of crosslinks tend to

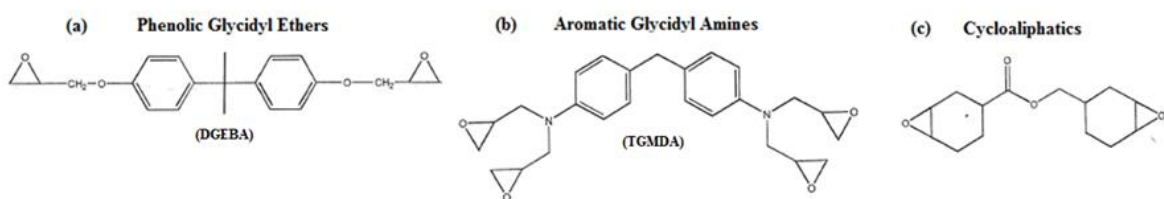
form materials with higher toughness, resisting to the crack propagation. (MOLONEY, *et al.*, 1987; CHEN, *et al.*, 2013)

The glass transition temperature of a cured epoxy resin is completely conducted upon the molecular structure that is developed in the matrix during the curing process, coming from resin and curing agent reactivity, defined by the reactive groups per molecular weight. This drives properties as the cross-link density, backbone stiffness, intermolecular interactions, among many others. The T_g is therefore strongly related to the curing temperature and enthalpy, and will change as the curing temperature changes. Epoxy resins cured at low temperatures will result in a low T_g material, while a higher T_g material will be found when the same system is cured in a higher temperature. Although all systems will have an ultimate T_g determined by its formulation, that cannot be enhanced by an increase in curing temperature. (DEKKER, 1988; TOMUTA, 2014)

Another important characteristic that rules the resin stability for its use is the epoxy equivalent weight (EEW) that can be defined as the resin weight per epoxy groups. The equivalent weight will be used to calculate the stoichiometric ratio between the epoxy, curing agent, and modifiers when it is the case. The calculation is defined by dividing the molecular weight of the resin by the number of epoxide groups per molecule. (DEKKER, 1988; TOMUTA, 2014)

High-temperature performance resins are those that cure to yield somewhat inflexible molecular structures. Rigidity can be created into the cured material by various methods: Through the incorporation of aromatic groups, an increase in the number of reactive sites (epoxy groups) and therefore, the cross-link density, or a reduction on the distance between the reactive sites. The three primary classes of epoxies used in composite applications are phenolic glycidyl ethers, aromatic glycidyl amines and cycloaliphatics. Figure 2 (a, b and c) show the chemical structure of each one of these classes, respectively. (DEKKER, 1988)

Figure 2 – Chemical structure of (a) diglycidyl ether of bisphenol-A, (b) tetraglycidyl methylene dianiline, (c) cycloaliphatic epoxy resin



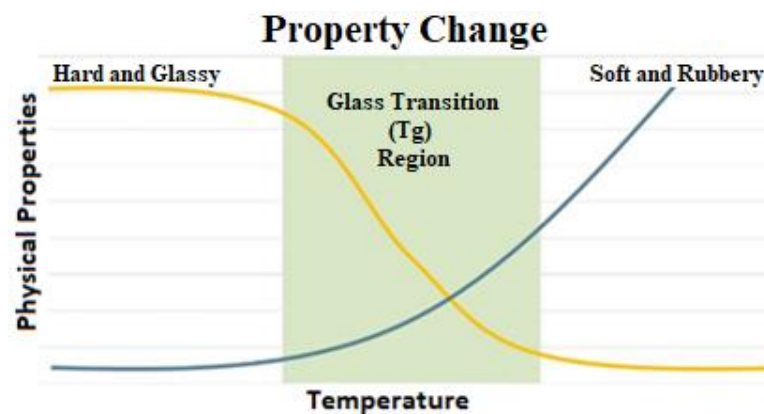
Source: Adapted from Dekker, 1988

3.2. Curing Agents for Epoxy Resin

Curing agents achieve an important role in the cross-linking kinetics, gel time, curing degree, viscosity, curing cycle and basically the cured material performance. Epoxy resin will react with a great number of chemical species, being those curing agents or hardeners (MIRACLE, 2001). There are essentially three types of curing agents. The first type of curing agents includes active hydrogen-containing compounds and their derivatives. The second type of curing agents includes anionic and cationic initiators. These curing agents are used to catalyze the homopolymerization of epoxy resins, like tertiary amines, imidazoles, among others. The third type of curing agents is called reactive crosslinkers. They usually have higher equivalent weights and cross-link with the secondary hydroxyl groups of the epoxy resins or by self-condensation, like commercial IPDA, TETA, and others. (MIRACLE, 2001)

It is possible to formulate the epoxy resin in an infinite number of combinations in order to manipulate the material final properties, such as physical form, T_g , mechanical performance, chemical resistance, among others. This can be done not only by changing the hardener, but the composition itself, curing time, curing temperature, additives, and others. Curing times can range from seconds to days, with some heat-activated systems being latent for months to years at room temperature. The uncured formulated resin can be solid, rubbery or liquid, tacky or dry, and can cure at temperatures from 5 to 260 °C. The cured product can be soft and pliable or rigid and glassy, with glass transition temperature ranging from below room temperature to 260°C, and tensile elongations from 1 to over 100%. (HAMERTON, 1997) As a general overview of the epoxy properties as a function of temperature, as described above, can be illustrated by Figure 3

Figure 3 – Epoxy resin physical properties as a function of the temperature



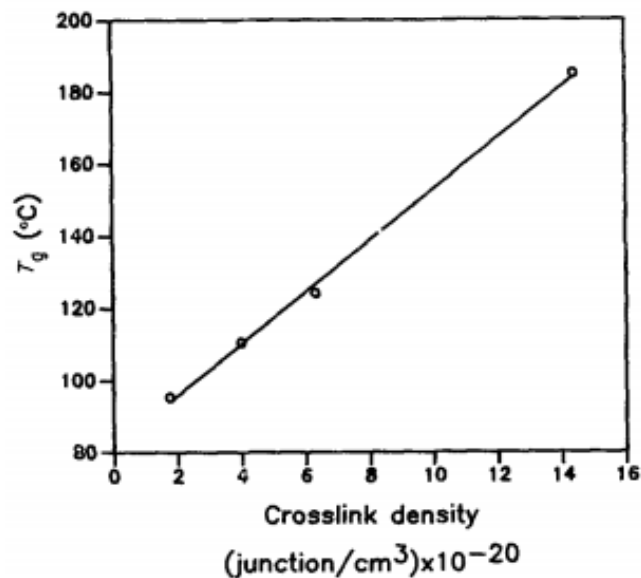
Source: Hamerton, 1997

The physical properties as well as the T_g will be then, related to the crosslink density. This property by its time, will be reached in the curing process. Therefore, all these properties will follow the parameters of the curing process. (HAMERTON, 1997)

There are several characteristics of the hardener which directly affect the crosslink density. The two more important are the molecular weight and the number of functional groups. The molecular weight reduction will correspond to more compact structures, where more reactive groups have the opportunity of bounding in a given space, compared to a large molecule, with the same number of reactive groups. The number of reactive groups by its time, will directly come out as the number of possible bindings that one single molecule can achieve, that evidently will apply that larger is the number of reactive groups, large is the crosslink density.

In the literature (LEVITA, *et al.*, 1991; UEBERREITER, 2010), it is possible to notice description in detail of the relation between molecular weight, crosslink density, and the T_g . The crosslink density appears to increase linearly with the decrease of molecular weight, as well as the T_g . Figure 4 shows very clearly a practical result of this combination.

Figure 4 – Glass transition temperature as a function of crosslink density



Source: Levita, *et al.*, 1991

The number of reactive groups though, cannot exist without the increase of molecular weight, and therefore, cannot be analyzed isolated. However, it is possible to see an increase in the epoxy resin T_g comparing curing agents with a different number of reactive groups.

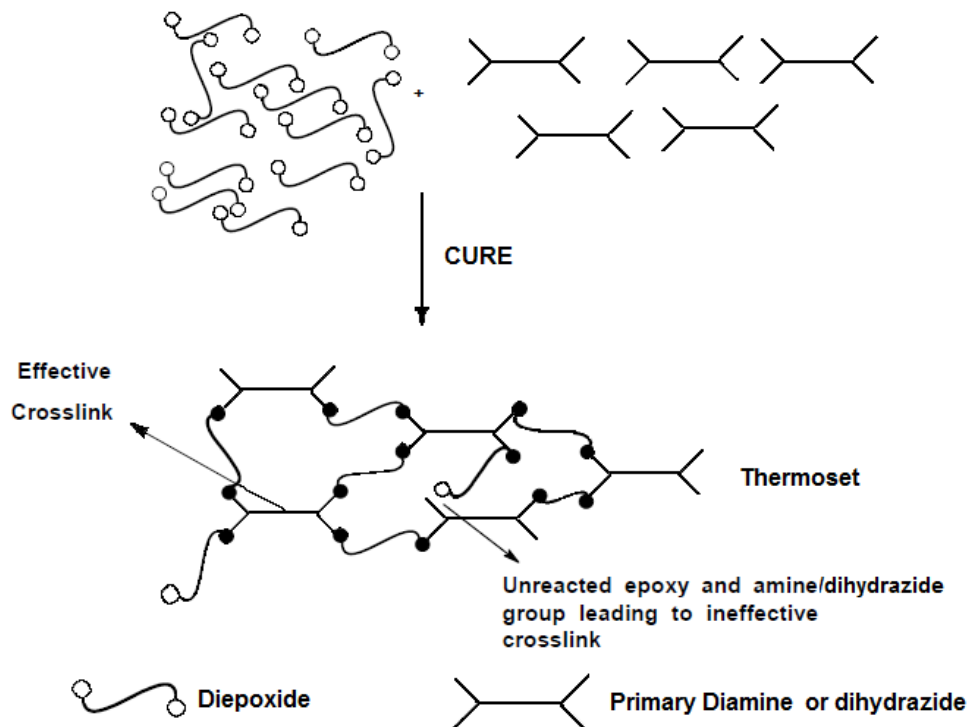
3.3. Network Structure

The network will strongly depend on the ratio of resin and hardener used for the curing resin. Similarly, both curing agent and resin structure will affect the material characteristics. For this reason, it can be said that epoxy materials are extremely versatile thermosets. (MIRACLE, 2001).

The crosslink extent can be measured from the conversion. The most important properties are achieved with the maximum crosslink density. The curing temperature therefore, will be a vital key of this process. Heating increases molecular mobility, resulting in higher crosslink density, which in turn affects the chemical resistance of the cured matrix positively. (TOMUTA, 2014)

The reactivity of resin-hardener systems can be determined by measuring the heat evolved, which vary with the existence of unreacted structures, or also by the T_g achieved after the formation of the network structure. The kinetics of curing can also be measured by this principle, allowing prediction of the curing schedule, which will be of great importance in the technological application. Figure 5 shows a representation of the network formation. (MIRACLE, 2001)

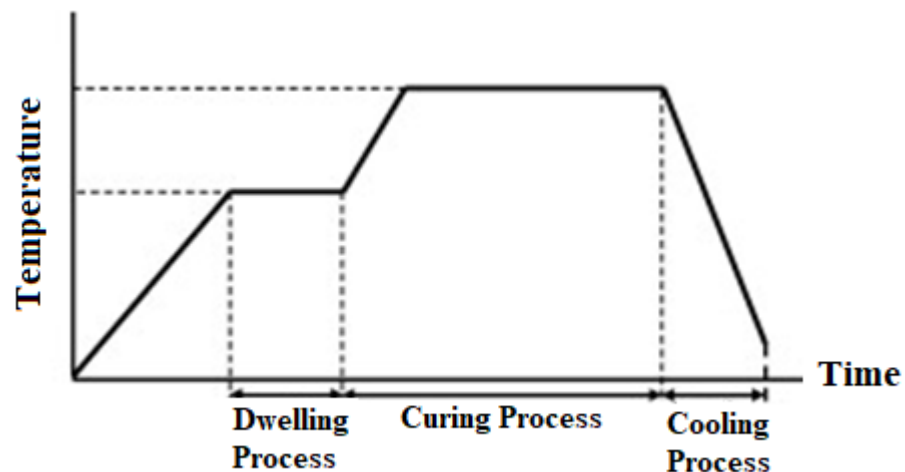
Figure 5 – Formation of resin-hardener networks through the curing process



Source: Miracle, 2001

The curing cycle is then responsible for determining the kinetics and the formation of the network structure. Several curing cycles can be arranged for different combinations of epoxy resins and curing agents. Although, the curing cycle consists of a first heating ramp, where the isothermal represents the dwelling moment, used to allow the resin to flow and volatiles to escape. The second ramp and hold is the polymerization portion of the cure cycle. During this period, the resin viscosity initially drops slightly due to the application of additional heat, when needed, and then rises dramatically as the kinetics of the resin start the cross-linking process, as illustrated in Figure 5. (MIRACLE, 2001) Figure 6 represents a common curing cycle model in a relation of temperature and time.

Figure 6 – Straight ramp-up of a common curing cycle of epoxy resin system



Source: Adapted from Miracle, 2001

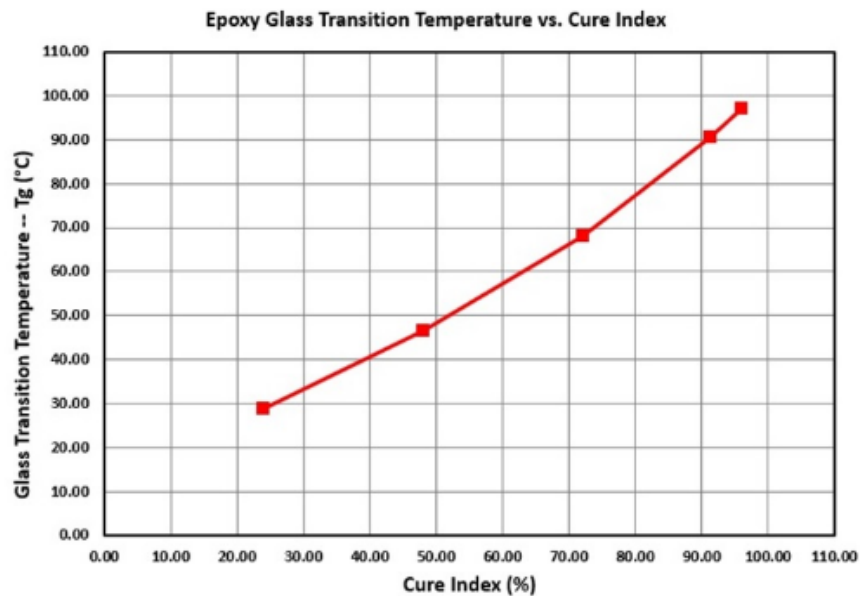
The use of the material for this purpose will be below the glass transition temperature of the cured resin $T_{use} < T_g$. For higher thermal performances there is continuous research in epoxy-hardeners system with higher T_g and therefore higher T_{use} . In many applications of epoxy resins, it is their glassy state elastic modulus that is of paramount importance. There will be a need to perform the structure-property relationships for thermosetting resins. The elastic properties will be a function of the network structure and the measurement temperature relative to the glass transition temperature of the cured resin. (DEKKER, 1988; TOMUTA, 2014)

The literature suggest that the glass transition temperature can be used as a measure of cure index, C . (DEKKER, 1988) Their proposal has been slightly modified by replacing T_g

$$C = \frac{T_g - T_{g0}}{T_{g\infty} - T_{g0}} \quad (1)$$

where T_{g0} is the initial and $T_{g\infty}$ is the “fully cured” glass transition temperature. Such a definition requires that T_g is a measure of the structure of the cured resin regardless of the precise cure treatment, that is, cure temperature and cure time. Regarding this definition C increases from zero to unity as cure progresses. (DEKKER, 1988) Figure 7 brings a simulation of this method applied.

Figure 7 – Glass transition temperature as a function the cure index

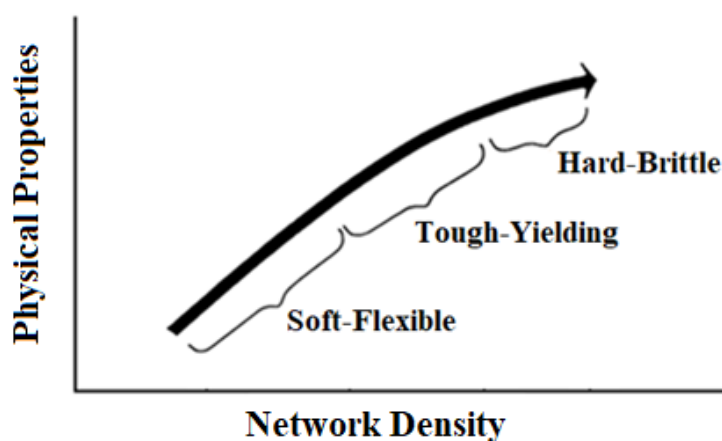


Source: Carbas, *et al.*, 2013

Although, it is interesting to notice how the number of reactive sites (later on the crosslink density) changes the mechanical behavior of this material. Polymers with high crosslink density are usually infusible, insoluble and dimensionally stable under load. This occurs once the distance between crosslinks gets lower, disabling chain motion, making the material more brittle, with a higher T_g (above 140 °C). (CARBAS, *et al.*, 2013) Crosslink density will be inversely related to the distance between crosslinks. Resins with low network density will present a tendency to a behavior soft-rubbery behavior, followed by a lower T_g (below 140 °C). (CARBAS, *et al.*, 2013) The high network density is also associated with stiff and stable structure, which lead to a lower interaction with chemicals components, once the structure is more compact. As this network space is increased, it is believed that the

interaction with chemicals components increases with it. (CARBAS, *et al.*, 2013) Figure 8 presents the general physical relationship between the intermolecular sites and the material physical state.

Figure 8 – Effect of molecular weight between crosslinks on the physical state of epoxy resin



Source: Adapted from Dekker, 1988

3.4. Fracture Mechanics

Regarding good mechanical properties, low shrinkage and thermal stability, the epoxy resins are found in an increased rate of use, inside a wide range of engineering applications, from civil engineering, automotive field to aviation and aerospace industry. (GRELLMANN, *et al.*, 2015) In almost all of its applications, properties as strength, stiffness and toughness are essential requirements. The results of local stress and inconvenient defects can be very expressive. Attention must be given to assessing the influence of structure (crosslink density, chemical composition, etc.) as well as the application conditions (temperature, load, etc.) on the basic fracture properties of epoxy resins. (GRELLMANN, *et al.*, 2015; ELLIS, 1993)

Theoretical observations have shown that the stress to cause cleavage fracture in a brittle solid should be approximately 10% of Young's modulus of the material. Griffith (1920) who identified the significant influence of small defects on the load-bearing properties of a brittle isotropic material. In modern-days, linear elastic fracture mechanics is based on two interrelated conditions for fracture, the energy analysis (G approach) and localized stress field approach (K approach) at plain strain conditions. The former supposes that fracture will occur when sufficient energy is released by crack growth to supply the requirement for the creation of new fracture surfaces. Linear elastic fracture mechanics is applied to materials which obey

Hooke's law, where the measured strain is proportional to the applied stress. Although all epoxies exhibit some inelastic deformation around the crack tip, the fact that the bulk of the remaining material behaves elastically permits the successful application of this analysis. (ELLIS, 1993; GRELLMANN, *et al.*, 2015)

Using an energy balance argument to a linearly elastic cracked body of thickness B under an applied load, it makes possible to determine the critical strain energy release rate G_C for fracture to occur.

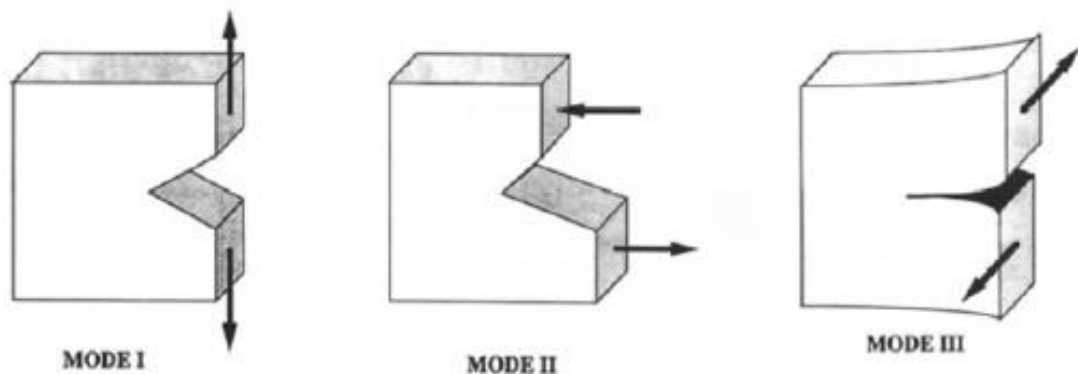
$$G_C = \frac{P_C^2}{2B} \frac{\partial C}{\partial a} \quad (2)$$

where C is the compliance of the cracked specimen for a given crack length a and P_C being the critical load for the onset of crack propagation. Equation 3 represents the basis for most G_C calculations with the fundamentals requirements being a knowledge of the variation of specimen compliance with crack length. It is crucial to note that are different kind of loading found in operational service (modes I, II and III), shown in Figure 9. (ELLIS, 1993)

$$G_{IC} = \frac{U}{BD\phi} \quad (3)$$

where U is the energy under the load-displacement curve, B the specimen thickness, D the specimen height and ϕ a calibration factor taking account of the specimen geometry and crack length.

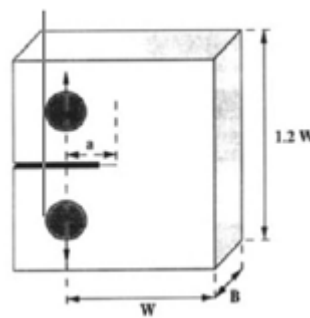
Figure 9 – Modes of loading: Mode I opening mode, mode II in-plane shear, and mode III anti-plane shear



Source: Ellis, 1993

The fracture energies associated with I, II and III modes of deformation are denoted G_{Ic} , G_{IIc} and G_{IIIc} , respectively. Between these three models, Mode I deformation is technically the most used of the three since it represents the most commonly found loading condition and generally has the lowest associated fracture energy. Mode I-type loading is also much more readily simulated in laboratory conditions. Figure 10 brings the more common specimen used for test the I-type load. (GRELLMANN, *et al.*, 2015; ELLIS, 1993)

Figure 10 – Typical test geometry for characterizing epoxy toughness by compact tension test



Source: Ellis, 1993

In choosing the precise dimensions for the selected specimen geometries, a range of size criteria have to be first respected. It is believed that the most important of these concerns is the specimen thickness B . Such a thickness dependency relates to the state of stress at the crack tip. This can vary from plane stress conditions in a thin plate to plane strain conditions in a much thicker specimen. Since the stress at which a material yields is greater in a plane strain field than in a plane stress field, a smaller plastic zone size is observed under plane strain conditions. The effect of this smaller plastic zone is to reduce the measured toughness of the specimen. Afterwards, the equation was adapted to the strain energy analysis for the specimen as it is described in Equation 3. (ELLIS, 1993)

The other frequently used approach for analyzing fracture resistance for the epoxy material is the critical stress intensity factor (K_I). In this method, the stress field around a sharp crack in a linear elastic material is defined by a stress intensity factor. The general form of K_I will be given by:

$$K_I = Y\sigma \sqrt{a} \quad (4)$$

where Y represents a geometrical factor (specimen high, width, among others), a as the crack length and σ is the applied nominal stress. Afterwards, is assumed that fracture will occur when the K_I value reaches a critical value termed K_{IC} , a material property for a given test condition. Considering a finite plate, K_{IC} is given by:

$$K_{IC} = Y\sigma_c \sqrt{a} \quad (5)$$

where σ_c will be now the applied stress at the onset of fracture. (ELLIS, B., 1993)

The presence of localized shear-yielding in areas of high-stress concentration is therefore beneficial, once it will result in crack tip blunting, a local re-distribution in the stress field, and an increase in the measured fracture toughness. As would be conventional, the strain immediate to the crack tip is significant. It is interesting to note, however, that the maximum value of strain is approximately 15%, whereas the elongation at break of this resin when measured in a standard tensile test is typically only 1.5%. This significant difference almost certainly relates to the presence of small defects or local variations in the network density, which are clearly going to be more numerous in a larger volume. (GRELLMANN, 2015)

3.4.1. Modes of crack propagation

The mechanisms of inelastic deformation will take place at the tip of a sharp crack in an epoxy resin, and therefore, will have a significant effect upon how this crack will subsequently propagate. Extensive testing of several pure and rubber-modified epoxies was highlighted with three modes of crack propagation, (ELLIS, 1993) being these:

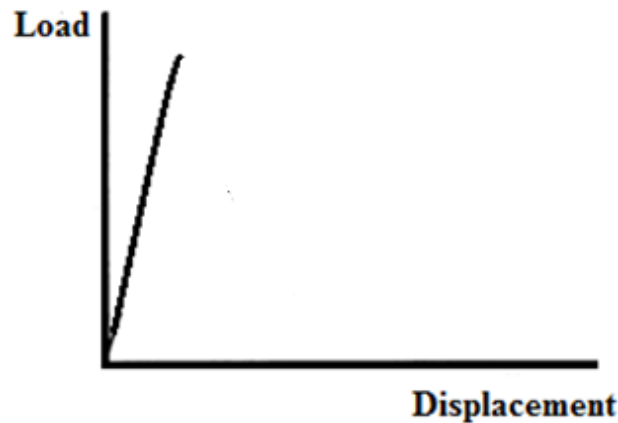
- Unstable brittle propagation
- Stable brittle propagation
- Stable ductile propagation.

Unstable brittle propagation

This kind of propagation results in a flat, featureless fracture surface. Basically a smooth continuous double-torsion load displacement curve (Figure 11). This behavior is understood to be common in brittle fracture. Some literature has already shown that this failure mode can be successfully characterized by a unique value of crack tip opening

displacement. These materials usually present a very low K_{IC} value, and almost no displacement, once the first crack propagates really fast through the whole material. (ELLIS, 1993)

Figure 11 – Schematic representations of unstable crack propagation in a load-displacement relation



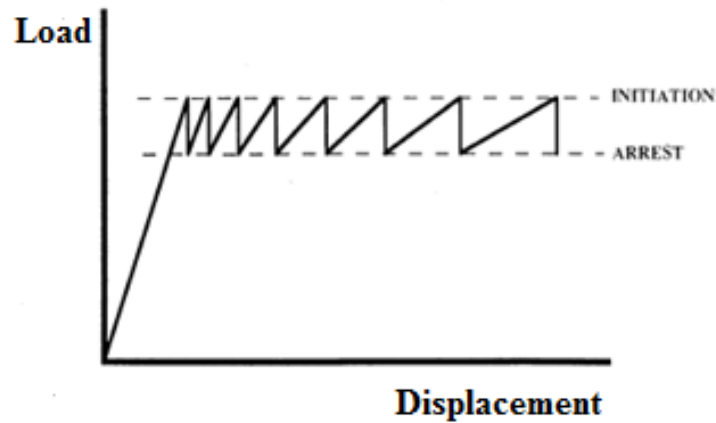
Source: Adapted from Ellis, 19983

Stable brittle propagation

This crack advancing behavior is defined by a jump-like shape, often referred to as stick-slip behavior as shown in Figure 12. The transitions at which crack propagation changes from stable brittle to unstable brittle (or from unstable brittle to stable ductile) will depend upon several conditions of both material and test parameters. (ELLIS, 1993)

Several researchers have identified the fundamental role of plastic flow, and subsequent crack-tip blunting around stress concentrations in epoxy resins. Localized plastic deformation is clearly a fundamental mechanism in this respect, and many of the observations presented in the literature have been explained, at least quantitatively in terms of this plastic flow process. In general, stable brittle failure occurs at lower temperatures and higher rates of loading. Under these conditions, the material modulus is likely to be high and the extent of plastic flow and therefore crack blunting low. By increasing temperature and decreasing load rate, the material failure will tend to appear in the stick-slip manner combined with the unstable brittle propagation. Here, the yield stress of the material is lower and greater plastic deformation can appear at the crack tip. When the crack finally does re-sharpen, the release of energy is significantly greater than that required to create a fracture surface and the crack accelerates, sometimes up to several hundreds of meters per second, and may eventually bifurcate. (ELLIS, 1993) Figure 12 shows an illustration of this kind of propagation.

Figure 12 - Schematic representations of stable brittle crack propagation in a load-displacement relation



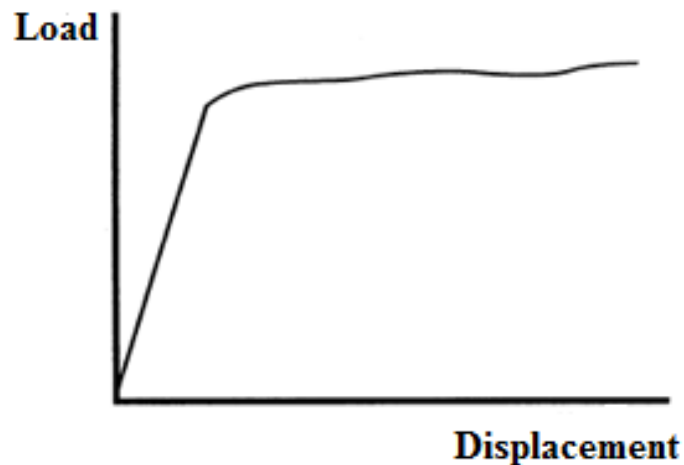
Source: Adapted from Ellis, 1993

Stable ductile propagation

This failure model will usually be yielded by a smooth load displacement, under stable brittle conditions as shown in Figure 13. This failure kind will be led by high energy dissipation, relatively rough fracture and also, high toughness.

Testing over high temperatures and very low strain rates lead cracks to frequently advance through a tearing process, in which much energy is absorbed, deforming plastically the material and creating multiple finger-like markings. The original model considers the advance of a meniscus between a less-dense and a more-dense fluid. (ELLIS, 1993)

Figure 13 - Schematic representations of stable ductile propagation in a load-displacement relation



Source: Adapted from Ellis, 1993

3.4.2. Microstructural Effects

The fundamental physical properties regarding an epoxy resin will be determined by the nature of its network density. Eventually, the molecular architecture of epoxy resins will directly influence the ability to carry the load by how the energy is absorbed. (ELLIS, 1993)

Generally, the network density influences the glass transition temperature of the polymer, its ability to undergo localized plastic deformation is responsible for toughness characteristics at a given temperature. Epoxies that have high crosslink densities tend to have high T_g s but are frequently prone to brittle failure. A low crosslink density therefore, will lead to a less rigid network structure that is capable of undergoing greater amounts of plastic deformation, which in turn may result in higher fracture toughness. Further researches established a direct relationship between the square root of the average molecular mass of the network strands and the fracture energy for crack arrest (KINLOCH, 2010). These results also indicated that K_{IC} at initiation improved with an increasing molecular mass of strands. Similar observations following fracture mechanics tests on a DGEBA-DDS epoxy were identified. A 100% increase in fracture toughness was reported over a range of molecular weights from approximately 300 to 3800 g/mole. (LEVITA, *et al.*, 1991,) The experimental results also suggested a linear dependence over this range of molecular weights. The calculated crack tip opening displacement can be related to the effective molecular mass between crosslinks. And also that the deformation zone length and width at the crack tip are directly proportional to the molecular mass of the network strands. (MIRACLE, 2001; KINLOCH, 2010; PALUVAI, *et al.*, 2014)

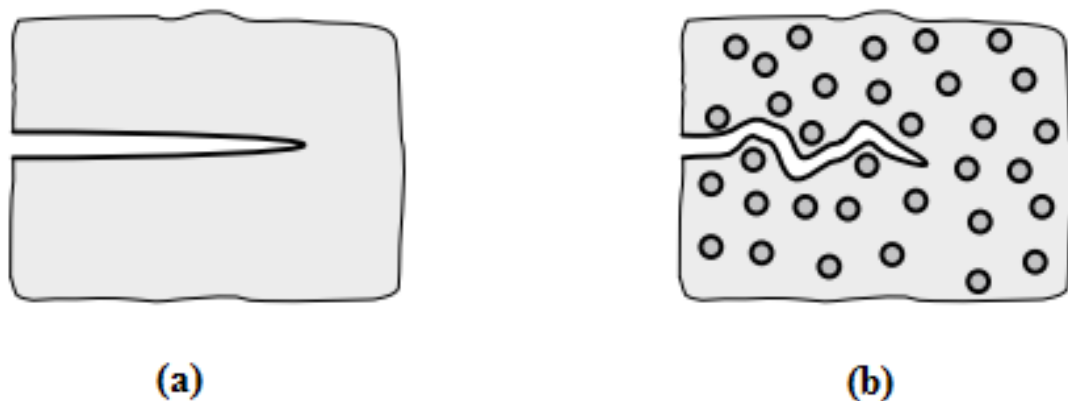
3.5. Toughness Modifiers

Many of the epoxy resin applications are often limited by their relatively brittle property and susceptibility to failure. Therefore, many investigations have been conducted during the years in an attempt to provide methods which would allow significant improvements in toughness, maintaining the important epoxy resins properties (UTALOFF, *et al.*, 2018). As far as this, the most successful method described by the state of the art is known as the toughness modifiers (rubber-based, block copolymers, fillers, among others).

Various investigations have shown that the addition of fillers in the epoxy matrix increases the toughness of various epoxy formulations, maintaining the epoxy resin properties. Possibly the greater development here is that this can be achieved with an improvement in modulus, although rubber modification usually provides a more efficient

means of toughness performance. For these modifiers, variables like particle size, particle size distribution, modifiers concentration, surface chemistry have been studied by several researches, which have indicated the most important variables necessary for optimizing toughness performance (TAMUTA, 2014; HUANGM and KINLOCH, 1992). They proposed to explain the toughness improvements through a mechanism based upon the concept of “crack pinning”, as shown in Figure 14.

Figure 14 – (a) Crack behavior without the presence of particles, (b) Crack pinning mechanism as toughening with the use of particles



Source: Adapted from Grellmann, *et al.*, 2015

The explanation behind this theory is quite simple, involving the idea that a propagating crack front, when encountering an inhomogeneity, becomes temporarily pinned at that point, thus, increasing the amount of energy needed to propagate this crack. A rise in load increases the degree of bowing between pinning points resulting in both new fracture surface and gaining length of the crack front. As these effects become more common and more intensive, the energy absorption increases as well, leading improvement in toughness. (GRELLMANN, *et al.*, 2015; TAMUTA, 2014)

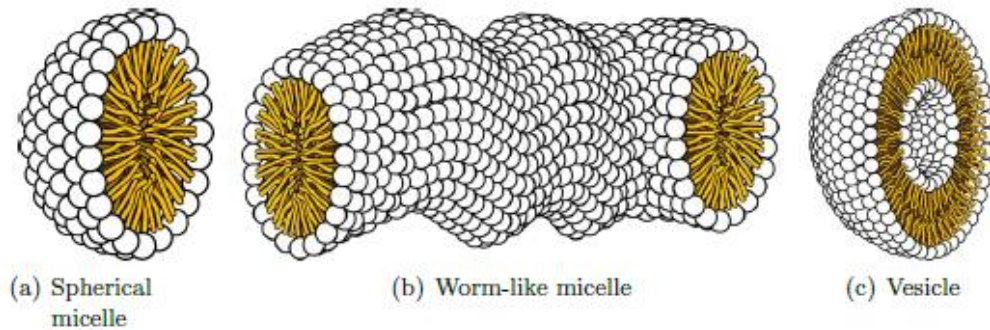
3.5.1. Polysiloxane-Based Core-Shell Particles

These modifiers are among the most important tougheners types due to their excellent properties of miscibility and low viscosity combined with the toughening itself. Besides unreactive rubbers, there are reactive ones which are able to react with the epoxy resin during the curing process. The formation of chemical bonds will lead to a greater interaction between the epoxy matrix and the toughener particles. Moreover their widespread applications as toughener, rubbers can suffer from several disadvantages, like the dependence on the phase separation on the curing cycle, lowering the network density and therefore the T_g , later on, a deterioration of the thermal properties. (UTALOFF, *et al.*, 2018; RATNA, *et al.*, 2004; BAIN, *et al.*, 2017) As it is shown in several reports, (CHEN, *et al.*, 2013; BAIN, *et al.* 2017; UTALOFF, *et al.*, 2018), these modifiers bring a strong increase of the K_{IC} associated with a small drop of the T_g in most of the cases. In Utaloff's *et al.* (2018) report, using isophorone diamine (IPDA) curing agent (relatively high crosslink density polymer), the addition of nanosized polysiloxane-based core-shell particles in a volume fraction of 5% was able to increase the toughness resistance in 35% from 0.72 MPa m^{1/2} to 1.00 MPa m^{1/2}, with a relatively low decrease in the T_g . Chen, *et al.* (2013) by the other hand, using a relatively low crosslink density epoxy resin (epoxy resin cured with polyetheramine), was able to show a 200% increase in the fracture resistance, with also a relatively low decrease in the T_g , also with a 5% volume fraction of microsized modifier. Among others, this dependency was found to be valid for the dendritic polymers. Other works where the increase of K_{IC} came associated with no change of the T_g at all, can be found in literature (FRIEDRICH, 1993). The general conclusion from these papers are related to the interaction of the rubber-based modifier and the epoxy matrix. The interaction between the particle and the epoxy matrix can afterwards, influence in the resin curing rate, degradation, among many others properties. (CHEN, *et al.*, 2013)

These rubbery modifiers are defined as copolymer, comprise of two different monomers species covalently bonded together through copolymerization. There will be several possible combinations of these block copolymers, that will later on define the material properties. (CHONG, 2015) These molecules have an epoxy-miscible block and an epoxy-immiscible block, which allows microphase separation at the length scale of the polymer chains (~ 10 nm) due to the thermodynamic immiscibility of the blocks. The epoxy-miscible block will aggregate to form the outside of the micelle in contact with the epoxy, like a shell, to shield

the epoxy-immiscible block in the center as the core. Figure 15 illustrates the aggregated core-shell particles. (CHONG, 2015)

Figure 15 – Possible self-assembly micellar structures for core-shell particles



Source: Chong, 2015

The Literature suggest that the effect of these complex particles morphology on the fracture performance of epoxies is still relatively unknown (CHONG, 2015).

3.5.2. Particle Size Effects

The modifiers particle size will play a fundamental roll in the material performance, defined as a parameter that influences both the fracture toughness and the operative toughening mechanisms in rubber-modified epoxy polymers (HAMERTON, 1997). The most recent findings for rubber-modified epoxy polymers suggest the use of an optimal particle size in the range from 0.1 to 5 μm (PALUVAI, *et al.*, 2014; PEARSON and YEE, 1991). Recent studies used an argument of particle-plastic zone interaction to explain the effect of particle size on the toughness of rubber-modified epoxies. These investigations demand that particles smaller than the size of the plastic zone of the neat epoxy are more efficient toughening agents. This happens because these particles are able to interact with the crack-tip plastic zone and, therefore, cavity and promote shear yielding mechanism. It has been also proved that particles larger than the size of the plastic zone of neat epoxy do not enhance the shear yielding in the matrix at the crack tip, but simply bridge the two crack surfaces. (HAMERTON, 1997; PEARSON and YEE, 1991)

It is believed that larger particle size will deform the organization of the chains with more magnitude, what can later on, bring a decrease in the material T_g , strength modulus, among others. This will naturally, be directly coupled with the epoxy network density and structure. (PEARSON and YEE, 1991)

3.5.3. Volume Content Effects

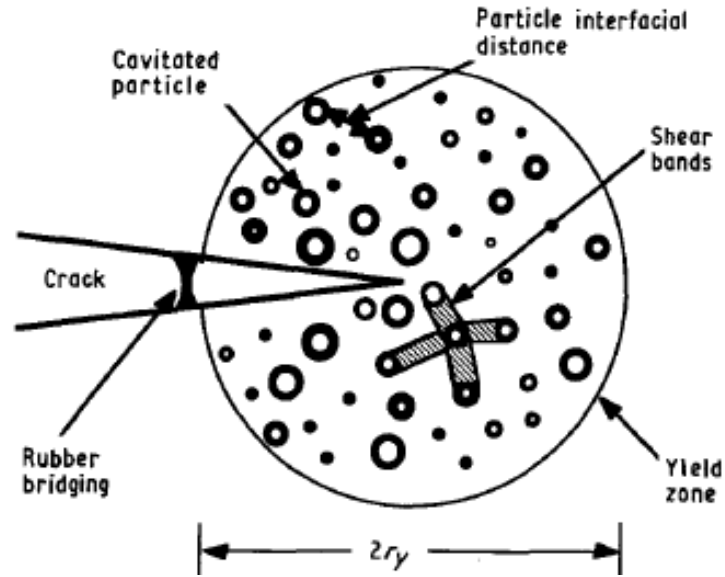
In several previous reports (PEARSON and YEE, 1991; BAIN, *et al.*, 2017) the importance of rubber volume fraction content in the particle-plastic zone has been registered. The most important fact to be noticed in a volume fraction dependent toughness modifier will be the interparticle distance, and also its distribution in the plastic zone. Most of the reports related to the addition of rubber modifiers in epoxy matrix have shown that the rise in the modifiers volume fraction will increase the material toughness, but decrease others properties (like T_g , strength modulus, etc.). It is also reported that too high volume fraction can cause a decrease in the toughening mechanism (above 15% for example). All these details will be once more related to the epoxy resin, the curing agent and the modifier. The combination of network density, chains structure, particle size, particles distribution, among many others, will directly correlate in the volume fraction optimization concerning to these rubber-modifiers. (PEARSON and YEE, 1991; BAIN, *et al.*, 2017; UTALOFF, *et al.*, 2018)

It is also well described by literature that the addition of particles can reduce the tensile strength of thermoset polymers. Giannakopoulos *et al.* (2010) measured that the addition of the rubber-based core-shell particles did indeed reduce the tensile strength, and this reduction was approximately linear with increasing particle content.

3.5.4. Math Modeling of Toughening

Along the years, several models have been proposed to correlate the microstructure and fracture properties of epoxy polymers toughened by the addition of rubbery modifiers. Kunz-Douglass *et al.* (1980) developed a model where the energy dissipation during the deformation is correlated with the bridging of the crack surfaces by these rubbery particles. Although further literature already bring addition of much more complex mechanisms, it is evident that a satisfactory model will require various energy dissipation mechanism models, which later on will correlate the respective contribution to the increase in the fracture energy of these materials. (KUNZ-DOUGLASS, *et al.*, 1980) The latest reports about modeling the fracture toughness of rubber-toughened epoxies have shown that there are three main mechanisms contributing to the overall increase in the fracture energy: Localized shear banding, plastic void growth, and rubber-bridging mechanism. These and others aspects are illustrated in Figure 16.

Figure 16 – A schematic representation of the different toughening mechanism involved in the fracture



Source: Huang and Kinloch, 1992

Here, the $2r_y$ are the diameter of the plastic (or process) zone. The typical equation found in literature for the fracture energy of this system is established as

$$G_{Ic} = G_{IcU} + \Psi \quad (6)$$

where G_{IcU} represents the fracture energy of untoughened epoxy, and Ψ represents the overall three toughening contributions, described as

$$\Psi = \Delta G_s + \Delta G_V + \Delta G_r \quad (7)$$

The ΔG_r describes the rubber-bridging model. (KUNZ-DOUGLASS, *et al.*, 1980) The localized shear banding (ΔG_s) and the plastic void growth (ΔG_V) are related to the size of the plastic zone, as it is arranged in the Huang and Kinloch (1992) report, and can be calculated from the following equation

$$\Delta G_s \text{ or } \Delta G_V = 2 \int_0^{r_y} U(r) dr \quad (8)$$

Afterwards, the plastic zone size has to be estimated through linear elastic fracture mechanism concepts, combined with yield stress. (HUANG and KINLOCH, 1992)

4. Materials and Methods

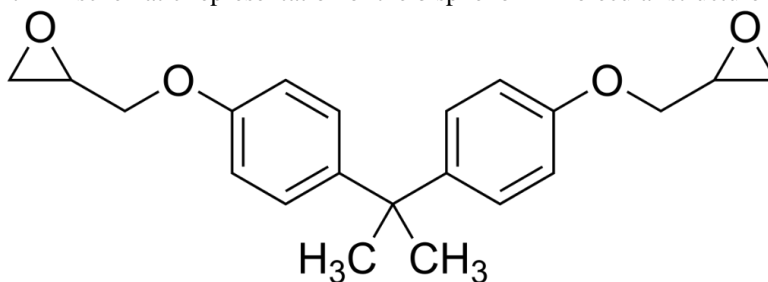
4.1. Materials

This chapter describes the formulations of the epoxy resin, curing agent and additives that were used. One unique epoxy resin system based on (bisphenol-A) was used, combined with two different curing agents. One of these curing agents was indicated to formulate a low network density system (polyetheramine). The second curing agents was indicated to produce high network density systems (norbornene methyl anhydride). It was incorporated two different types of PCS particles. The microsized particles were handed as preformed masterbatch, while the nanosized particles were incorporated as block copolymer, and assembled as core-shell particles during the curing process.

4.1.1. Epoxy Resin

The base epoxy resin for this system was a standard diglycidylether of bisphenol-A (DGEBA) with an epoxide equivalent weight of 182 - 192 g/eq, commercialized as D.E.R.TM 331 Epoxy Resin from company Olin Corporation (Stade, Germany). The DGEBA molecular structure can be seen in Figure 17.

Figure 17 – A schematic representation of the bisphenol-A molecular structure



Source: Adapted from Dekker, 1998.

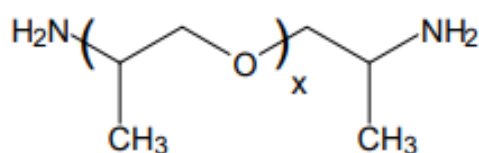
The uncured resin D.E.R.TM 331 is a low viscous (11000 - 14000 mPa.s at 25°C) transparent material. Is the most widely used liquid epoxy resin for general purpose. It is recognized as the standard industrial grade from which material formulations have been developed.

4.1.2. Curing Agent

Polyetheramine (PEA)

Polyetheramine is a low T_g curing agent characterized by repeating oxypropylene units in the backbone. As shown by the representative structure (Figure 18, where $x = 2.5$), polyetheramine is a tetrafunctional, primary diamine with an average molecular weight of about 230 g/mol. The primary amine groups are located on secondary carbon atoms at the end of the aliphatic polyether chain.

Figure 18 – Illustrative molecular structure of polyetheramine



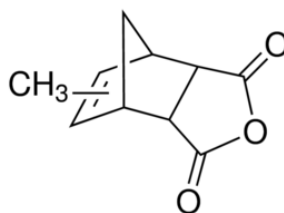
Source: Huntsman® official website, 2019

The curing agent utilized is produced by the Huntsman®, commercialized with the name Jeffamine D230. The molecule has an amine equivalent weight of 60 g/eq, and a functionality of four. The curing temperature when formulated with DGEBA is approximately 90°C. As an outcome, the DGEBA-D230 (DGEBA-PEA) resin system should result in a low network density system, with glass transition temperature around 90°C.

Norbornene Methyl Anhydride (NMA)

Norbornene Methyl Anhydride, known as NMA, is a yellow to colorless liquid, with molecular weight of 178 g/mol, and its hydrogen equivalent weight is estimated as 170 g/eq. It is supplied by the Huntsman®, commercialized with the name of Aradur HY 906. Figure 19 illustrates the chemical structure of this molecule.

Figure 19 – Illustrative molecular structure of NMA



Source: Huntsman® official website, 2019

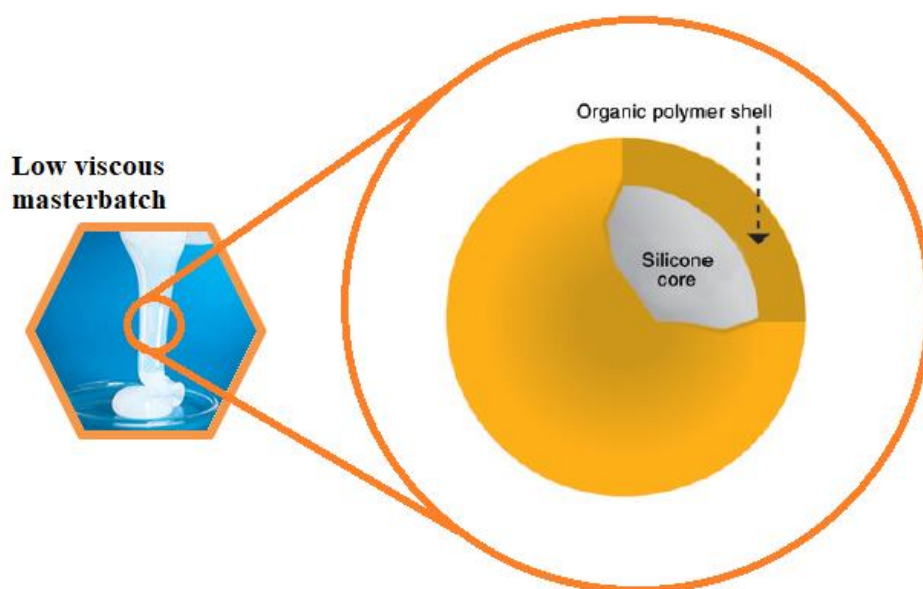
The molecule is composed of two reactive groups. The system DGEBA-NMA performs a high network density structure, with glass transition temperature from 170 to 200°C, according to the curing cycle, which temperature is given around 200°C. The curing of this material is relatively slow, which is generally followed by a catalyst substance. This catalyst substance is a useful synthetic intermediate, which can be used as a building block for active ingredients as well as in epoxy curing. The catalyst substance used for DGEBA-NMA formulation was 2-Ethyl4-Methylimidazole, commercially known as 2E4MZ, supplied by TCI Chemicals.

4.1.3. Toughness Modifier

Microsized particles

The polysiloxane core-shell microsized particles were utilized by a masterbatch of DGEBA epoxy resin with 40% of presynthesized core-shell particles (0.3 – 0.5 μm) finely distributed. The particles are composed by an elastomeric polysiloxane core with a Polymethyl methacrylate (PMMA) organic shell structure, which is compatible in polarity to the epoxy resin. The siloxane rubber domains are already preformed and not built during the curing process. The material used was supplied by Evonik®, commercialized by the name Albidur EP 2240 A. Figure 20 presents the masterbatch physical form, and an illustration of the particles structure.

Figure 20 – Physical form of the low viscous masterbatch and the illustration of the PCS particles preformed

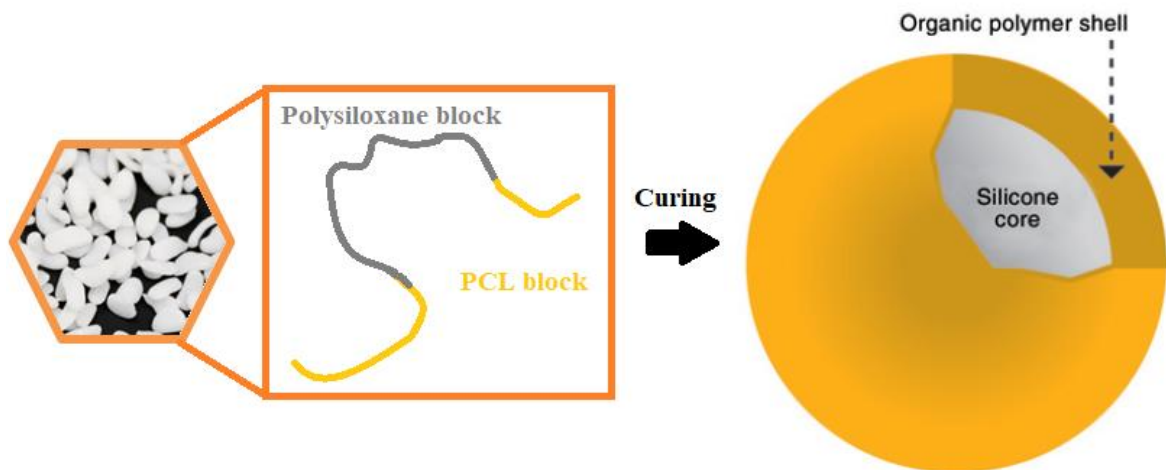


Source: Adapted from Ebenoch, 2004

Nanosized particles

The nanosized polysiloxane-polycaprolactone (polysiloxane-PCL) copolymer is provided as a solid flake structure, as a block copolymer type (A-B-A). When dissolved in an epoxy resin system, the nanosized chains perform a self-assembling mechanism during curing process, forming particles less than 100 nm diameter. This core-shell particle is provided by Wacker®, commercialized as GENIOPERL W36. Figure 21 presents the toughener physical form, the polysiloxane-PCL chains illustration, and the system self-assembled as a core-shell particle.

Figure 21 – Physical form of the toughener, followed by its copolymer structure, and its final form as self-assembled core-shell nanoparticle after curing



Source: Adapted from Ebenoch, 2004

4.2. Methods

This chapter outlines the various test methods and procedures that were utilized to characterize the material properties and microstructure. Also, the sample preparation procedures and standards associated to the given characterization.

4.2.1 Material Formulation and Testing

The formulation was designed based on the epoxy equivalent weight stoichiometric with the curing agent and particle system used. For epoxy resin, the equivalent weight (*EEW*) is a ratio of the molecular weight to its number of epoxy groups, given by

$$EEW = \frac{\text{Epoxy monomer molecular weight}}{\text{Number of epoxy groups in molecule}} \quad (9)$$

The curing agent equivalent weight (*AEW*) follows the same idea, but in function of its reactive groups, given by

$$AEW = \frac{\text{Curing agent monomer molecular weight}}{\text{Number of hydrogen groups from amine in molecule}} \quad (10)$$

To maintain stoichiometric equivalency (proper crosslinking), the number of moles of epoxy should be the same as the number of moles of curing agent is related as

$$\frac{EEW}{AEW} = \frac{We}{Wca} \quad (11)$$

Where *We* is the epoxy final weight, and *Wca* is the curing agent final weight. The final formulation weight for the system (epoxy-curing agent-particle-additives), will be given by the some of their fraction, always maintaining the ratio of epoxy resin and curing agent stablish by Equation 12.

$$FW = EW + CAW + PW + AW \quad (12)$$

Where *FW* is the total weight of the system, *EW* is the epoxy weight (notice that the epoxy resin weight contained on the masterbatch additive has to be included in this weight), *CAW* is the curing agent weight, *PW* is the particles weight, and *AW* will be the weight of any other additive (accelerator, for example).

Table 1 gives all the weight relations given by wt. % used for formulating the plates, as it is described on Equation 12. *FW* was always stablish as 140 g, once it is the standard weight of resin system necessary for a single material plate.

The formulation of all material-systems followed specifics methodology, given the nature of its composition. First, the DGEBA resin was mixed with the particles systems, disposed the specific concentration of it. In order to find perfect miscibility by dissolving the particles, these systems were settled on the oven, over 60°C. When the miscibility was found enough (around 1h), they were mixed by a Speedmixer DCA 150.1 FVZ (Figure 22), during 1

min, in a 200 rpm speed rotation. Evidently, for no particle system (0 wt. %), no particle compound was added, which led to skip this stage. Afterwards, the curing agents were added in their respective formulation. For the high network density system (DGEBA-NMA), the addition of accelerator was prescribed, and followed the addition of NMA. The mixing was then given once more by the speed-mixer, with the same mixing parameters.

Table 1 – Description of each material weight for the final material system, following the balance establish from the equations 9, 10, 11 and 12

Material Description			Weight Formulation					
Particle Parameter		Network Density System	Epoxy Resin	Curing Agents		Particles		Additives
Content (wt. %)	Size		DGEBA (g)	PEA (g)	NMA (g)	Albidur (g)	W36 (g)	2E4MZ (g)
0	--	Low	113.56	36.43	--	--	--	--
1	Micro	Low	105.29	33.31	--	3.50	--	--
3	Micro	Low	103.90	31.90	--	10.50	--	--
5	Micro	Low	102.55	30.40	--	17.50	--	--
1	Nano	Low	112.26	36.24	--	--	1.40	--
3	Nano	Low	109.66	35.84	--	--	4.20	--
5	Nano	Low	107.07	35.43	--	--	7.00	--
0	--	High	75.67	--	64.32	--	--	1.40
1	Micro	High	72.06	--	63.04	3.50	--	1.40
3	Micro	High	66.35	--	61.75	10.50	--	1.40
5	Micro	High	60.63	--	60.46	17.50	--	1.40
1	Nano	High	74.16	--	63.04	--	1.40	1.40
3	Nano	High	72.64	--	61.75	--	4.20	1.40
5	Nano	High	71.13	--	60.46	--	7.00	1.40

Source: From the author himself, 2019

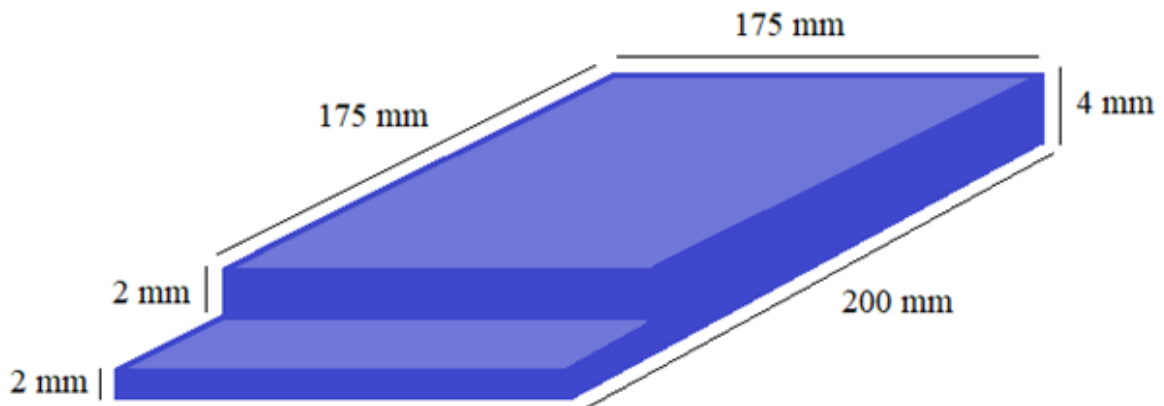
Figure 22 – Speedmixer DCA 150.1 FVZ



Source: Polymer Engineering Department – Universität Bayreuth official website, 2019

After mixing, the material was degassed, by inserting it in a low-pressure chamber. The degassing duration was 10 min for DGEBA-PEA system, and 30 min for DGEBA-NMA system. Once the systems was free of bubble airs controlled by eye, they were poured into the plate-molds. The plate-mold is a standard recipient for the liquid resin, with a specific cavity, resulting in the poured material shaped as this cavity. The cavity followed a specific geometry, resulting (varying not more than 0.5 mm dimensions from one mold to another), in a shape as is illustrated by Figure 23.

Figure 23 – Dimensions and geometry of mold cavity, consequently epoxy resin system dimensions and geometry resulting after curing



Source: From the author himself, 2019

With the liquid resin system already inside, the mold has been placed into the oven, where the followed material curing cycle was applied. Table 2 present the utilized curing cycle for each of the two systems, and Figure 22 the oven utilized for curing the materials, in consistency with the material's datasheet.

Table 2 – Curing cycle settled for DGEBA-D230 (left) and DGEBA-NMA (right) systems

DGEBA-PEA system			DGEBA-NMA system		
	Temperature (°C)	Duration (min)		Temperature (°C)	Duration (min)
Step 1	60	30	Step 1	100	120
Step 2	90	240	Step 2	160	120
Step 3	--	--	Step 3	200	60

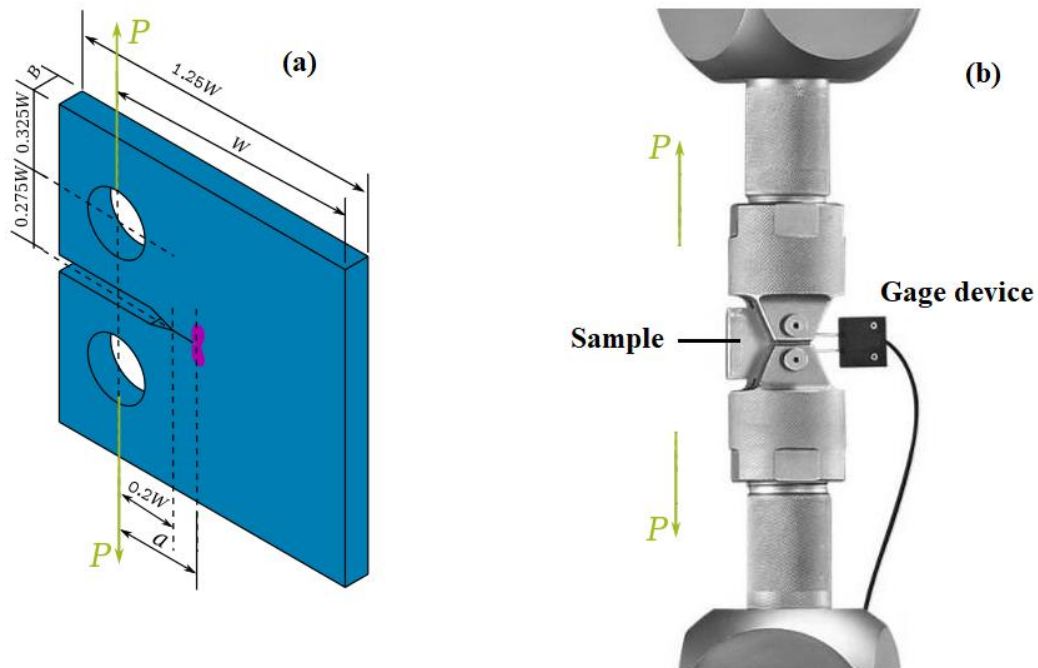
Source: From the author himself, 2019

4.2.1.1. Fracture Toughness Testing (K_{IC})

The fracture test is carried out in displacement control at a constant rate of increase of stress intensity while recording load and crack opening displacement data, until the specimen breaks. Following the common methods, a gage device is needed to measure the crack opening displacement. After the specimen fails, the fatigue pre-crack and any crack extension are measured accurately at intervals along the crack front and then recorded.

For polymeric materials, the common standard used is ISO 13586. The specimen geometry and dimensions are shown in Figure 24a, while the test procedure is shown in Figure 24b, following the ISO 13586.

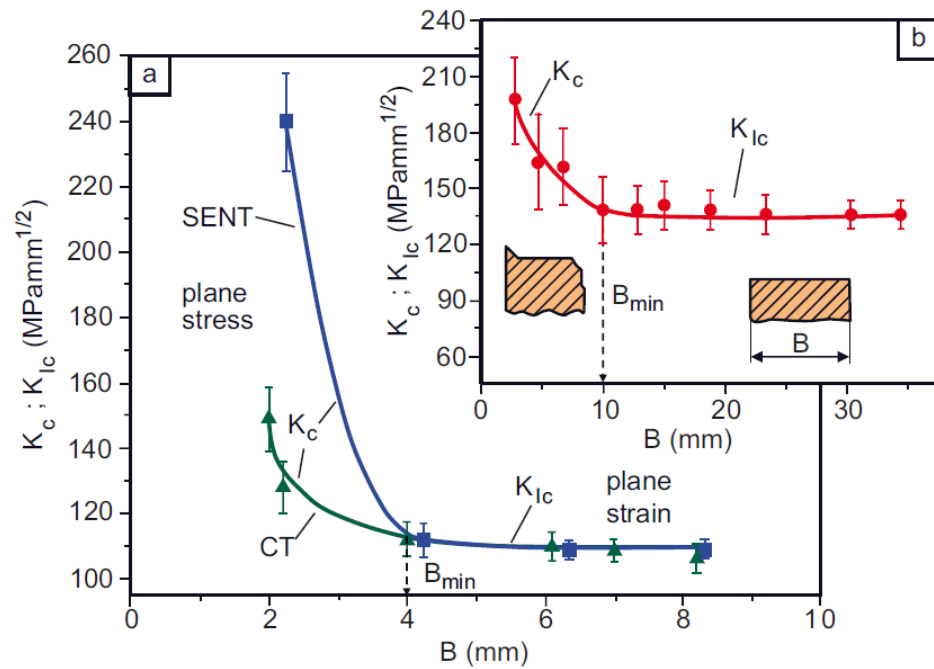
Figure 24 – (a) Specimen geometry and dimensions associated with ISO 13586 as a function of the size W , (b) schematic illustration of K_{IC} testing on the universal testing machine



Source: (a) Bower, 2009, (b) Adapted from Bower, 2009

For the fracture toughness measurements, the test specimen were cut out from the initial plate (Figure 23), following the dimensions of ISO 13586. The width B is defined by the plate thickness ($4 \text{ mm} \pm 0.5$), while W was defined as 33 mm. A complete explanation about the use of B as $4 \text{ mm} \pm 0.5$ can be found in Grellmann, *et al.* (2015), pages 252 – 254, where two polymers (relatively ductile and fragile behavior at break) were tested in several different thickness, and the 4 mm thickness presented to be the transition from plane stress to plane strain state, as follows the Figure 25.

Figure 25 – Dependency of fracture toughness K_C , K_{Ic} at room temperature on specimen thickness (a) under quasi-static load for PVC-C with $K_{Ic} = 110 \text{ MPa mm}^{1/2}$ and for PP with $K_{Ic} = 139 \text{ MPa mm}^{1/2}$ (b) at traverse speed $V_T = 8.3 \times 10^{-4} \text{ m s}^{-1}$

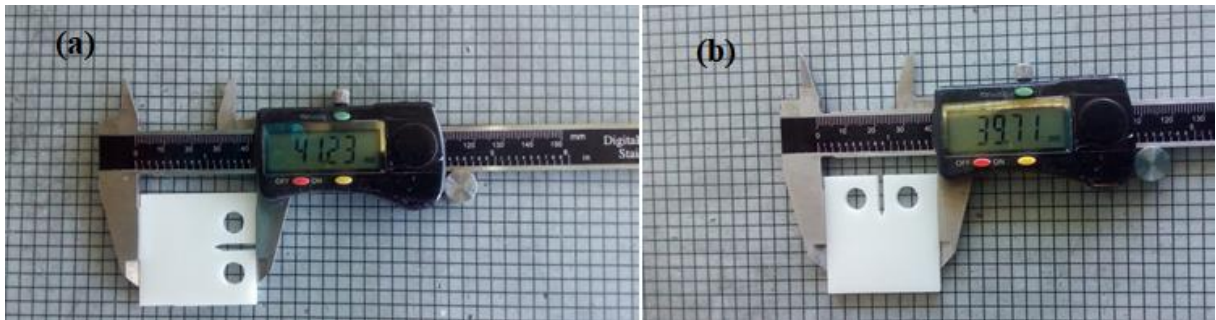


Source: Grellmann, *et al.*, 2015

This model is usually performed for situations where the Yield strength is unknown. Several reports like Utaloff *et al.* (2018); Chong (2015); Giannakopoulos *et al.* (2011); Wetzel *et al.* (2006) can present the same methodology.

The result from that is a $41.25 \pm 0.15 \text{ mm}$ length size ($1.25W$), and a $39.60 \pm 0.15 \text{ mm}$ height ($2 \times [0.275W + 0.325W]$). Afterwards, two holes were drilled in the sample, using a specific geometry mold. The notch was also made by a specific geometry mold, given a single cut through the mold cavity, following the dimensions illustrated in Figure 24a. Figure 26a and 26b show the sample geometry after the cutting stage.

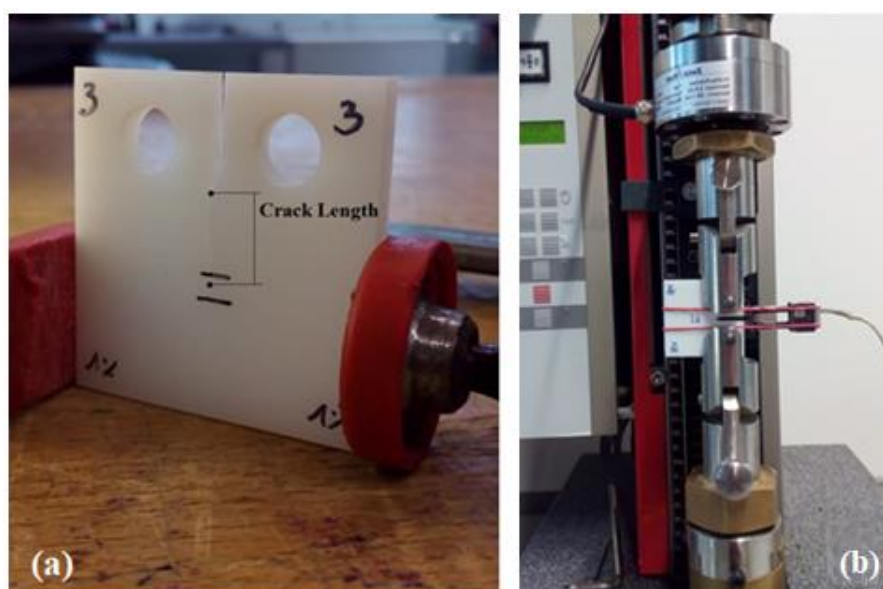
Figure 26 – Specimen geometry and dimensions following ISO 13586



Source: From the author himself, 2019

Afterwards, a sharp crack was generated using a sharp razor blade. The pre-crack length also followed the specifications of ISO 13586. The K_{IC} values were determined on a universal tensile testing machine (2.5 kN, Zwick, Germany) with a load cell of 500 N, according to the standard ISO 13586. The test was performed in a controlled environmental, guaranteeing temperature of 23°C during all process. Six specimens were tested for each set of data. Figure 27a presents a sample ready for testing after the pre-crack introduction, and Figure 27b shows the schematic practical measurement.

Figure 27 – (a) Specimen ready for K_{IC} testing, (b) schematic view of the practical testing



Source: From the author himself, 2019

4.2.1.2. Scanning Electron Microscope (SEM)

The micrographs images were recorded using a Zeiss Leo 1530 (Figure 28), in order to obtain high resolution pictures of the fracture surfaces. The samples were first cut shorter with a Struers Accutom- 5 precision cutter, equipped with a saw blade. The samples were then mounted on aluminum pin-stubs using conductive tape. To prevent charging, the cross-sections of resin samples were sputtered with Platinum using a Cressington Platin-Sputter Coater 208 HR. An accelerating voltage of 5 kV and a typical working distance of 6 to 8 mm was used.

One surface fracture of each resin system was analyzed through SEM. The surface was taken from the K_{IC} fractured samples. In order to have sufficient representability, the chosen surfaces were taken from the samples with K_{IC} value closest to the average.

Figure 28 – Scanning Electron Microscope Zeiss Leo 1530

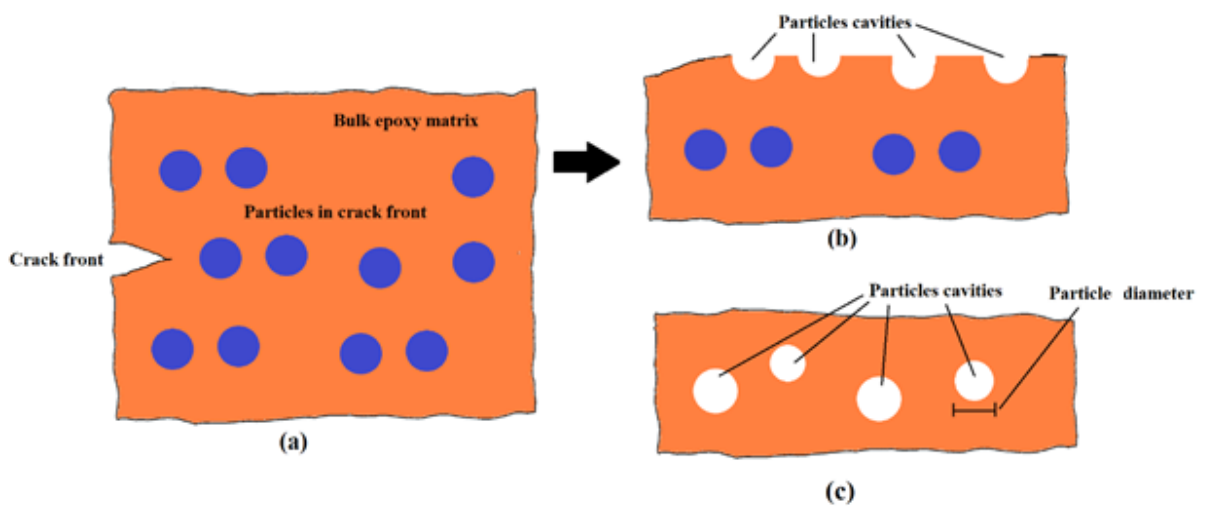


Source: Polymer Engineering Department – Universität Bayreuth official website, 2019

4.2.1.3. Particle Size and Distribution Evaluation

The particle size and size distribution of the particles could be determined from the SEM images. The SEM images were able to show clearly the particles cavities. The cavity represents the particle diameter, once it is related to the space where the particle was occupying before being pulled out. Figure 29 illustrates the process of cavity formation, and what is given in the SEM images.

Figure 29 – Schematic illustration of cavity formation on the bulk, (a) side view before the crack propagation, (b) side view after the crack propagation, (c) top view from surface fracture



Source: From the author himself, 2019

Using the software ImageJ®, it was possible to evaluate the diameter of these cavities, related to the real particles diameter. The software allows a counting tool where is possible to evaluate an average diameter of every single cavity, repeating the action until a desired amount of particles counted. From each cavity, two diameters are measured (vertical and horizontal), giving an average diameter for that specific cavity. The process was repeated for all the cavities in the picture. For each resin system, two pictures were analyzed, covering a range of 75 – 150 particles cavities counted.

4.2.1.4. Tensile Testing

For the sample preparation of this test it was used the DIN EN ISO 527-2 Type B, representing the specimen prepared through machining. A nominal width of 10 mm and thickness of 4 mm was defined by the standard. As the K_{IC} samples, the tensile samples were machined from the resin plate shown in Figure 30. The dimensions were defined as $l_0 = 50$ mm, $l_1 = 60$ mm, $l_2 = 110$ mm, $L = 115$ mm and $l_3 = 150$ mm. Figure 30 shows the practical machined sample.

Figure 30 – Tensile testing specimen machined following DIN EN ISO 527-2 Type B



Source: From the author himself, 2019

A gauge length of 25 mm and a test speed of 50 mm/min were used. The tests were performed with a Zwick Z1475 universal testing machine, as can be seen in Figure 31. To proceed with the test, every width and thickness were measured. The test was done in a controlled

environmental, guaranteeing temperature of 23°C during all process. Six samples were tested for each formulation.

Figure 31 – Universal testing machine Zwick Z1475



Source: From the author himself, 2019

4.2.1.5. Dynamic Mechanical Analysis (DMA)

Dynamic mechanical analysis (DMA) utilizes a system of clamps for mechanical testing of solid polymers materials, inside an oven, where load can be applied over the effect of temperature. Because it is applied a sinusoidal force, it is possible to express the modulus as an in-phase component, the storage modulus, and an out of phase component, the loss modulus, as it is described in standard D4065. The ratio of the loss to the storage is the $\tan \delta$ and is often called damping. It is a measure of the energy dissipation of a material. The storage modulus (E'), loss modulus (E'') and $\tan \delta$ can be calculated as a function of temperature, given by

$$\tan \delta = \frac{E''}{E'} \quad (13)$$

The T_g is then determined as the peak $\tan \delta$ value.

For DMA measurements, the standard used is ASTM D4065. The samples were cut from the plate produced, using a thin saw, obtaining rectangular shapes with sides 10×50 mm. with a fixed thickness of 2 mm. The specimen sides did not vary more than ± 0.5 mm. and the thickness did not vary more than ± 0.2 mm. It is possible to see an image of the sample ready to test in Figure 32.

Figure 32 - (a) Schematic structure of a DMA measurement. (b) General results of storage modulus in function of temperature



Source: From the author himself, 2019

The DMA was performed to obtain the T_g and the E' , using a Gabo Eplexor 500N DMA from TA Instruments (Figure 33). The test frequency was 1 Hz, the static load 1 %, and the dynamic load 0.5 %. The temperature range was specific to the network density system, changing the temperature at a heating rate of 3 K/min. For the D230 systems, the temperature range was from -150 °C to 120 °C, for the NMA systems, the temperature range was from -150 °C to 220 °C. For each material composition, two samples were measured.

Figure 33 – Gabo Eplexor 500N DMA machine utilized for DMA measuring



Source: Polymer Engineering Department – Universität Bayreuth. Official Website

4.2.1.6. Network Density Calculation

The crosslink density (ν_c) can be determined from the experimental data, using the rubbery modulus (E_R) from the viscoelastic curve and applying the theory of rubber elasticity. (NAKKA, 2010) According to that theory, the network density (ν_c) is defined as the number of moles of elastically effective network chains per unit volume of the sample

$$E_R = 3A\nu_cRT \quad (14)$$

where A is the front factor often assumed to be unity. R is the gas constant 8.314 J/mol/K. T is the absolute temperature in Kelvin and ν_c is the measure of the network density in mol/g. Removing the front factor A , the direct correlation between the network density and the rubber elasticity modulus is followed by Equation 15. (NAKKA, 2010)

$$\nu_c = \frac{E_R}{3RT} \quad (15)$$

Here, the E_R will be the value of storage modulus E' at the Rubbery Plateau region. Conventionally, this point was defined as the value E' at $T_g + 30$ °C.

Some others literature brings different approaches to calculate the system network density, like Flory-Rehner, Bellenger, Scalan model. Although these methods are more focused in a theoretical relationship, exploring the molecular structure and molecular weight.

In this work, the Equation 15 was utilized for determining the network density values of all resin systems. The E' and T_g values were measured by the DMA testing, being then applied to the equation. As it was measured two DMA samples, two values of network density were obtained for each resin system.

5. Results and discussion

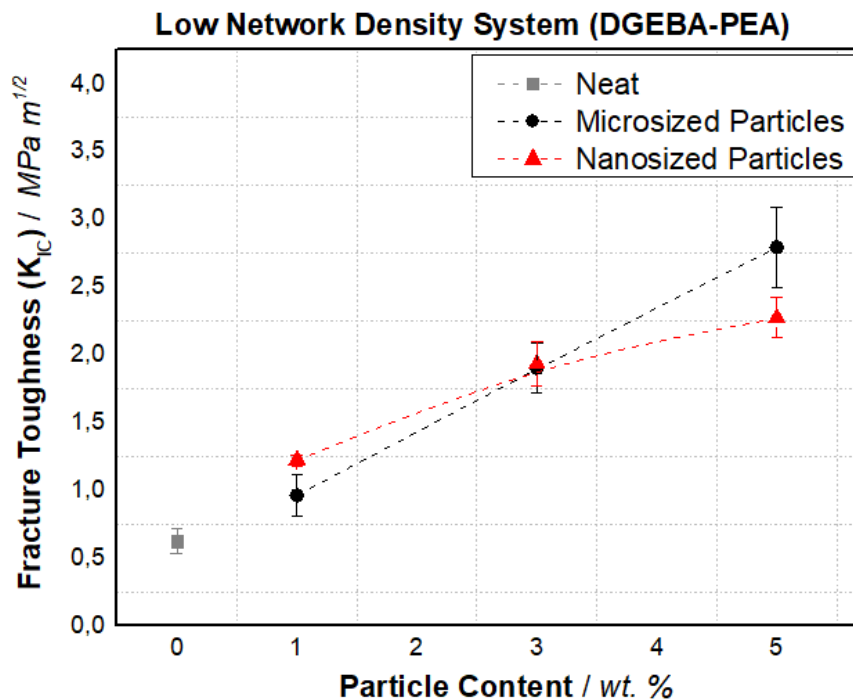
5.1. Mechanical Properties

Firstly, the fracture toughness of all epoxy resin systems was measured and analyzed, as a function related to the particle size and weight content. Supporting the fracture toughness measurements, the fracture toughness images obtained from SEM were also analyzed. Afterwards, the tensile properties systems with and without particles were also evaluated, in order to identify the material stiffness, mechanical resistance and elongation at break as a function of PCS particle addition. The tensile properties results also give support to the fracture toughness evaluation.

5.1.1. Fracture Toughness

Figure 34 represents the fracture toughness for the low network density system (DGEBA-PEA), as a function of particle content, for both microsized and nanosized particles addition. The K_{IC} value for the unmodified system was measured to be $0.62 \text{ MPa m}^{1/2}$, and increased almost 100% with the addition of 1 wt. % of particles. For 5 wt. % of particles, the values of microsized and nanosized achieved 2.79 and $2.27 \text{ MPa m}^{1/2}$ respectively.

Figure 34 – Fracture toughness for DGEBA-PEA-Particle systems as a function of particle size and content



Source: From the author himself, 2019

The addition of 1 wt. % of PCS particles has shown to be sufficient for toughening the epoxy low network density system. Nanosized particles have proven to be more efficient at the 1 wt. % content addition, while systems with microsized particles presented the highest fracture toughness value, much probably related to the lower mean free path among particles. It is believed that the lower distance between one particle with the other promotes more intensive toughening mechanisms. Even though, it can be safely considered that the particle size has no significant influence on fracture toughness improvement of low network density systems, once both proved great enhancement.

It is proven in literature (PEASON, 1991; KINLOCH, 2010) that after a limit content, the improvement rate starts to decrease as more particles are add. In this work, for the low network density system, both particle size systems showed 5 wt. % particle content to keep a positive rate of improvement on K_{IC} , indicating that a higher fracture toughness value can be achieved with more particle content. The fracture toughness improvement was above 200% for both particle size, achieving until 350% higher K_{IC} value when compared with the unmodified system.

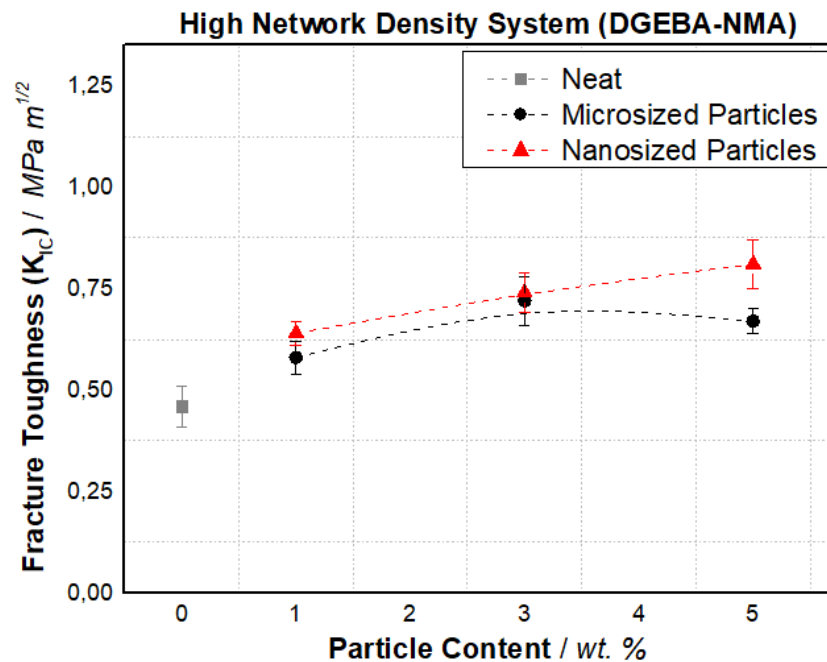
Figure 35 represents the fracture toughness for the high network density system (DGEBA-NMA), following the same procedure. The K_{IC} value for the unmodified system was measured to be $0.46 \text{ MPa m}^{1/2}$, and an increased much lower than 100% was found at 1 wt. % of both particle size content. For 5 wt. % of particles, the values of fracture toughness were still below $1.0 \text{ MPa m}^{1/2}$, although nanosized particles showed a better performance.

Comparing both Figures 34 and 35, it is possible to notice that the crosslink amount on the structure has an expressive effect on the improvement rate of fracture toughness by the use of PCS. Eventually, the micromechanical deformation mechanisms of epoxy resin by the use of PCS are strongly related to the network density, and therefore, how the particles interact with the network.

Analyzing Figure 35, it is noticed better performance of nanosized particles on fracture toughness improvement. For 5 wt. % use of PCS nanosized particles, the value of $0.81 \text{ MPa m}^{1/2}$ can be considered relatively high for a very high network density system resin. Eventually, the addition of microsized PCS particles showed an even lower increase on the fracture toughness, achieving the maximum improvement at 3 wt. % content, evaluated as $0.72 \text{ MPa m}^{1/2}$. It is important to notice that for microsized particles, a limit on the particle content was achieved, which directly indicates that increasing the microsized particle content above 3 wt. % cannot bring better performance. Even if there is a higher tendency of greater

toughening of nanosized particles in the 1 and 3 wt. % contents, it is statistically correct to establish that the particle sized present no influence.

Figure 35 – Fracture toughness for DGEBA-NMA-Particle systems as a function of particle size and content



Source: From the author himself, 2019

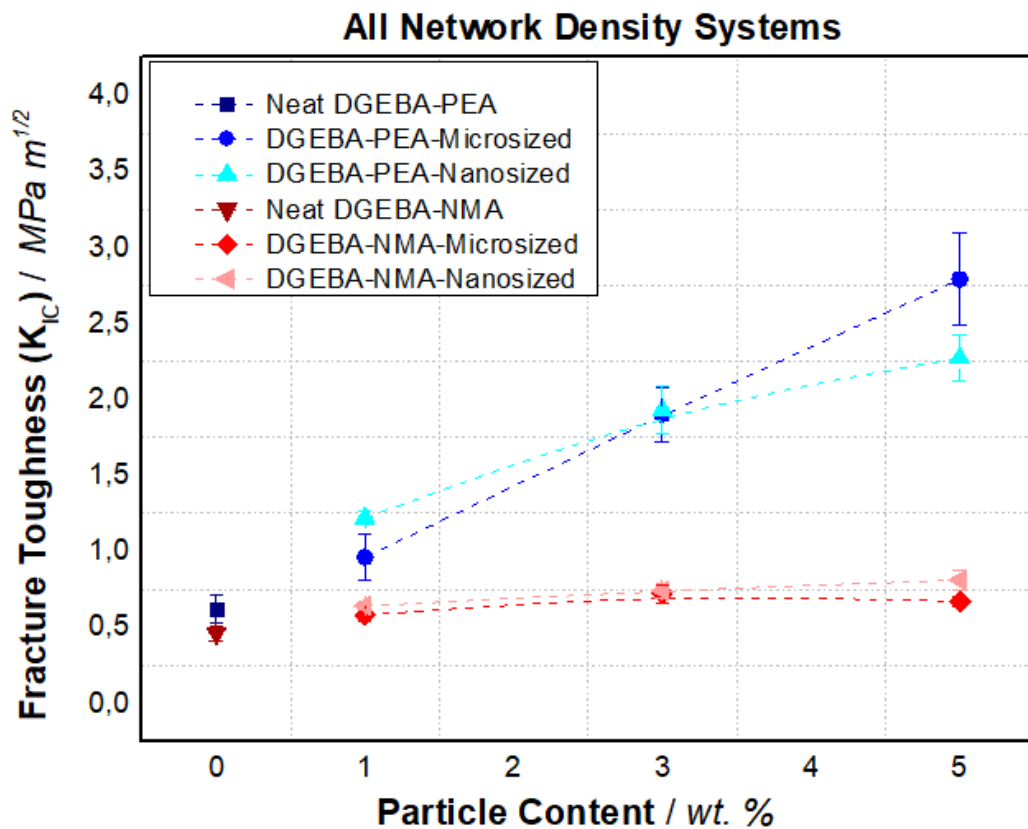
As a general analysis, Figure 36 shows a single comparison from the fracture toughness of all systems regarding particles sizes and contents. Levita *et al.* (1991) also compared modified and unmodified epoxies varying the network density, and noticed the same lack of toughenability in high network density systems.

Utaloff's *et al.* (2018) and Chong (2015) used several different modifiers on a relatively high network density system, and the K_{IC} values were also less than 1.0 MPa m^{1/2}. Therefore, it is still very clear the complexity of toughening a high network density system. It is believed that the addition of particles on the resin system, besides the addition of new deformation mechanisms, disturb the network structure. Therefore, as these mechanisms can no longer be improved, given a wt. % content limit, the network disturbs starts to emerge more intensively, showing decrease on the fracture toughness improvement. This also explains why the low network density system is less influenced by the particle size, and why it does not present an improvement limitation at 5 wt. % particle concentration. Levita *et al.* (1991) describes that the reduction in toughness caused by crosslink can be attributed either to the decrease of the volume of the plastic zone at the notch tip or, above all, to a lack of post-

yield deformability as confirmed by tensile test. The influence of the network density becomes more complex as increases, and fragile behaviors start to lead the fracture much easier than low network density systems.

Kinloch (2010) discusses the relation between the particle size with the deformation mechanisms and the material stiffness. The dependence of particle size shown appears credible for conventionally scaled materials. For the material tested in this work, with microsized particle radius, possibly cavitation and bridging effects were more pronounced, which should also deflect on the material stiffness. Lower particles size should be more related to mechanisms as shear band yielding and crack pinning. As the same particle volume is distributed in a lower scale, the mean free path is much lower. This combination should lead to an improvement on fracture toughness without significant change on the material stiffness.

Figure 36 – Fracture toughness for resin systems as a function of particle size and content



Source: From the author himself, 2019

Finally, Table 3 presents all the K_{IC} results related to their systems.

Table 3 – Fracture toughness general results for all resin-particles systems

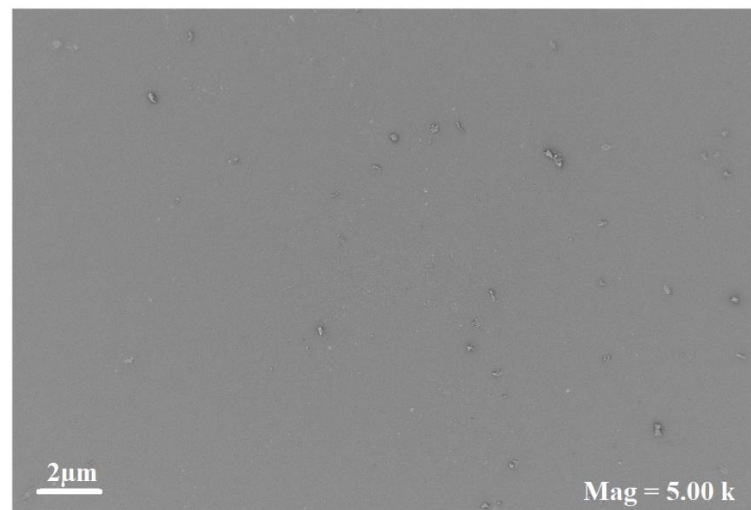
Fracture Toughness Properties (K_{IC}) in MPa m ^{1/2}					
System	Particle Size	Neat	1 wt. %	3 wt. %	5 wt. %
Low network density	Microsized	0.62 ± 0.09	0.96 ± 0.15	1.90 ± 0.18	2.79 ± 0.30
	Nanosized		1.22 ± 0.04	1.93 ± 0.16	2.27 ± 0.15
High network density	Microsized	0.46 ± 0.05	0.58 ± 0.04	0.72 ± 0.06	0.67 ± 0.03
	Nanosized		0.64 ± 0.03	0.74 ± 0.05	0.81 ± 0.06

Source: From the author himself, 2019

5.1.2. Fractography

Scanning Electron Microscopy (SEM) of the fracture surfaces were conducted aiming to observe the toughening mechanisms. The surface roughness and crack propagation direction of the selected images shown pronounce the energy dissipation effects. Figure 37 shows the fracture surface of the neat DGEBA-PEA system. The fracture surfaces of the unmodified epoxies were smooth and glassy, where the only method of energy dissipation found was the creation of new surfaces. This process is related to a very brittle and low fracture toughness value, as are both unmodified epoxy resin systems. Figure 38 presents the DGEBA-PEA modified with 1 wt. % microsized particles, and shows already track of roughness and fracture energy absorption mechanisms. As mentioned in Section 5.1.1., the particle cavitation and plastic void growth are most associated with bigger particles, which are associated with the surface shown in Figure 38.

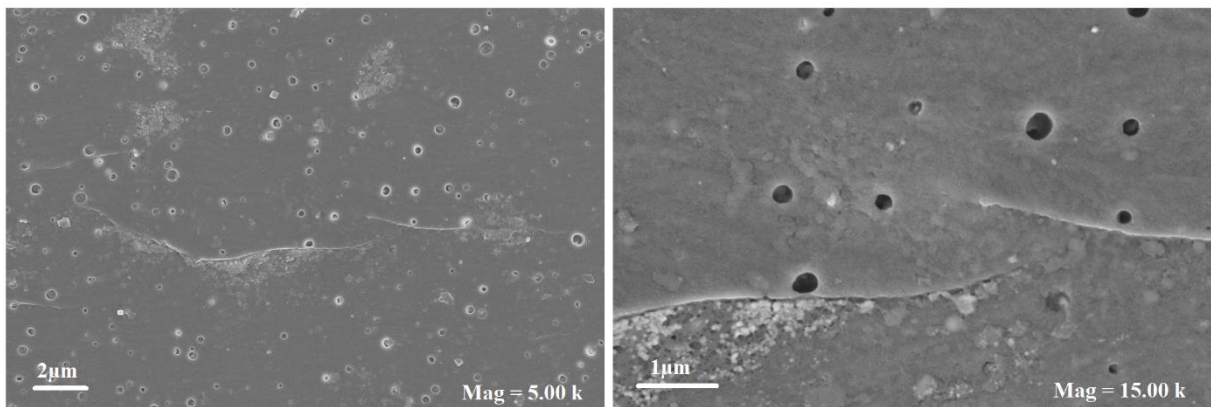
Figure 37 – Fracture surface SEM image for the DGEBA-PEA neat system



Source: From the author himself, 2019

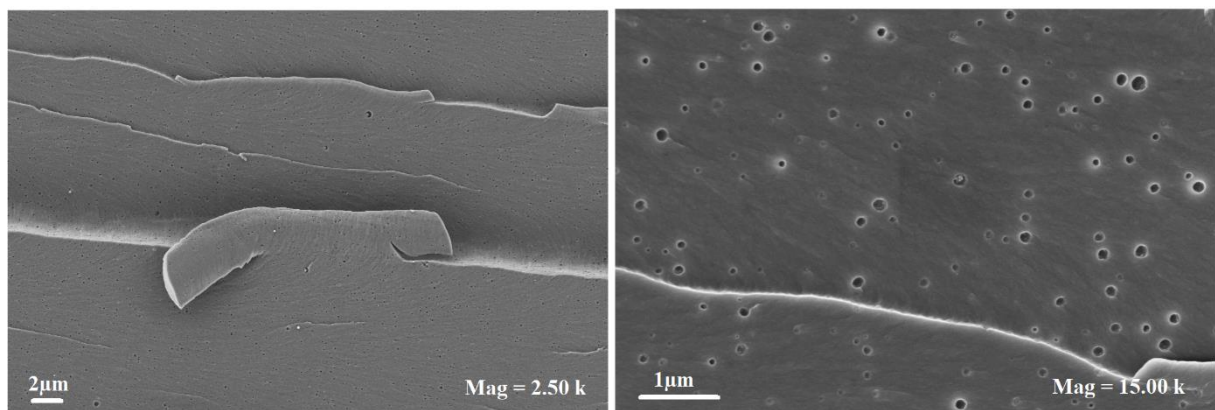
Figure 39, representing the DGEBA-PEA modified with 1 wt. % of nanosized particles, presents also surface roughness and tracks of fracture energy dissipation. The shear band yielding now was very expressive and continuous, what would match with a very expressive increase on the fracture toughness of the system, as it was shown to be much closed to 100%.

Figure 38 – Fracture surface SEM image for the DGEBA-PEA modified with 1 wt. % of microsized particle system with different magnifications, left (5.00 k), right (15.00 k)



Source: From the author himself, 2019

Figure 39 – Fracture surface SEM image for the DGEBA-PEA modified with 1 wt. % of nanosized particle system with different magnifications, left (2.50 k), right (15.00 k)

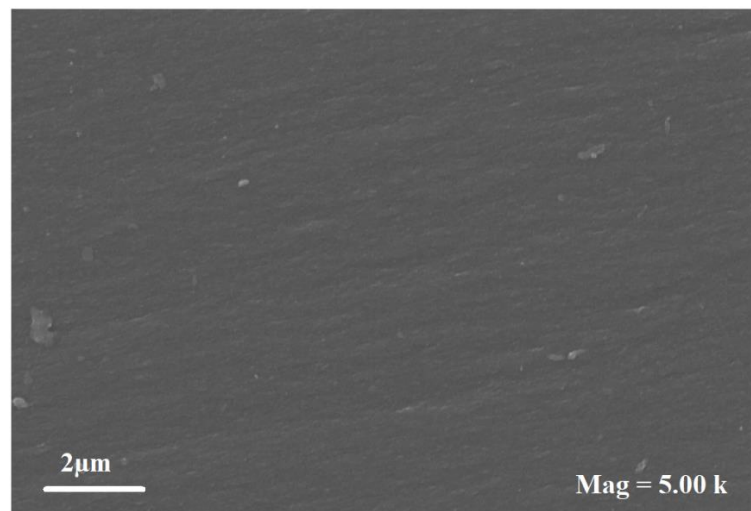


Source: From the author himself, 2019

Similar discussion can be made for the high network density system (DGEBA-NMA), where the unmodified system showed the same glassy and smooth single phase fracture surface, as can be seen in Figure 40. Figures 41 and 42 represents the fracture surface of DGEBA-NMA systems modified with 1 wt. % microsized and nanosized particles, respectively. Unlike the unmodified resin system, the modified material was again able to

present fracture energy absorption mechanisms. The degree of band shear yielding and crack pinning was much expressive on the nanosized modified system (Figure 42). This can be associated with the better distribution and lower distance among the particles, allowing more presence of the energy absorption. The fracture surface of microsized modified systems are quite similar (Figure 41), although the distance among particles looks much larger. It is believed that the larger distance among particles decrease the effect of band shear yielding and crack pinning, which is associated with a lower increase in the fracture toughness. Nevertheless, Figure 41 present more the effect of particle cavitation and plastic void growth, which matches with larger particles sizes.

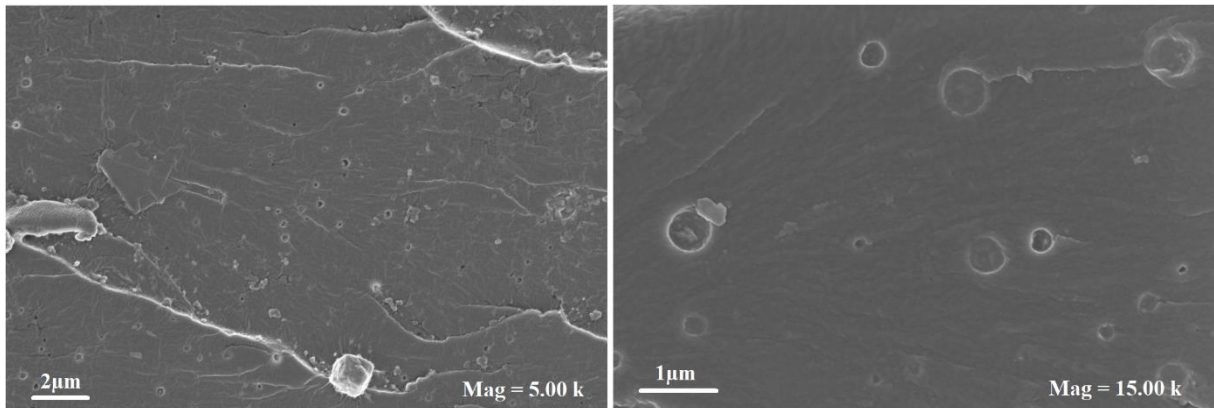
Figure 40 – Fracture surface SEM image for the DGEBA-NMA neat system



Source: From the author himself, 2019

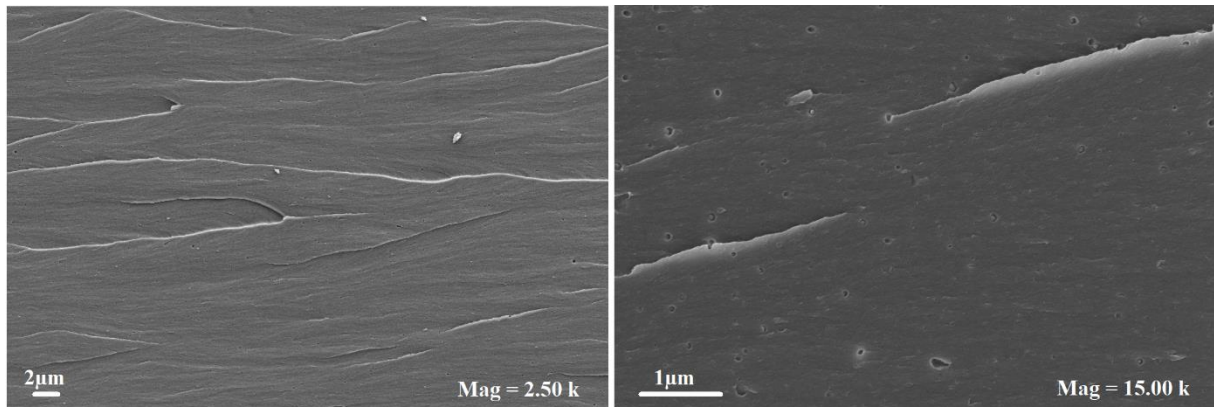
The morphology of both modified system presents significant degree of roughness and waveness, mostly in nanosized modified systems. All those models of plastic deformation are related with the fracture toughness improvement showed in the Figure 34. The SEM pictures also reveals the crack propagation around the epoxy inclusions through the matrix, rather than through the inclusions, which increases the amount of energy needed to crack growth.

Figure 41 – Fracture surface SEM image for the DGEBA-NMA modified with 1 wt. % of microsized particle system with different magnifications, left (5.00 k), right (15.00 k)



Source: From the author himself, 2019

Figure 42 – Fracture surface SEM image for the DGEBA-NMA modified with 1 wt. % of nanosized particle system with different magnifications, left (2.50 k), right (15.00 k)

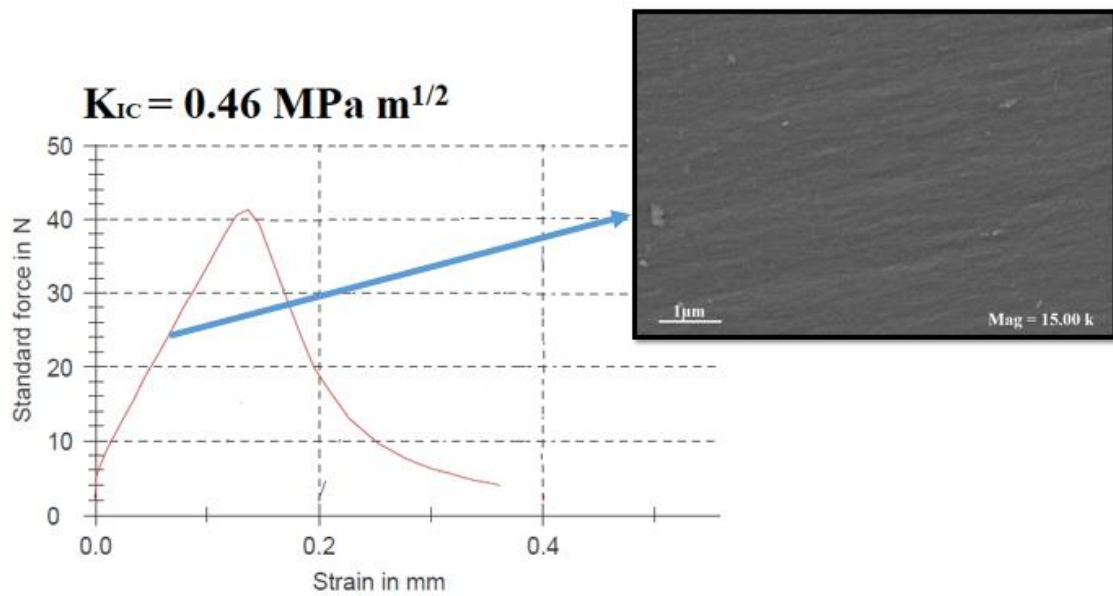


Source: From the author himself, 2019

The formation of shear ribs and steps along the crack growth direction encouraged by microcracking in different planes was more definite for static fracture than for fatigue. Instead of shear steps, crack pinning could be resolved in fatigue. (KARGER-KOCSIS and FRIEDRICH, 1993) This feature can be explained by reduced plastic and process zones under fatigue conditions as discussed before.

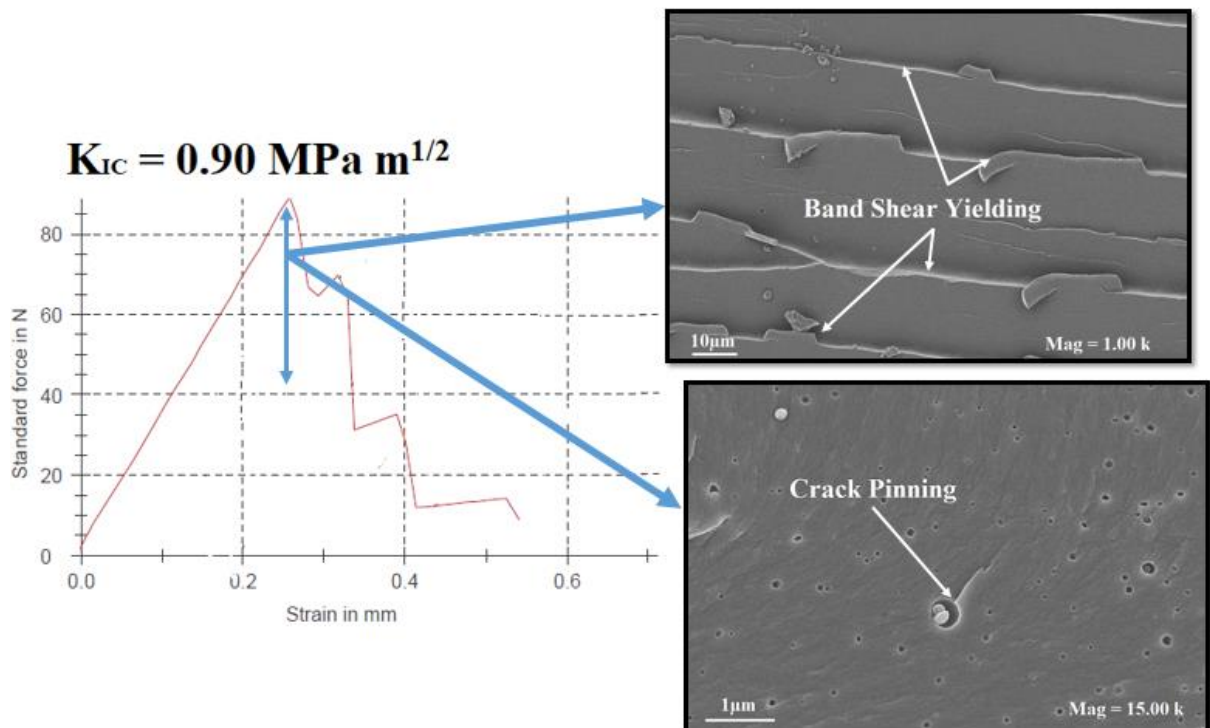
Figure 44 can show very clearly the toughening mechanisms provided by the addition of 5 wt. % of nanoparticles, which cannot be seen in the unmodified epoxy resin system (Figure 43).

Figure 43 – Practical measurement of fracture toughness (K_{IC}) from one DGEBA-NMA unmodified specimen, attached with a SEM image from the specimen fracture surface



Source: From the author himself, 2019

Figure 44 – Practical measurement of fracture toughness (K_{IC}) from one DGEBA-NMA modified with 5 wt. % nanosized PCS specimen, attached with a SEM image from the specimen fracture surface



Source: From the author himself, 2019

The clear fracture surface of DGEBA-NMA neat resin indicates that practically all curing agents had formed a perfect cross-linked structure system, which results in a continuous and smooth phase. Chong (2015) claims that a lower degree of curing would possibly indicate discontinuous phases and plastic deformation traces. This fracture toughness function can be directly compared with a brittle propagation function as presented in Figure 11.

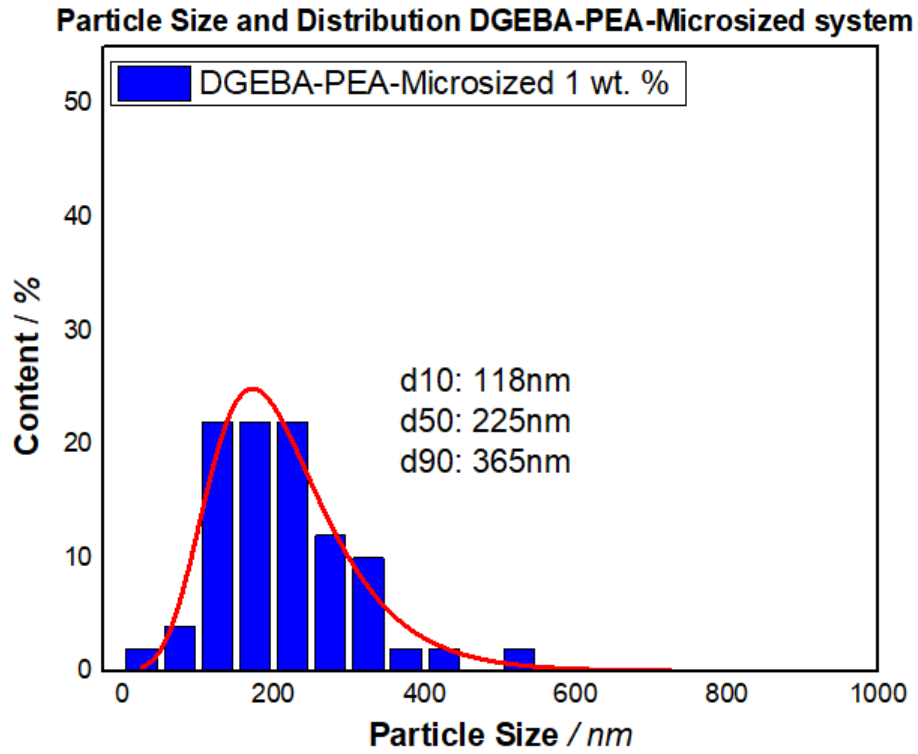
Figure 44 presents the DGEBA-NMA toughened with 5 wt. % of nanosized particles. Here it is possible to see the increase in fracture toughness by the introduction of energy absorption effects, as band shear yielding and crack pinning, as is pointed on the SEM pictures. Eventually, these mechanisms will require additional amount of energy allow crack propagation through the structure, which is responsible for toughening the material. In Figure 43, the unmodified resin shows a clear and smooth fracture surface, and the K_{IC} is therefore much lower. Eventually, this function can be associated with the stable-brittle propagation fracture toughness presented in Figure 12.

5.1.3. Particle Size and Size Distribution

The particle size measured was estimated to be 10 to 20% smaller than the real size. This is given by the inaccuracy of measuring a 3D cavity through a 2D image, where the apparent radius is smaller than the real radius. Although, the particle size and distribution is very close to the datasheet information. Even so, the particle size distribution is independent of this inaccuracy, and can be very well defined.

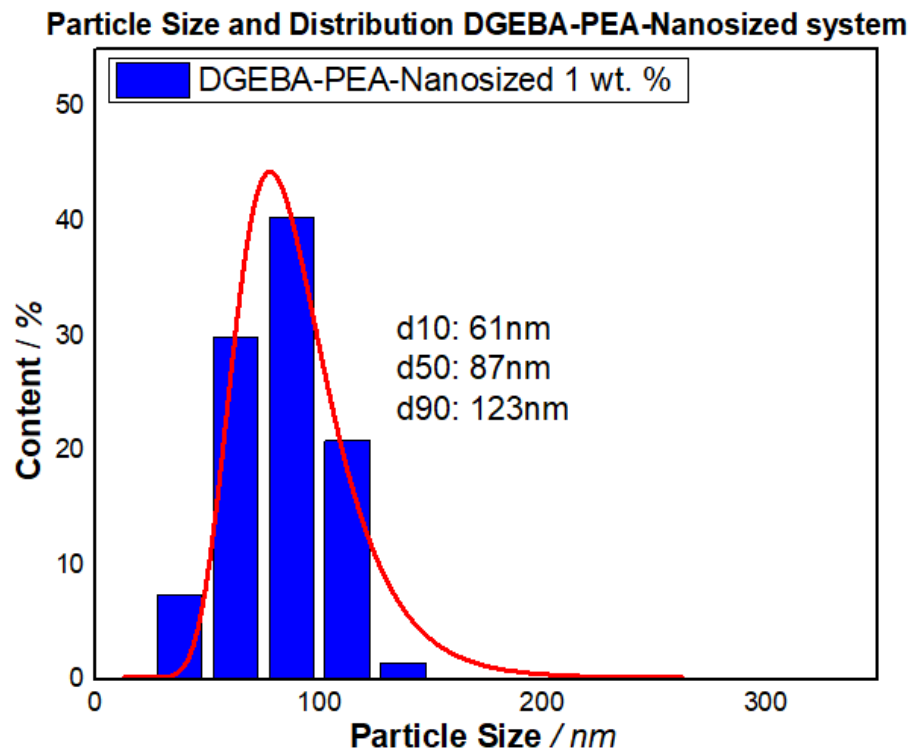
For the low network density system the particle size was considered very closed to the value provided by the datasheet. The particle size distribution for this case was considered large, once particles from below 100 nm and above 500 nm were found. Even though, considering the d50 method and the imprecision, the average was approximately 250 nm. The nanosized particles were estimated as an approximately 90 nm, considering the same methodology. The particle size distribution for the nanosized particles was much more reduced. Figure 45 and 46 presents the particle size and size distribution for the low network density system.

Figure 45 – Particle size and size distribution for DGEBA-PEA-Microsized system



Source: From the author himself, 2019

Figure 46 – Particle size and size distribution for DGEBA-PEA-Nanosized system

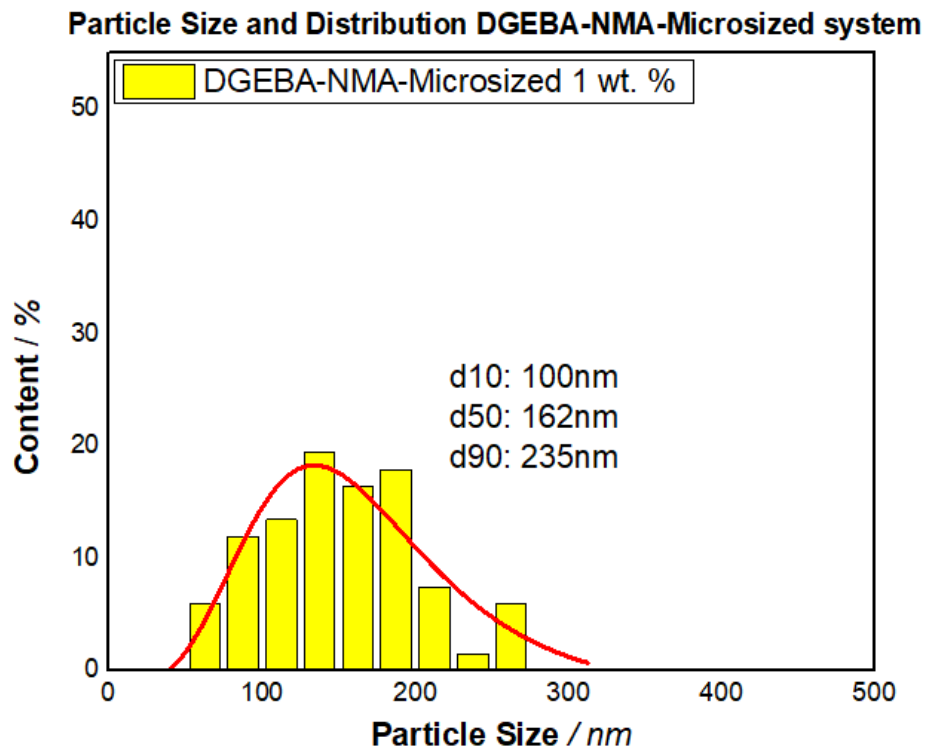


Source: From the author himself, 2019

For the high network density system the particle size was lower than the expected from the datasheet. As it is discussed in the material datasheet, the particle size can possibly vary with the curing cycle temperature. Considering that all particles are agglomerates of block copolymers (as it is shown in the material description, section 4.1.3.), the higher temperature should give more mobility to these chains. As the curing cycle temperature gets higher, there was a greater tendency of these copolymer chains to dissociate from the particle agglomerate, making it progressively smaller.

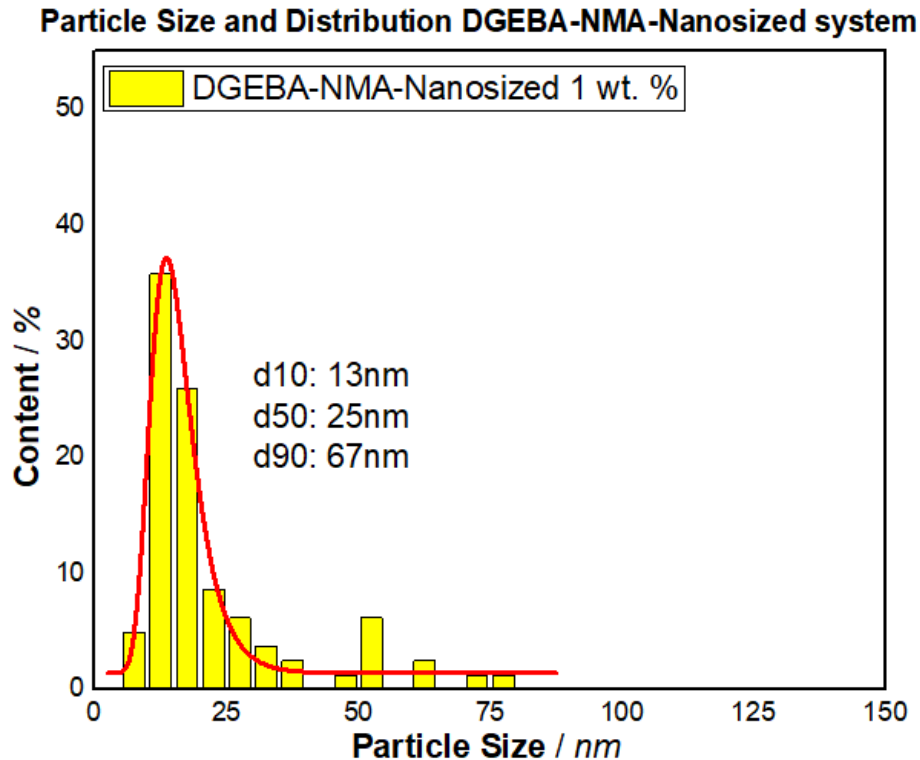
It is also possible to see that the microsized particles in both cases presented a higher particle size distribution. Conceivably, This was given by the existence of few very small (50 – 100 nm) particles, present in conjunction with the microsized particles. This very small particles included in the microsized could also explain why the d50 was evaluated lower than the expected. For the nanosized particles the distribution was lower, and the particle size was evaluated as the expected from the datasheet for both cases. Particles formed by copolymers structures tends to deviate more from each other as the final particle size increases. Figure 47 and 48 presents the particle size and size distribution for the high network density system.

Figure 47 – Particle size and size distribution for DGEBA-NMA-Microsized system



Source: From the author himself, 2019

Figure 48 – Particle size and size distribution for DGEBA-NMA-Nanosized system



Source: From the author himself, 2019

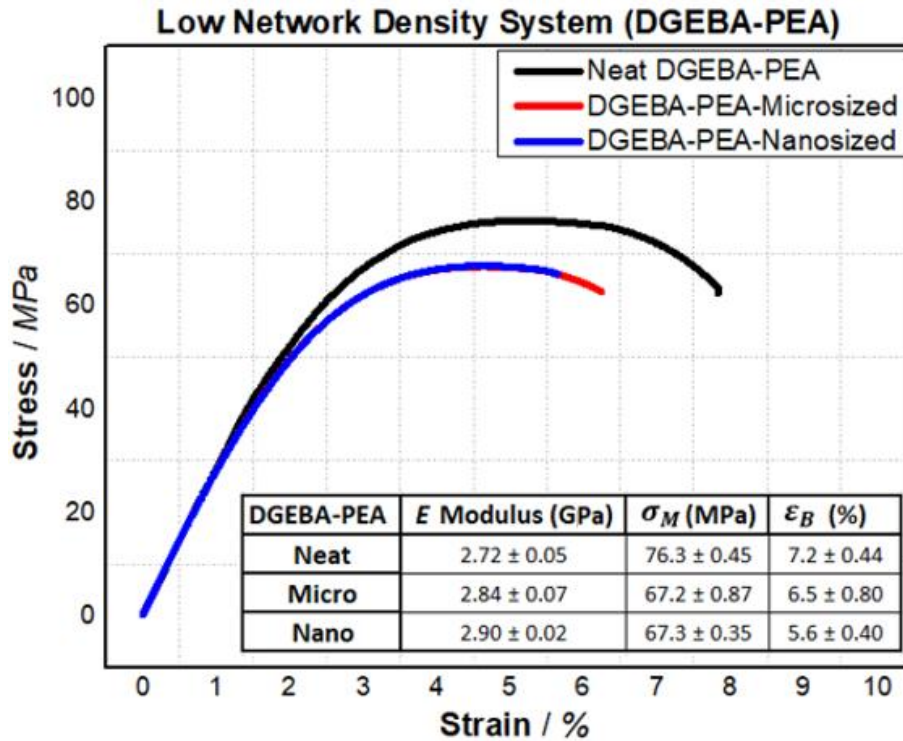
5.1.4. Tensile Properties

A tensile modulus of 2.7 GPa was measured for the unmodified DGEBA-PEA system. The modulus increased approximately 0.15 GPa by the use of 1 wt % of polysiloxane core-shell particles, for both microsized and nanosized systems. Considering the standard deviation of the values, it is possible to declare that the stiffness was not influenced by the use of 1 wt. % of PCS particles. Figure 49 presents the stress as a function of the elongation for the low network density system, for the specimen which the behavior was closest to the average, with the values attached as a table, where E modulus represents the Young's modulus, σ_M the maximum stress, and ε_B the elongation at break.

For the low network density, the maximum tensile stress was evaluated as 76.3 MPa, while the values with particles were found closed to 67 MPa. The decrease should be related to the facility of fracture mechanisms created in the interface of matrix-particle generated by a tensile load. These mechanisms are usually crazing and particle cavitation effects. Eventually, as the maximum tensile strength goes lower, the elongation at breaks decreases. The particles have a very low influence on a low network density resin tensile behavior, where stiffness

was maintained, and the material tensile strength decreases. As the matrix-particle interface is very miscible, these effects were not very significant.

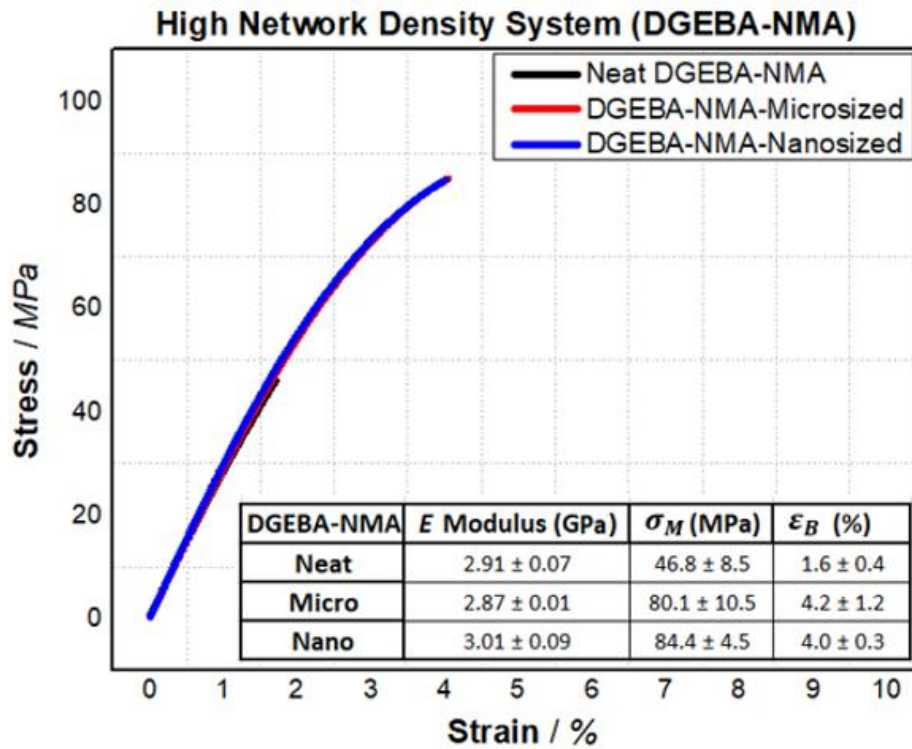
Figure 49 – Practical tensile curves for DGEBA-PEA neat and modified with 1 wt. % PCS particles, attached with the most important results



Source: From the author himself, 2019

For the high network density system, a 2.91 GPa Young's modulus was found. Related to the low network density system, the stiffness behavior were very similar. This property is ruled by the nature of atomic bonds, and therefore, by the number of crosslinks in the network. However, here the number of crosslinks in the network for both systems is sufficient high to the elastic modulus be independent of the network density, being only a function of the atomic bonds, which is the same for both cases. The other properties though, are significantly different. Figure 50 provide the same tensile structure described in Figure 49 but for DGEBA-NMA.

Figure 50 – Practical tensile curves for DGEBA-NMA neat and modified with 1 wt. % PCS particles, attached with the most important results



Source: From the author himself, 2019

Regarding the tensile strength, the unmodified DGEBA-NMA was evaluated with a 46.8 MPa value. This was surprisingly low, as tensile strengths of approximately 81 and 83 MPa are typically measured for this epoxy polymer (CHEN, *et al.*, 2013). However, such unmodified thermoset polymers are extremely sensitive to the presence of surface defects, and it is likely that such imperfections caused these relatively low values to be measured. Indeed, for the formulation containing 1 wt. % of PCS particles, a mean tensile strength of 80 and 84 MPa was measured for microsized and nanosized particles, respectively, which is close to the value reported by Giannakopoulos *et al.* 2011. The use of PCS particles grants stability to the measurements, where higher values of maximum tensile strength are measured compared to the low network density system. In this case, where the network density is so high, it is believed that the use of particles increase the material elongation and plastic deformation, different from the low network density case. Eventually, the higher crosslinks amount decreases significantly the elongation at break, which was reduced for 1.6 % to the unmodified DGEBA-NMA resin, and closed to 4.0 % to the DGEBA-NMA-Particles systems, compared with the DGEBA-PEA-Particles systems.

5.1. Thermomechanical Properties

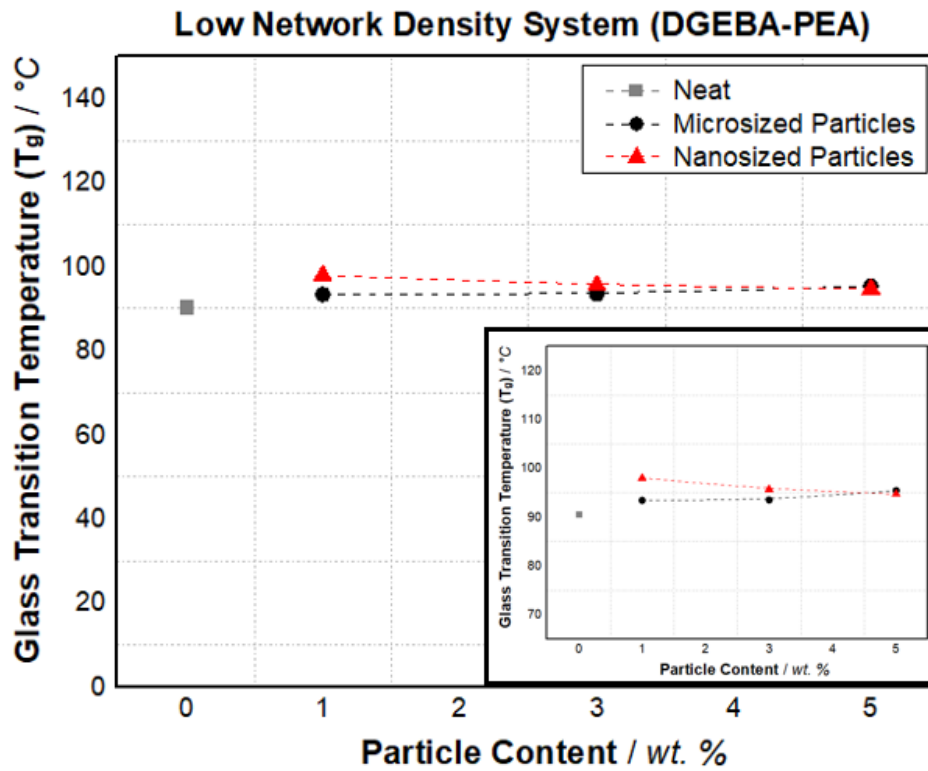
The thermomechanical analysis was made by DMA evaluations, and the data collected by the TA Orchestra software®. The $\tan \delta$ curve was directly provided by the software, where the T_g was then obtained for each system. The loss modulus E'' was also provided by the software, allowing the calculation of the network density, by the use of Equation 13.

Appendix A provides the curves obtained from DMA data (E' , E'' , $\tan \delta$) for low and high network density systems. From these data, the values of T_g and network density were taken.

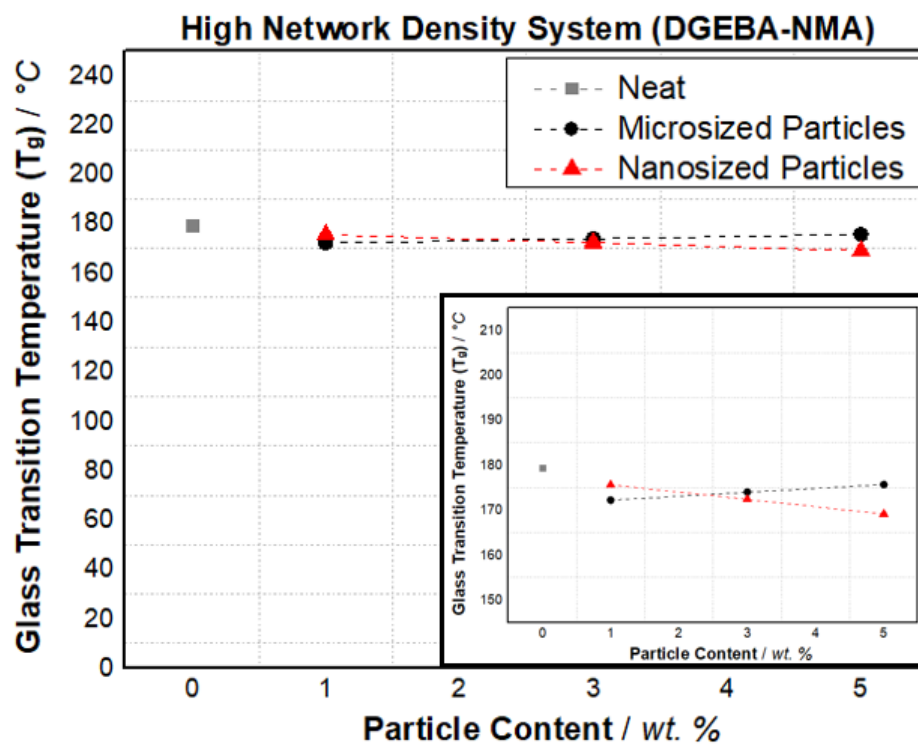
5.2.1. Glass Transition Temperature

Unmodified low network density system DGEBA-PEA showed a T_g of 90.60 °C, as expected from its curing cycle. The addition of particle has proved to increase the T_g value, in a range of 3 to 8 °C. The nanosized system shown a highest increase on the T_g at low concentration value (1 wt. %), and a smooth decrease, which still remains above the neat resin. The microsized particle addition showed a linear smooth increase almost indistinguishable, keeping the T_g around 5 °C higher than the neat resin system, as it is shown in Figure 51.

For the high network density system DGEBA-NMA, the unmodified T_g was measured as 179.40 °C. The addition of PCS particles decreased the T_g in a relatively high amount. The use of 1 wt. % of these particles showed to decrease more with more intensity for the microsized particles (172.20 °C), while the nanosized particles showed lower difference with the neat (175.60 °C). Although as the particle content increased, the T_g decreased more significantly to the nanosized particles, as the 5 wt. % amount was evaluated with a 169.10 °C T_g value. On the other hand, for the use of 5 wt. % of microsized particles, the T_g was still lower than the unmodified resin, but higher than the 1 wt. % of microsized particles, being evaluated as 175.70 °C. The Figure 52 shows the T_g behavior of these systems.

Figure 51 – T_g evaluated from DMA for DGEBA-PEA-Particle systems as function of particle size and content

Source: From the author himself, 2019

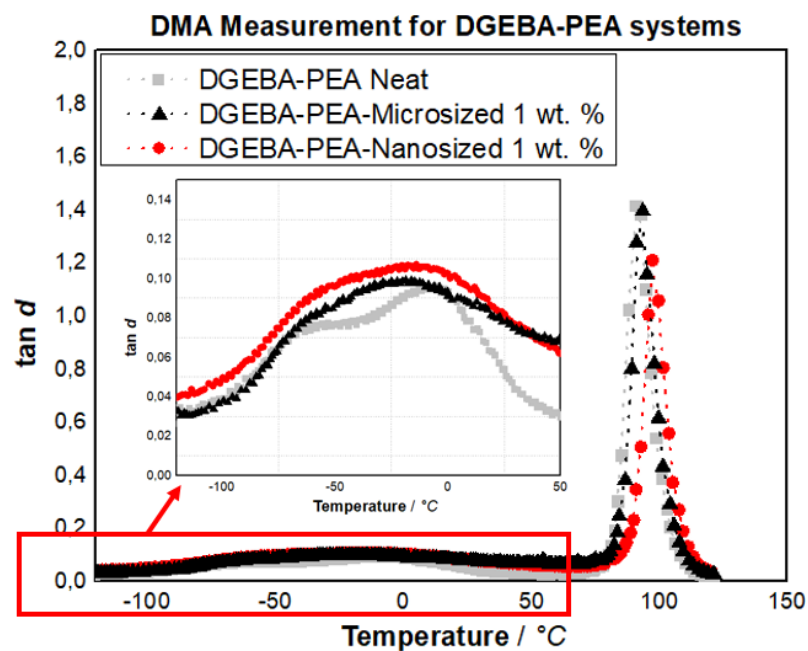
Figure 52 – T_g evaluated from DMA for DGEBA-NMA-Particle systems as function of particle size and content

Source: From the author himself, 2019

Analyzing these specific results, it is believed that there are two different mechanisms affecting on the material T_g . The first one is related to the crosslinks formation constraint from the network structure by the introduction of a particle in that volume. This mechanism is associated with a decrease on the material T_g , as can be seen in Figure 4, Chapter 3. The second mechanism is a mechanical mobility restriction of the chains created by the introduction of the PCS particles. Once these particles are a core-shell system, the thermal vibration behavior should be similarly to the epoxy resin structure. The combination of these two mechanisms in different epoxy systems results in a wide range of possible behaviors, where is related the network density, particle size and particle content.

For the low network density system, the amount of crosslink formation constraint from the network has a lower magnitude than the mobility restriction generated by the particles introduction, which led the material to obtain a higher T_g value than the unmodified resin. In fact, it is possible to detect in the DMA results, for the DGEBA-PEA system, that the $\tan \delta$ as a function of the temperature presents in the β -transition, much more extent transition for the modified systems than for the unmodified system, in the PCS glass transition region (Figure 53). This indicates that the network system takes more energy in other to increase the mobility. The DGEBA-PEA modified with 1 wt. % of nanosized particles presented the higher T_g , and therefore, corresponding with the higher extension of the β -transition.

Figure 53 – $\tan \delta$ curve as a function of temperature for DGEBA-PEA modified with 1 wt. % of particles



Source: From the author himself, 2019

The DGEBA-NMA have shown more complex behavior regarding to the possible interaction between particle and network. The first analysis is that in a high network density structure, the restriction of crosslinks formation by existence of particles will be more expressive, while the mobility restriction is less pronounced. As a result, the T_g will be lower with particles compared with the unmodified system. Apparently, the microsized particles were able to increase the mobility restriction as the particle content increased, while the crosslink impediment rate keeps similar. This factor would be related to an increase on the T_g value. Chen, *et al.* (2013) used a high network density system with microsized PCS particles, and was able to detect the same T_g pattern by the use of PCS particles, as is shown in Table 4. Although, the author claims that the behavior is insignificant, and is related to experimental uncertainty.

Table 4 – T_g for a high network density system as a function of a microsized particle content

S-CSR content		T_g (°C)
(wt%)	(vol%)	
0	0	148
2	3.1	145
6	8.4	145
10	11.6	147

Source: Chen, *et al.*, 2013

Similarly to Figure 52, Table 4 presents a first drop on the material T_g as the microsized particles are introduced, and a smooth increase as the content is raised. On the other hand, the use of nanosized particles have shown a linear decrease in the material T_g , achieving a lowest value of 169.10 °C in 5 wt. % particle content. This decrease is significant, and indicates that the elimination of crosslinks was more expressive than the mobility restriction. It is possible that due to the low particle size, the mobility was not as much influenced, although the high distribution of particles is sufficient to eliminate high amount of crosslinks.

Finally, Table 5 presents all the T_g results related to their systems.

Table 5 – Glass transition general results for all resin-particles systems

Glass Transition Temperature (T_g) in °C					
System	Particle Size	Neat	1 wt. %	3 wt. %	5 wt. %
Low network density	Microsized	90.60	93.40	93.50	95.40
	Nanosized		98.00	95.70	94.70
High network density	Microsized	179.40	172.20	174.00	175.70
	Nanosized		175.60	172.40	169.10

Source: From the author himself, 2019

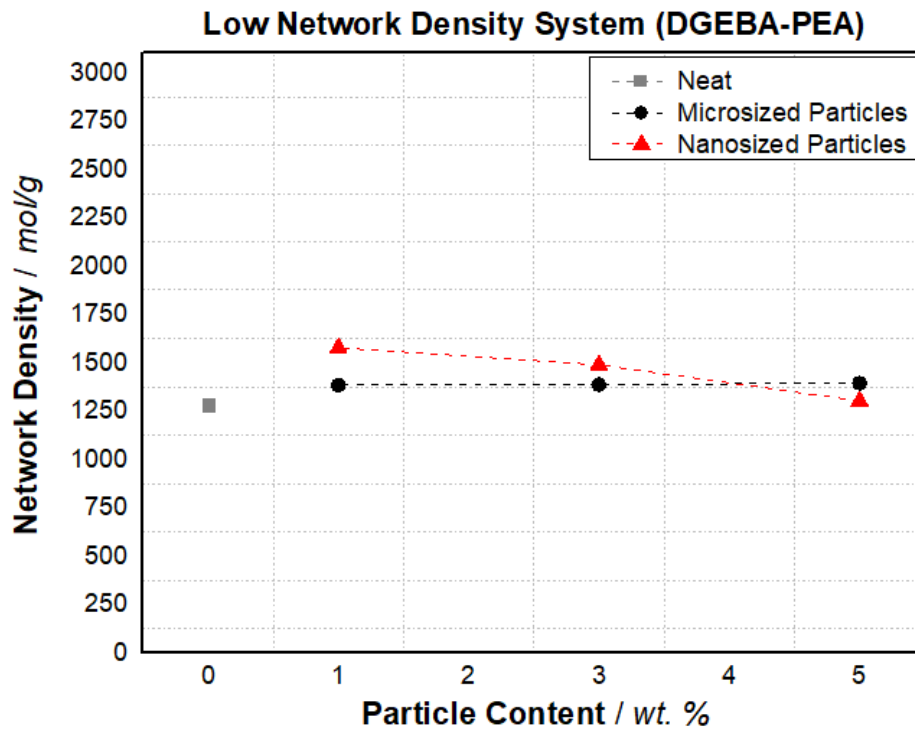
5.2.2. Network Density

The network density for the DGEBA-PEA system showed to be strongly related to the T_g behavior, as it is seen in Figure 54. Higher network densities were actually calculated for the modified system compared to the unmodified system. The network density calculation is dependent on the loss of modulus E' , and a decrease in the network mobility indicates higher network density value, which does not necessarily mean higher amount of crosslinking.

Figure 54 provides support to the discussion on the increase on the DGEBA-PEA thermomechanical performance, where the PCS introduction provides a more stable and compact structure. Eventually, the curve provides information of a network density reduction tendency as the particle content is increased to further values.

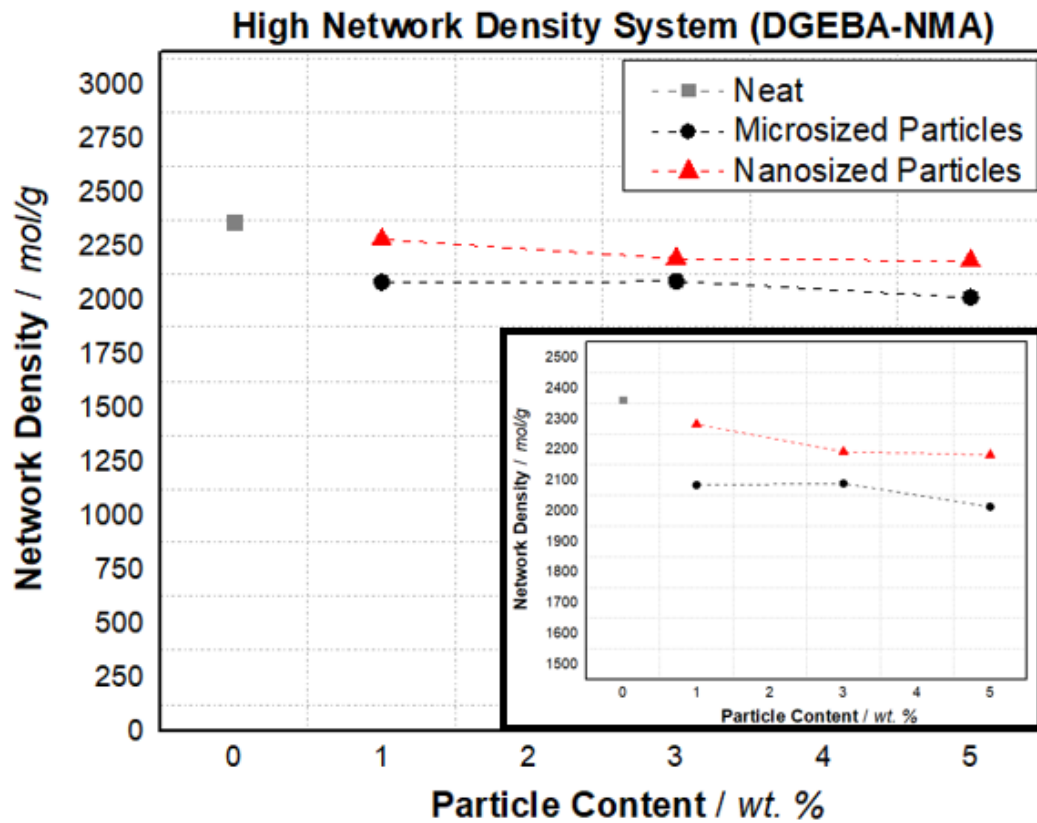
The DGEBA-NMA system presents a different pattern of network density compared to the T_g behavior shown in Figure 55. Here it was noticed that the network density decreases much more expressively with the addition of microsized particles compared with the addition of nanosized particles. The introduction of microsized particles in the high network density system shows to decrease the loss modulus E' , and the network density by sequence, more expressively than by the introduction of nanosized particles. This suggests that larger particles eliminate more crosslinks than smaller particles. The T_g though, is not associated only with the crosslink content, and therefore do not decrease proportional to the network density.

Figure 54 – Network density for DGEBA-PEA-Particle system as a function of the particle size and content



Source: From the author himself, 2019

Figure 55 – Network density for DGEBA-NMA-Particle system as a function of the particle size and content



Source: From the author himself, 2019

Table 6 presents the network density evaluated to each system.

Table 6 – Network density general results for all resin-particles systems

Network Density in mol/g					
System	Particle Size	Neat	1 wt. %	3 wt. %	5 wt. %
Low network density	Microsized	1279.3	1382.5	1385.2	1393.7
	Nanosized		1576.6	1488.2	1302.4
High network density	Microsized	2361.1	2083.8	2088.6	2012.5
	Nanosized		2281.8	2192.6	2182.4

Source: From the author himself, 2019

6. Conclusions

Different epoxy systems were modified with microsized and nanosized polysiloxane core-shell particles in different particles content. The DGEBA epoxy resin was formulated with Polyetheramine (PEA) and Norbornene Methyl Anhydride (NMA) in order to bring low a high network density system analysis, respectively. The mechanical, morphological and thermomechanical properties were analyzed and related to the particles parameters.

For the low network density system, the particle size showed to have no significant influence on the mechanical and thermomechanical properties. The PCS particle content on the other hand showed to increase expressively the fracture toughness as it was raised. The fracture toughness of this system was highly improved, reaching 100% higher K_{IC} already with 1 wt. % particle addition. The fracture toughness kept increasing with the particle content, reaching values above 2.00 MPa m^{1/2}. The fracture toughness improvement for this case was kept positive, which indicates that higher K_{IC} value can be achieved with more particle content. The tensile properties were very similar for both modified and unmodified system, where the elastic modulus was evaluated between 2.70 and 2.90 GPa. The T_g was proven to be higher with addition of particles, proving that the core-shell system acts similarly to the resin network in terms of thermal vibration. Also, that the higher network space indicates lower crosslink eliminations.

For the high network density system, the particle size and content were proven to be significant in both mechanical and thermomechanical behavior. The K_{IC} improvement was much lower than the low network density system, and was kept below 100% even with 5 wt. % content of particles. The nanosized particles demonstrated better performance on fracture toughness, indicating more efficient toughening mechanisms. On the other hand, the microsized particles presented a lower gain in K_{IC} values, which were also decreased from 3 to 5 wt. %, establishing a limit on fracture enhancement. The elastic modulus for this system was also very similar for both modified and unmodified system, granting low influence from the particles, giving values between 2.87 and 3.00 GPa. The thermal performance presented decrease in both T_g and network density values, for both particles sizes. A combination between crosslink elimination and network movement restriction was estimated given the T_g pattern. Microsized particles showed lower decrease on the T_g compared to nanosized particles. The highest drop on the T_g was found in 5 wt. % of nanosized particles, achieving 10 °C difference.

This work investigated the PCS particles parameters related to the mechanical and thermomechanical properties. Several toughening mechanisms were identified and discussed between the fracture toughness values and the fractography SEM images. Afterwards, a brief relation with tensile properties was supported. Nevertheless, the thermomechanical stability brought a new topic of discussion relating particles parameters and network structure. It is noteworthy that this topic is not much discussed in the literature, and for this reason, further examinations indicates promising analysis for the state of the art.

Regarding to the engineering overview, for low temperature applications, low network density system proved to easily present K_{IC} values above $1.00 \text{ MPa m}^{1/2}$ by PCS particles addition, which are indicated to engineering applications. If further fracture toughness values are required, the increase on particle content is recommended. The rise on T_g for this case only ensures thermal stability for these applications. For high network density the addition of particles has to be more careful analyzed. The use of nanosized PCS brought better K_{IC} performance, although it was still less than $1.00 \text{ MPa m}^{1/2}$. The microsized particles led to improvement values lower than $0.75 \text{ MPa m}^{1/2}$, and even lower when 5 wt. % was add, which suggest less indication of use compared to the nanosized particles. The T_g drop by 5 wt. % nanosized particles addition indicates careful application for high temperature applications, what would probably restrict the particle content when related to the final application.

Nevertheless, the use of particles prove to increase significantly the epoxy resin performance, and it is estimated as essential to engineering applications. Several combinations of fracture toughness and thermal stability can be associated with the particles parameters and the resin network system, which can be arranged with the final application. In applications where no thermomechanical high-performance is required (low network density systems), a very pronounced toughening can be done with both nanosized and microsized particles in a 5 wt. % content, without signs of decreasing T_g or Elastic modulus. Yet, further toughening can be achieved with higher particles content. In applications where thermomechanical high-performance is required (high network density systems), the nanosized particles are more indicated, with content not higher than 5 wt. %, since the T_g appears to be very affected by the use of particles.

7. Suggestions for Future Works

A very important measurement for simulating real dynamic fracture toughness is the Fatigue Crack Growth Rate measurement (da/dN), designed to determine the rate of crack loading conditions once a flaw has been initiated in the specimen. This measurement should be considered to be tested in the systems utilized in this work, for further investigations in the mechanical behavior of these materials. Nevertheless, this measurement provides an important engineering property for high performance materials utilized in harsh stress situations, which should be significantly improved by the use of PCS particles (CHONG, 2015; UTALOFF, *et al.*, 2018).

In order to study a more comprehensive range of mechanical and thermomechanical results, different materials on the core-shell particles can be applied, aiming to evaluate the possible behaviors with the resin network. For low network density systems, higher particle sizes and content can be safely tested to evaluate different enhancements in mechanical properties. For high network density systems, more distributed particle content can be investigated for optimized engineering applications.

Given all results presented in this work, a math model relating the particle size and content with K_{IC} values can be created, given further support to the investigation. The fracture energy (G_{IC}) math model is more investigated in the literature, which could also be associated with the results evaluated in this work.

The topics discussed in the thermomechanical results can be more deeply investigated by setting isolated parameters. A separated model between crosslink elimination and thermal vibration restriction can be analyzed, indicating clear mechanisms and math models.

References

ASM International. Characterization and Failure Analysis of Plastics. The Materials Information Society. **2003**. ISBN: 0-87170-789-6.

ASM International. Introduction to Tensile Testing. 2nd ed. The Materials Information Society. **2004**. ISBN: 978-0-87170-806-9.

ASKELAND, D. R., PHULE, P.P., The science and engineering of materials. Pacific Grove: Brooke/Cole, Thompson Learning, **2003**.

AZIMI, H. R., PERSON R. A., HERTZBERG, R. W., Fatigue of rubber-modified epoxies: Effect of particle size and volume fraction, J. Mater. Sci. 31. **1996**. 3777–3789. doi:10.1007/BF00352793.

BAIN, E. D., *et al.*, Failure processes governing high rate impact resistance of epoxy resins filled with core shell rubber nanoparticles, Conf. Proc. Soc. Exp. Mech. Ser. 1B. **2017**. 271–283. doi:10.1007/978-3-319-41132-3_36.

BOWER, A., Applied Mechanics of Solids. CRC Press, October 5, **2009**. ISBN: 9781439802472.

CARBAS, R., *et. al.* Effect of post-cure on the glass transition temperature and mechanical properties of epoxy adhesives. Journal of adhesion science and technology. **2013**. v27. 2542 – 2557.

CHEN, J., *et al.*, The mechanical properties and toughening mechanisms of an epoxy polymer modified with polysiloxane-based core-shell particles. Polymer, v54. **2013**. 4276–4289. doi:10.1016/j.polymer.2013.06.009.

CHERRY, B. W., THOMPSON, K. W., The fracture of highly crosslinked polymers. Part 1. Characterization and fracture toughness. J. Mater. Sci. **1981**. v16: 1913–1924.

CHONG, H. M., Toughening mechanisms of block copolymer and graphene nanoplatelet modified epoxy polymers, Imp. Coll. London. **2015**.

DEKKER, M., Epoxy Resin: Chemistry and Technology, New York, **1988**. ISBN: 0-8247-7690-9.

DOMPAS, D., *et al.*, Cavitation debonding during deformation of rubber-modified poly(vinyl chloride). Polymer. **1995**. v36, 437–441.

ELLIS, B., *Chemistry and Technology of Epoxy Resins*, 1st ed., Springer, **1993**, ISBN: 978-94-010-5302-0. doi:10.1007/978-94-011-2932-9.

EVANS, A. G., FABER, K. T., Crack-growth resistance of microcracking brittle materials. *J. Am. Ceramic. Soc.* **1983**. v67. 255–260.

FIEDLER, B., HOJO, M., *et al.* Failure behavior of an epoxy matrix under different kinds of static loading. *Compos Sci. Technol.* **2001**. v61, 1615–1624.

FRIEDRICH K., Microstructure-related fracture toughness and fatigue crack growth behavior in toughened, anhydride-cured epoxy resin, 48. **1993**. 263–272.

GIANNAKOPOULOS. G., *et al.*, Toughening of epoxy using core-shell particles. *Journal of Material Science.* **2011**. v46, 327-338. doi:10.1007/s10853-010-4816-6.

GRELLMANN, W., *et al.* *Polymer Testing*. Hanser Gardner Pubns. **2015**. ISBN-10: 1569904103, E-Book-ISBN: 978-3-446-44390-7.

HAMERTON, I., *Recent Developments in Epoxy Resins*, RAPRA Technology LTD. **1997**. ISBN: 1859570836.

HERTZBERG R., RICHARD W., *Deformation and Fracture Mechanics of Engineering Materials* (4th ed.). **1995**. Wiley. ISBN: 0-471-01214-9.

HUANG, Y., KINLOCH A., Modelling of the toughening mechanisms in rubber-modified epoxy polymers, *J. Mater. Sci.* 27. **1992**. 2763–2769. doi:10.1007/BF00540703.

HUANG, Y. G., KINLOCH A. J., The role of plastic void growth in the fracture of rubber-toughened epoxy polymers. *J. Mater Sci. Lett.* **1992**. v11, 484–487.

ISO 527-2:2012, specifies the test conditions for determining the tensile properties of moulding and extrusion plastics. Edition 2, **2012**. ICS: 83.080.001, Plastics in general.

KARGER-KOCSIS and FRIEDRICH, Microstructure-related fracture toughness and fatigue crack growth behavior in toughened, anhydride-cured epoxy resins. **1993**. 263-272, v48. doi: 10.1016/0266-3538(93)90143-5.

KIM, D. S., *et al.*, Effect of particle size and rubber content on fracture toughness in rubber-modified epoxies. *Polym. Eng. Sci.* **1996**. v36, 755–768.

KINLOCH, A., The mechanisms and mechanics of the toughening of epoxy polymers modified with silica nanoparticles, *Polymer (Guildf)*. 51. **2010**. 6284–6294.

KUNZ-DOUGLASS, S., et al., A model for the toughness of epoxy-rubber particulate composites, *J. Mater. Sci.* 15. **1980**. 1109–1123. doi:10.1007/BF00551799.

LE, Q. W., et al. Structure-property relations of 55 nm particle-toughened epoxy. *Polymer*. **2010**. v51, 4867–4879.

LEVITA, G., et al., Crosslink density and fracture toughness of epoxy resins, *J. Mater. Sci.* 26. **1991**. 2348–2352. doi:10.1007/BF01130180.

LIN, K. F., SHIEH, Y. D., Core-shell particles designed for toughening the epoxy resins. II. Core-shell-particle toughened epoxy resins. *J. Appl. Polym. Sci.* **1998**. v70: 2313–2322.

LU, F., CANTWELL, W. J., KAUSCH H. H., The role of cavitation and debonding in the toughening of core-shell rubber modified epoxy systems. *J. Mater. Sci.* **1997**. v32, 3055–3059.

MEEKS, A. C., Fracture and mechanical properties of epoxy resins and rubber-modified epoxy resins. *Polymer*. **1974**. v15. 675–681.

MIRACLE, D., *ASM Handbook: Composites*. Vol. 21, ASM International, Ohio. **2001**. ISBN:: 0-87170-703-9.

MOLONEY, A. C., et al., Parameters determining the strength and toughness of particulate filled epoxide resins, *J. Mater. Sci.* 22. **1987**. doi:10.1007/BF01160743.

NAKKA, J., Tailoring of epoxy material properties. Master of Science in Organic Chemistry, Andhra University, India. **2010**. ISBN/EAN: 978-94-91104-03-9.

O'HARA, G. P., Mechanical properties of silicone rubber in a closed volume. US Army Armament Research & Development Center, Benet Weapons Laboratory, **1983**.

PALUVAI, N. R., et al., Synthesis and Modifications of Epoxy Resins and Their Composites: A Review, *Polym. - Plast. Technol. Eng.* 53. **2014**. 1723–1758. doi:10.1080/03602559.

RATNA D., BANTHIA R. K., Rubber toughened epoxy, *Macromol. Res.* 12. **2004**. 11–21. doi:10.1007/BF03218989.

SCOTT, J. M., WELLS, G. M., PHILLIPS, D. C., Low temperature crack propagation in an epoxide resin. *J. Mater. Sci.* **1980**. v15, 1436–1448.

SUE, H. J., et al., Fracture behavior of core-shell rubber-modified crosslinkable epoxy thermoplastics. *Colloid Polym. Sci.* **1994**. v272, 456–466.

TOMUTA, A. M., New and Improved Thermosets Based on Epoxy Resins and Dendritic Polyesters. **2014**.

UEBERREITER, KANIG, K., Relation of Physical Behavior to Molecular Packing in Crosslinked Rubber. *Journal of Chemical Physics*, 18, 399. **1950**. doi: 10.1063/1.1732096.

UTALOFF, K., *et al.*, Improvement of fracture toughness and glass transition temperature of DGEBA-based epoxy systems using toughening and crosslinking modifiers, *Polym. Eng. Sci.* **59**. **2018**. 86–95. doi:10.1002/pen.24870.

VAN DER SANDEN, M. C., MEIJER, H. E. H, LEMSTRA, P. J., Deformation and toughness of polymeric systems: The concept of a critical thickness. *Polymer*. **1993**. v34, 2148–2154.

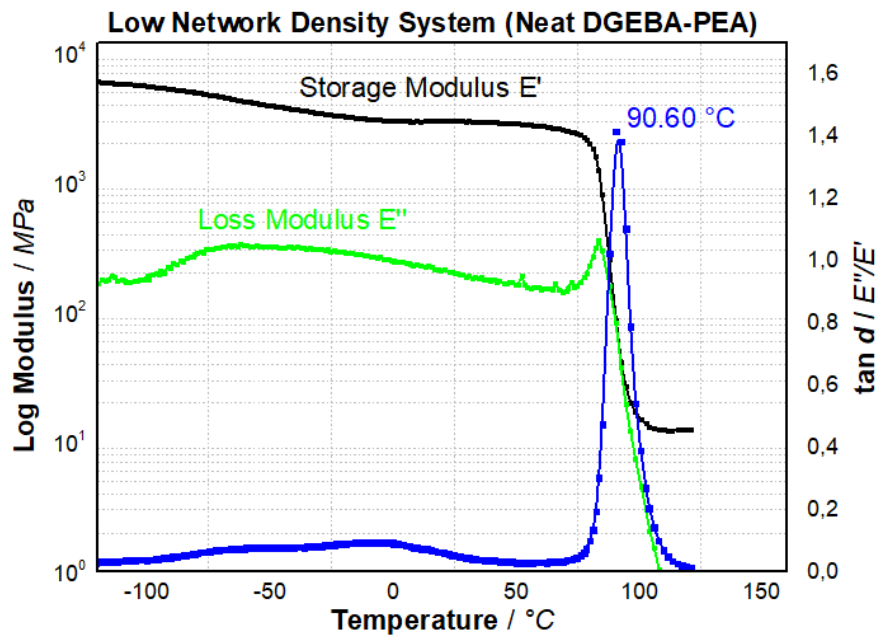
WETZEL, B., *et al.*, Epoxy nanocomposites – fracture and toughening mechanisms. *Science Direct, Engineering Fracture Mechanics* 73, 2375-2398. **2006**.

YEE, A. F., PEARSON, R. A., Toughening mechanisms in elastomer-modified epoxy resins – Part I. NASA Contractor Report. **1983**.

YOUNES, M., *et al.*, The curing of epoxy resins as studied by various methods. *Fachbereich Physik, Halle Saale, Germany*. **1994**.

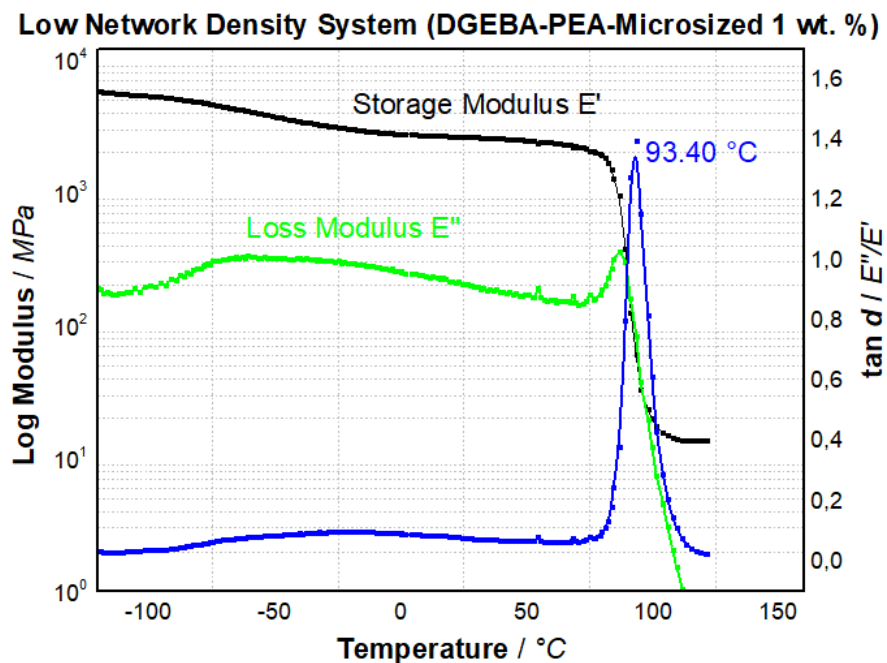
Appendix A

Figure 56 – DMA results as a plot of storage modulus (E'), loss modulus (E'') and $\tan \delta$ (E''/E') for low network system unmodified



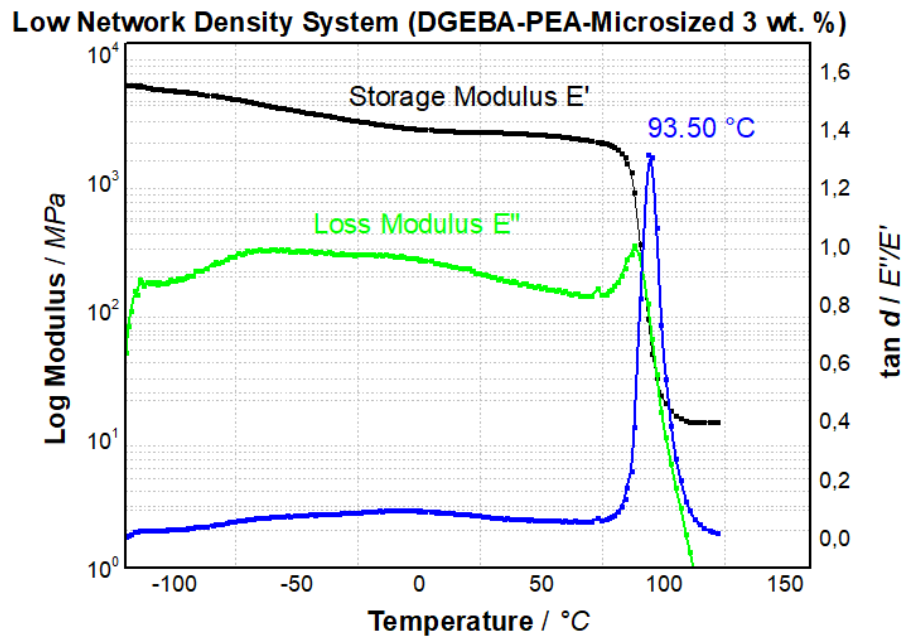
Source: From the author himself, 2019

Figure 57 – DMA results as a plot of storage modulus (E'), loss modulus (E'') and $\tan \delta$ (E''/E') for low network system modified with 1 wt. % of microsized particles



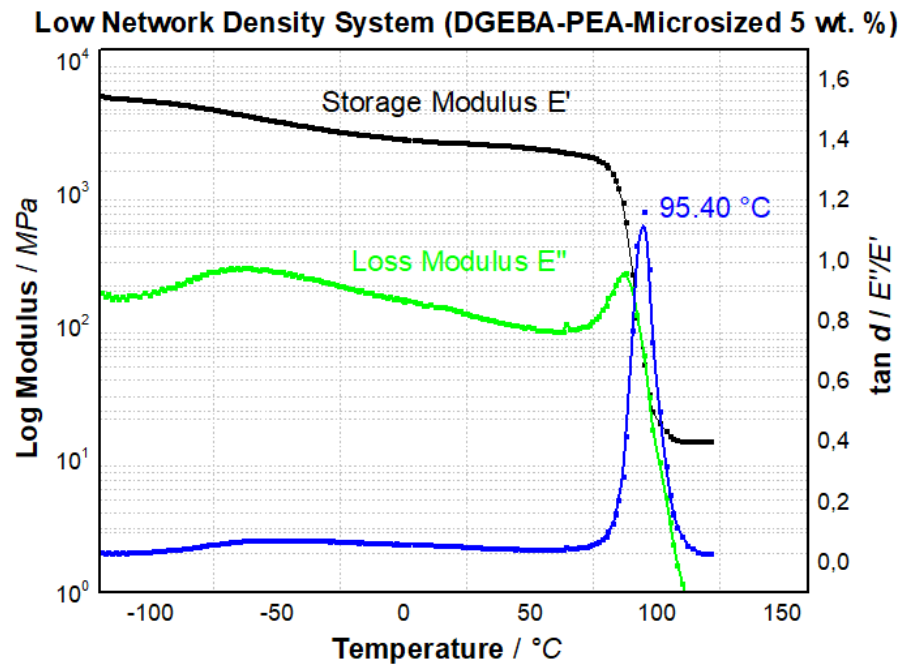
Source: From the author himself, 2019

Figure 58 – DMA results as a plot of storage modulus (E'), loss modulus (E'') and $\tan \delta$ (E''/E') for low network system modified with 3 wt. % of microsized particles



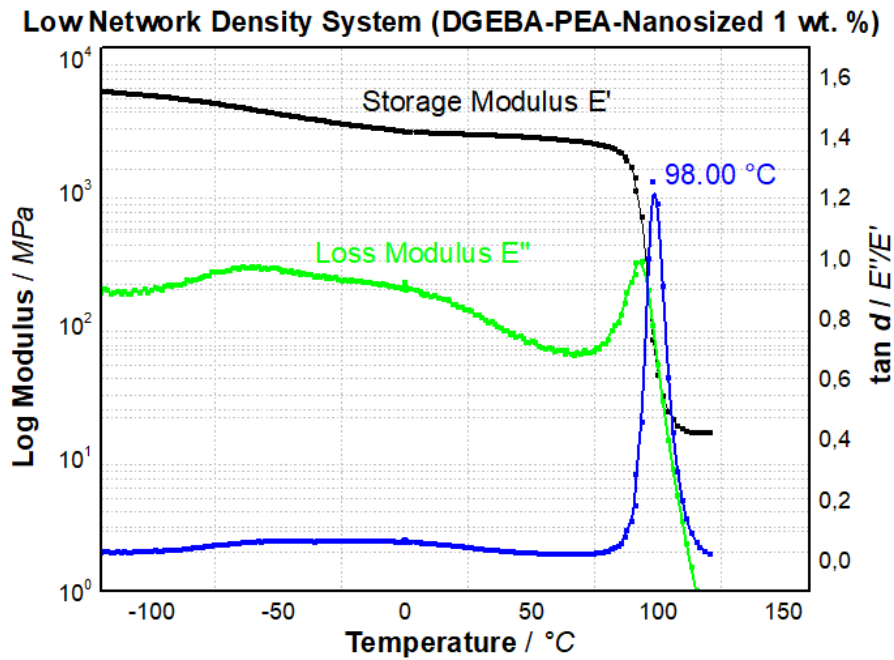
Source: From the author himself, 2019

Figure 59 – DMA results as a plot of storage modulus (E'), loss modulus (E'') and $\tan \delta$ (E''/E') for low network system modified with 5 wt. % of microsized particles



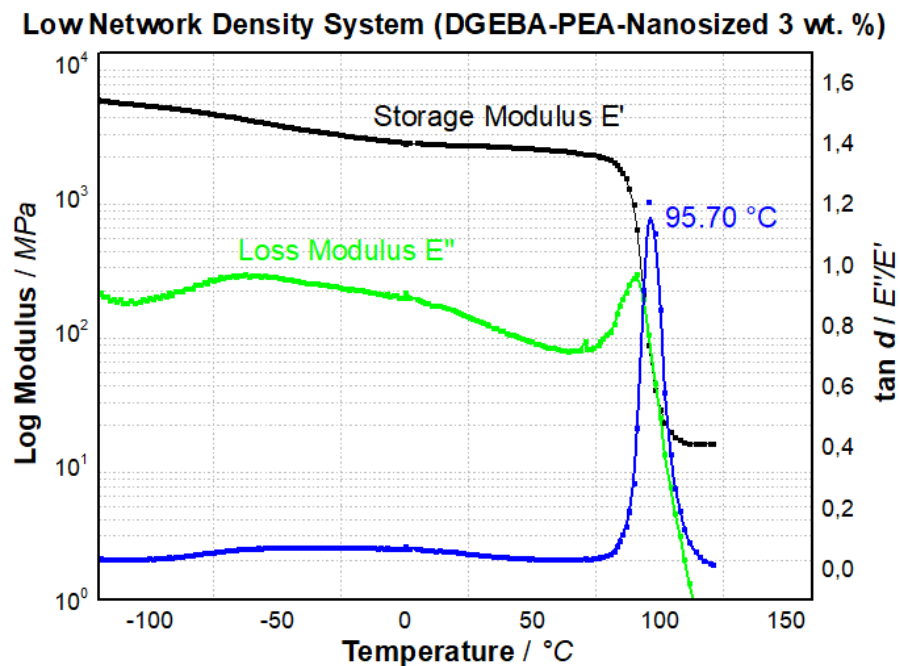
Source: From the author himself, 2019

Figure 60 – DMA results as a plot of storage modulus (E'), loss modulus (E'') and $\tan \delta$ (E''/E') for low network system modified with 1 wt. % of nanosized particles



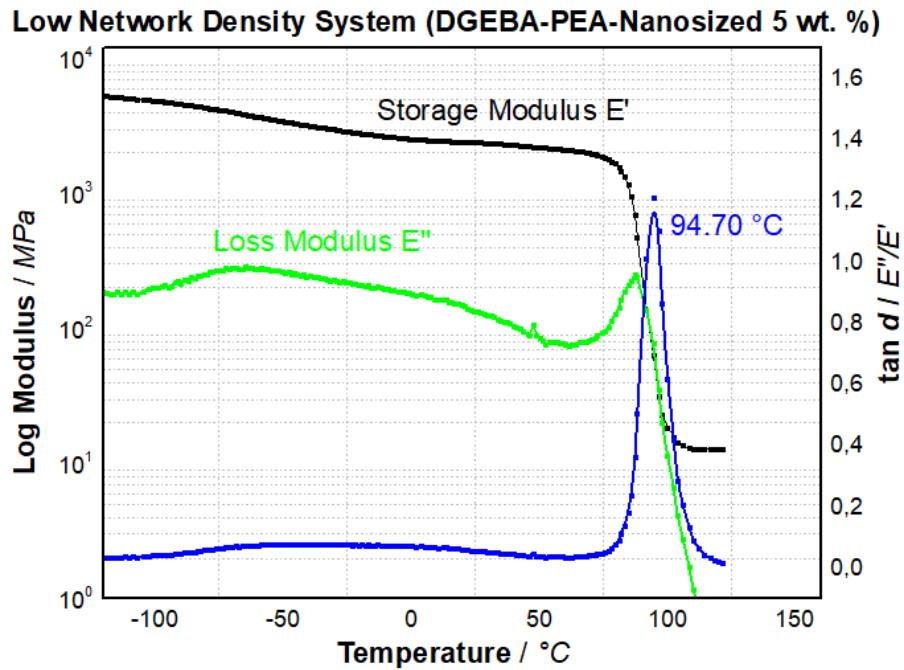
Source: From the author himself, 2019

Figure 61 – DMA results as a plot of storage modulus (E'), loss modulus (E'') and $\tan \delta$ (E''/E') for low network system modified with 3 wt. % of nanosized particles



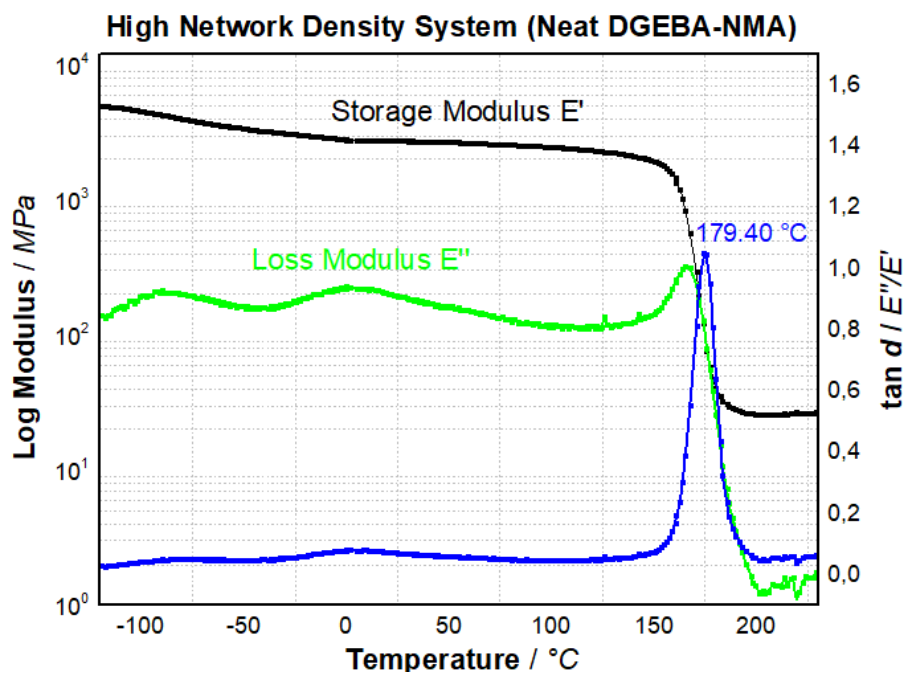
Source: From the author himself, 2019

Figure 62 – DMA results as a plot of storage modulus (E'), loss modulus (E'') and $\tan \delta$ (E''/E') for low network system modified with 5 wt. % of nanosized particles



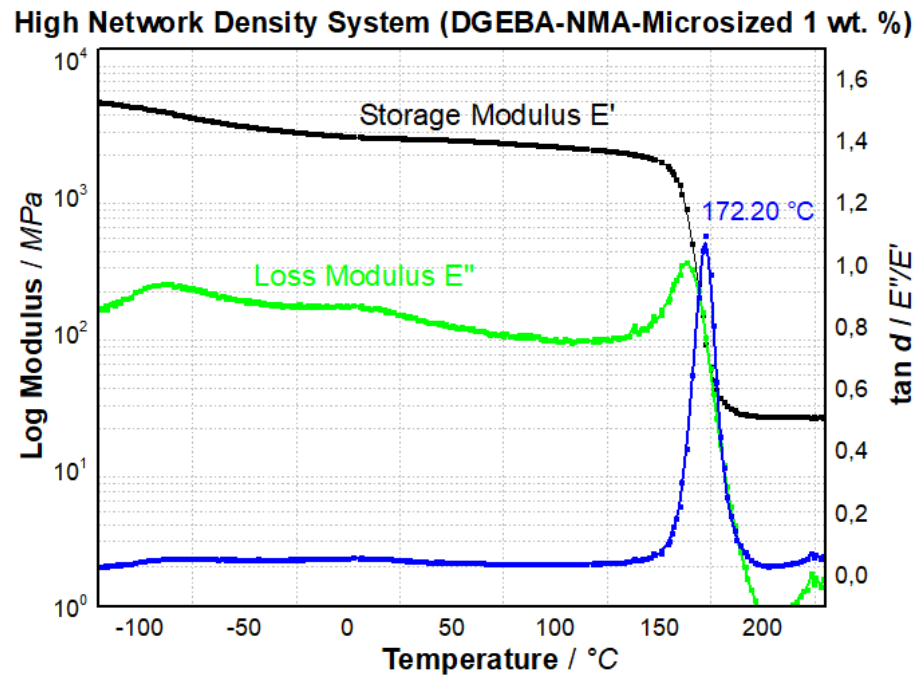
Source: From the author himself, 2019

Figure 63 – DMA results as a plot of storage modulus (E'), loss modulus (E'') and $\tan \delta$ (E''/E') for high network system unmodified



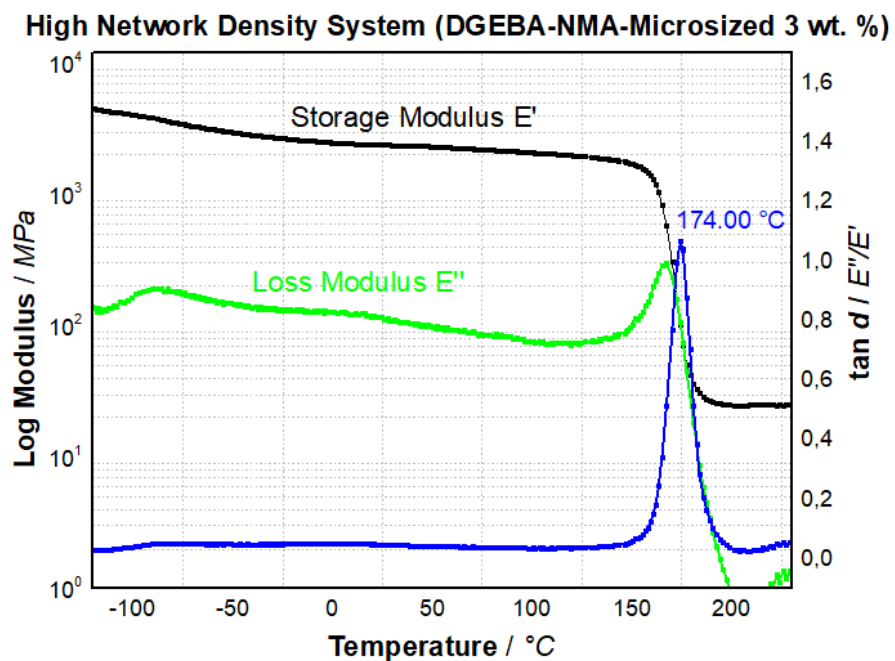
Source: From the author himself, 2019

Figure 64 – DMA results as a plot of storage modulus (E'), loss modulus (E'') and $\tan \delta$ (E''/E') for high network system modified with 1 wt. % of microsized particles



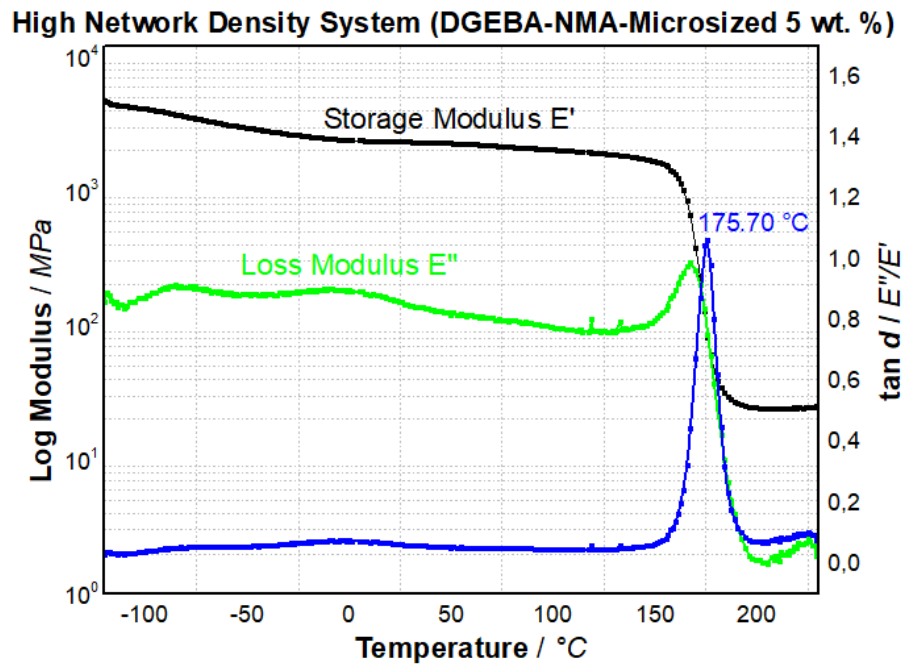
Source: From the author himself, 2019

Figure 65 – DMA results as a plot of storage modulus (E'), loss modulus (E'') and $\tan \delta$ (E''/E') for high network system modified with 3 wt. % of microsized particles



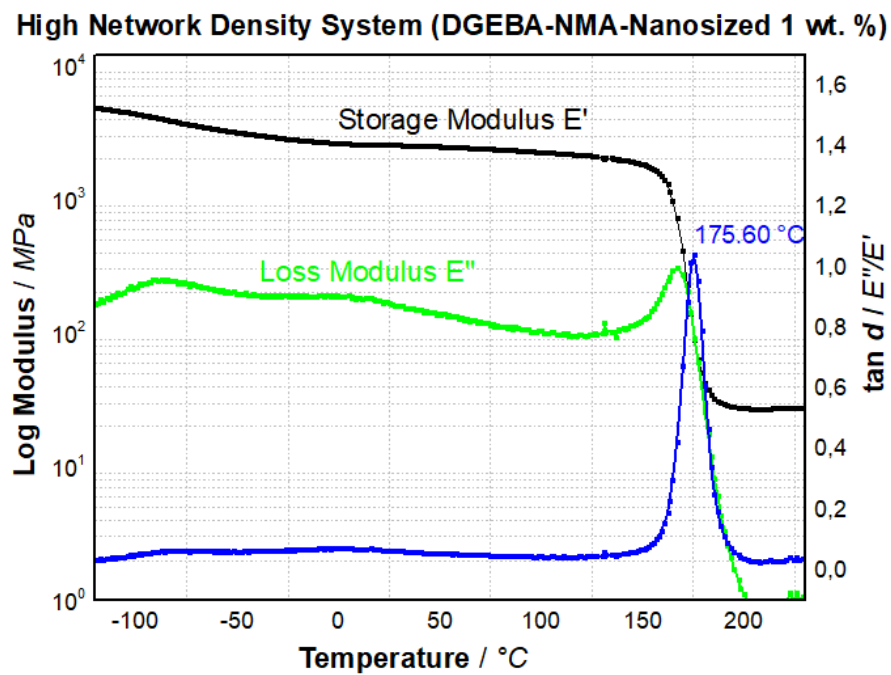
Source: From the author himself, 2019

Figure 66 – DMA results as a plot of storage modulus (E'), loss modulus (E'') and $\tan \delta$ (E''/E') for high network system modified with 5 wt. % of microsized particles



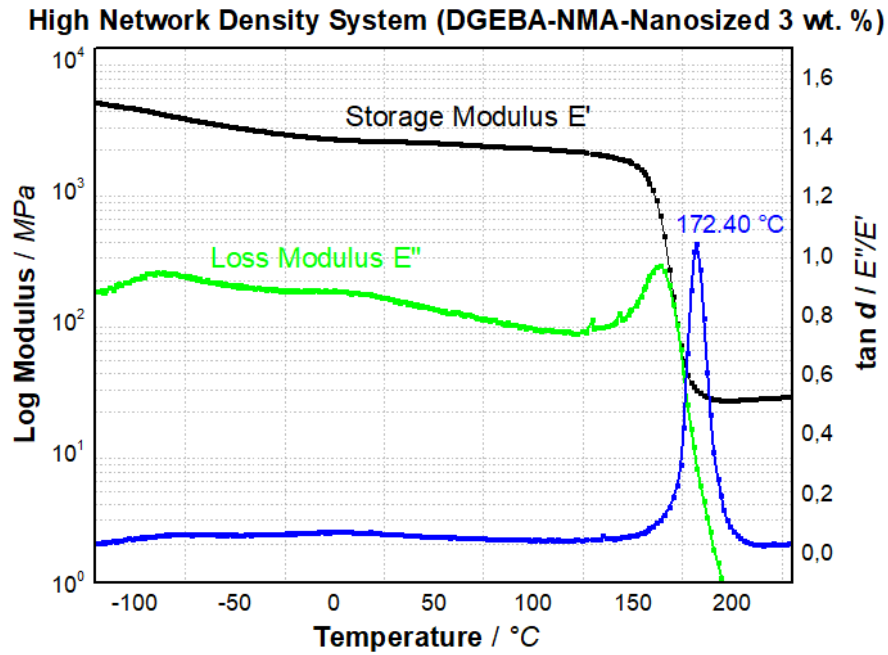
Source: From the author himself, 2019

Figure 67 – DMA results as a plot of storage modulus (E'), loss modulus (E'') and $\tan \delta$ (E''/E') for high network system modified with 1 wt. % of nanosized particles



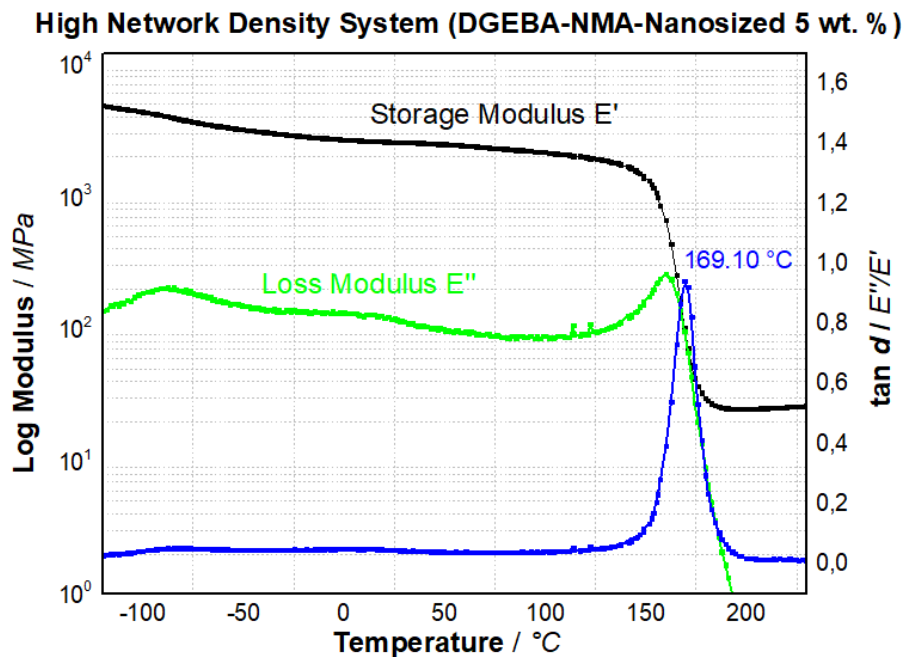
Source: From the author himself, 2019

Figure 68 – DMA results as a plot of storage modulus (E'), loss modulus (E'') and $\tan \delta$ (E''/E') for high network system modified with 3 wt. % of nanosized particles



Source: From the author himself, 2019

Figure 69 – DMA results as a plot of storage modulus (E'), loss modulus (E'') and $\tan \delta$ (E''/E') for high network system modified with 5 wt. % of nanosized particles



Source: From the author himself, 2019